QUANTITATIVE STUDIES OF POLYMER CRYSTALLIZATION UNDER NON-ISOTHERMAL CONDITIONS

A THESIS

Presented to

The Faculty of the Division of Graduate Studies

by

Donald Gene Bright

In Partial Fulfillment

of the Requirements for the Degree

Doctor of Philosophy in the School of Chemical Engineering

Georgia Institute of Technology

November, 1975

QUANTITATIVE STUDIES OF POLYMER CRYSTALLIZATION

UNDER NON-ISOTHERMAL CONDITIONS

Approved:

John D. Muzzy, Chairman

Charles J. Aloisio, Jr.

W.T. Ziegler

Date approved by Chairman: 4/4/75

DEDICATION

To All Those People Who Have Helped Me Thus Far In My Life

ACKNOWLEDGMENTS

The author wishes to thank his thesis advisor, Dr. John D. Muzzy, for his patience and guidance throughout the course of this work.

Appreciation is extended to Dr. W.T. Ziegler and Dr. C.J. Aloisio, Jr. of Bell Laboratories, Norcross, Georgia for having served on the reading committee. In addition, appreciation is extended to Dr. C.W. Gorton and Dr. W.C. Tincher for having served on the oral committee.

The Chemical Engineering Department is thanked for providing a Graduate Teaching Assistantship for the academic year 1972-73. Fellowships sponsored by Texaco Incorporated, the E.I duPont de Nemours & Company, the Procter and Gamble Company, and the Allied Chemical Company over the period of 1973-75 are greatly appreciated.

The author is indebted for the efficient assistance of the Chemical Engineering staff, especially Mr. C.J. Blackwood, Mrs. Dana Ritchie, and Mrs. Nancy Staton who always found the money from somewhere to pay for supplies and repair equipment.

The author thanks Mrs. Dana Ritchie for her excellent work, assistance, and dependability in typing both the rough and final drafts of this dissertation.

The author is grateful to have parents encouraging him to do his own thing in life and pursue a dream.

And last, but not least, the author thanks Casper, the friendly ghost, who shared the many lone hours and debated the many problems associated with this dissertation.

TABLE OF CONTENTS

Page

LIST OF TABLES

LIST OF FIGURES

Figure Page

Figure Page

NOMENCLATURE

Variable	Description	Units
a_o	Monomolecular Layer Width	cm
b_o	Monomolecular Layer Thickness	cm
c_1	WLF parameter	-
c_2	WLF parameter	°K
C_p	Specific Heat	cal/gm/°K
C_{p_c}	Specific Heat of Crystalline Polymer	cal/gm/°K
C_{p_m}	Specific Heat of Melt Polymer	cal/gm/°K
D	Spherulite Diameter	microns
D_i	Impingement Spherulite Diameter	microns
D_m	Maximum Spherulite Growth	microns
D_p	Programmed Scan Speed	°/min
D_s	Polymer Sample Scan Speed	°K/min
ΔF	Change in Free Energy	erg/molecule
$\Delta \bar{F}$	Change in Free Energy	cal/mol
G	Lamellar Growth Rate	cm/sec
G_o	Inherent Lamellar Growth Rate	cm/sec
ΔG_v	Change in Bulk Free Energy	erg/cm^3
h	Plank Constant	erg·sec
h_i	Coolant Heat Transfer Coefficient	$cal/sec/cm^2/°K$
Δh_c	Latent Heat for 100% Crystallinity	erg/cm^3
$\Delta \bar{H}$	Change in Enthalpy	cal/gm
$\Delta \bar{H}_a$	Apparent Activation Energy	cal/mol

Variable	Description	Units
$\Delta\bar{H}_c$	Latent Heat for 100% Crystallinity	cal/gm
k	Boltzmann Constant	erg/°K
k_{mw}	Thermal Conductivity of Mold Walls	cal·cm/sec/cm^2/°K
k_p	Thermal Conductivity of Polymer	cal·cm/sec/cm^2/°K
ℓ	Length of Monomolecular Chain Fold	cm
n	Avrami Exponent	-
Q	Heat Generation Rate	cal/cm^3/sec
R	Universal Gas Constant	cal/mol/°K
$\Delta\bar{S}$	Change in Entropy	cal/mol/°K
t	Time	second
Δt	Change in Time	second
T	Polymer Temperature	°K
T_g	Glass Transition Temperature	°K
T_m	Thermodynamic Melt Temperature	°K
T_i	Incipient Crystallization Temperature	°K
T_{peak}	Peak Crystallization Temperature	°K
T_F	Final Crystallization Temperature	°K
V	Spherulite Volume at Diameter, D	micron^3
V_m	Maximum Spherulite Volume at Maximum Growth, D_m	micron^3
x_{mw}	Mold Wall Thickness	cm
x_p	Polymer Slab Thickness	cm
Δx_p	Polymer Slab Increment Thickness	cm
x	Rectangular Co-ordinate	length
y	Rectangular Co-ordinate	length
z	Rectangular Co-ordiante	length

Variable	Description	Units
Z	Avrami Kinetic Parameter	sec^{-3}
α	Thermal Diffusivity	cm^2/sec
β	Degree of Crystallinity at Impingement of Spherulites	-
Δ	Change	-
η	Viscosity	poise
η_{T_g}	Viscosity at Glass Transition	poise
μ	Unit of Measure	micron
ν_o	Density of Growth Nuclei	cm^{-3}
π	Pi	-
ρ	Bulk Polymer Density	gm/cm^3
ρ_m	100% Melt Polymer Density	gm/cm^3
ρ_c	100% Crystalline Polymer Density	gm/cm^3
σ	Lateral Surface Fold Energy	erg/cm^2
σ_e	End Surface Fold Energy	erg/cm^2
x	Degree of Crystallinity	-
x_w	Maximum Degree of Crystallinity	-

SUMMARY

Cooling is a major step in any molding and extrusion process. For injection molding, the principal portion of the cycle time is devoted to cooling the molded part. In extrusion the length of the take-off system is dictated by the time to cool the extrudate. Furthermore, the cooling step can significantly alter the structure and consequently the properties of the product through variations in crystalline structure.

For crystalline polymers, analysis of the transient heat conduction occurring in bulk solidification must incorporate the latent heat of crystallization and the crystallization kinetics of the polymer. The problem lies in adequately representing and incorporating the crystallization kinetics and properly accounting for the associated latent heat contributions.

Historically, changes in crystallinity have been expressed through the classical Avrami kinetic relation. The inherent kinetic parameters are usually determined by curve fitting isothermal data; thus considerable data are required. These kinetic parameters do not adequately represent the phenomenological mechanisms of polymer crystallization. When the kinetic relation is used to represent the crystallization phenomena occurring under non-isothermal conditions, the validity of these empirical predictions is questionable.

This study incorporates a kinetic growth rate expression developed by Hoffman in the Avrami relation for predicting changes in crystallinity based on the phenomenological mechanisms of polymer

crystallization. It has been proven experimentally that with kinetic parameters determined from non-isothermal data, the Avrami relation can not be used to adequately describe the crystallization kinetics under non-isothermal conditions. Even in the differentiated form, the Avrami relation can not be applied on an incremental basis because of its temperature dependent, fundamental parameters.

The same kinetic growth rate expression was incorporated into an alternate relation, the volumetric growth relation, for predicting changes in crystallinity. The kinetic parameters can be determined from two data points collected under isothermal and non-isothermal cooling conditions: 1) the average size of the spherulites at impingement, and 2) the associated time and temperature at impingement. For simulations of isothermal and non-isothermal crystallizations, the volumetric growth relation predicted the correct crystallinity at the appropriate temperatures based solely on the crystallization kinetics.

By incorporating the volumetric growth relation into the heat generation term of the transient heat conduction expression, its solution gave time-temperature-position profiles of cooling temperature and crystallinity characteristic of cooled, injection molded parts.

Six crystalline polymers have been analyzed in this study: polyethylene, polypropylene, two polyethylene terephthalates, Nylon 6, and Nylon 66. All polymers were analyzed by a common procedure to determine their respective kinetic and heat conduction parameters under non-isothermal conditions. Since the analytical procedure and the volumetric growth relation were independent of any particular polymer studied, the procedure and growth relation should be suitable for the

analysis of non-isothermal crystallization in many crystalline polymers.

CHAPTER I

INTRODUCTION

Cooling is a major step in any molding and extrusion process. For injection molding, the principal portion of the cycle time is devoted to cooling the molded part. In extrusion the length of the take-off system is dictated by the time to cool the extrudate. Furthermore, the cooling step can significantly alter the structure and consequently the properties of the product through crystallinity.

Three factors are principally responsible for the lengthy cooling times in solidifying crystalline polymers: (1) low thermal conductivity, (2) the latent heat of crystallization, and (3) the time required for crystallization to occur. These same factors lead to some unusual time-temperature profiles which also vary substantially with distance from the cooling surface. The developing crystalline structure is highly dependent on the thermal history during cooling, frequently causing significant gradients in the structure and resultant properties of the solidified polymer. Therefore, heat transfer and crystallization are coupled processes which depend on both the cooling time and position within the material. Thus analysis of transient heat conduction must incorporate the latent heat of crystallization and the crystallization kinetics of the polymer in order to resolve this position dependent thermal and structural history.

A number of investigators (23,43,60,66) have analyzed heat

conduction in crystallizing polymers with considerable variations in the treatment of the crystallization kinetics. To date, the heat generation due to crystallization has been represented by relating the latent heat (1) to an equivalent temperature, (2) to an equivalent temperature change through heat capacity, and (3) through pre-determined, incremental changes in crystallinity. Obviously the first two techniques completely ignore the kinetic aspects of crystallization, and the third technique relates the corresponding energy release associated with an incremental change in crystallinity. Thus the problem in correctly solving transient heat conduction lies in the adequate incorporation of crystallization kinetics and the proper accounting of associated latent heat contribution.

The objective of this work is the development of a method for adequately representing the crystallization phenomena in solidifying crystalline polymers. The method begins with an enthalpic energy expression of phase change incorporating sensible and latent heat contributions. The latent heat portion is governed through changes in crystallinity expressed through a classical kinetic relation. This relation accounts for nucleation density, inherent crystallization, subsequent molecular crystallization, and molecular transport across the phase interface. As with all kinetic relations expressing phenomenological occurrences, experimental data are necessary to determine pertinent kinetic parameters. Historically, such data are usually collected under isothermal conditions. Since the kinetic parameters are typically determined through curve fitting the isothermal data, considerable data are required. But these kinetic parameters

do not necessarily represent any mechanisms of polymer crystallization. When the kinetic relation is used to represent the crystallization phenomena in different solidification processes, the validity of these empirical predictions is questionable.

This study incorporates a kinetic growth rate expression into the Avrami relation for predicting changes in crystallinity based on the phenomenological mechanisms of polymer crystallization. The kinetic parameters will be developed through isothermal and non-isothermal experiments which will be shown to require considerably less data. Finally, the resulting enthalpic expression incorporating crystallization kinetics represents the heat generation term within the transient heat conduction equation, solution of which yields the time-temperature-position profiles characteristic of cooling in injection molded parts. However, the kinetic model does not explicitly consider pressure and shear effects which will be the subject of future investigations.

In order to develop a method based on the theory and generality of the crystallization phenomena and be independent of any particular polymer, two polymers within each of three groups are utilized in this kinetic study. Polyethylene and polypropylene represent the polyolefins; two polyethylene terephthalates, polyesters; and Nylon 6 and Nylon 66, polyamides. Thus, a particular polymer identifies itself only through the following physical and thermal properties: thermodynamic melt point, glass transition, latent heat of crystallization, crystalline density, monomolecular layer thickness and width, and molecular chain fold energies.

CHAPTER II

LITERATURE SURVEY

The injection molding process can be divided into three major steps: filling, packing, and cooling. In the filling step, a molten polymer flows into an empty cavity which has a temperature below the solidification temperature range of the polymer. After filling, additional polymer is packed into the cavity to compensate for shrinkage caused by solidification. Actually, cooling starts with the filling step and continues until sufficient solidification of the polymer is achieved to permit its ejection from the mold without deformation. (38) Since a cooling material has a temperature profile, crystallization, if it occurs, does so at different rates throughout the polymer. Therefore, it is reasonable to expect that the degree of crystallinity and morphology are not uniform. Furthermore, the cooling history can significantly alter the structure and consequently the properties of the polymer.

For example, the mechanical properties and morphology depend strongly on the mold temperature employed during injection molding. For an ethylene and propylene copolymer, low mold temperatures yield a material with a fine morphological structure and high impact strength while high mold temperatures yield a material with a course morphological structure and a high heat distortion resistance. However, the tensile yield strength is largely unaffected by mold temperature. (28)

Transient Heat Conduction

Consider a cross-section of a typical polymer/mold wall/coolant arrangement as shown in Figure 1a and extract an elemental segment from somewhere within the arrangement for transient heat conduction analysis, Figure 1b. The mathematical relation representing heat conduction with heat generation in a rectangular, isotropic solid is expressed by (12):

$$\frac{\partial T}{\partial t} = \alpha\left[\frac{\partial^2 T}{\partial x^2} + \frac{\partial^2 T}{\partial y^2} + \frac{\partial^2 T}{\partial z^2}\right] + Q/\rho\, C_p \qquad (2.1)$$

In Equation (2.1), thermal conductivity is assumed to be constant. By assuming a rectangular geometry thin in the x-direction, heat transfer principally in the x-direction, and constant volume, Equation (2.1) reduces to a nonlinear parabolic, differential equation:

$$\frac{\partial T}{\partial t} = \alpha\, \frac{\partial^2 T}{\partial x^2} + Q/\rho\, C_p \qquad (2.2)$$

where Q represents the heat generation via polymer crystallization and is time and position dependent. Since Equation (2.2) is highly nonlinear and not amenable to explicit analytical solutions; it must be solved through numerical techniques.

Heat Generation

Several investigators (23,43,60,65,66) have analyzed the heat conduction phenomena in crystallizing polymers with considerable variations in the treatment of heat generation. Initial solutions were for non-crystallizing cellulosic or styrene polymers where no latent heat evolves during the melt/solid transformation; only a second order transition occurs. Reasonable solutions using these polymers were usually obtained

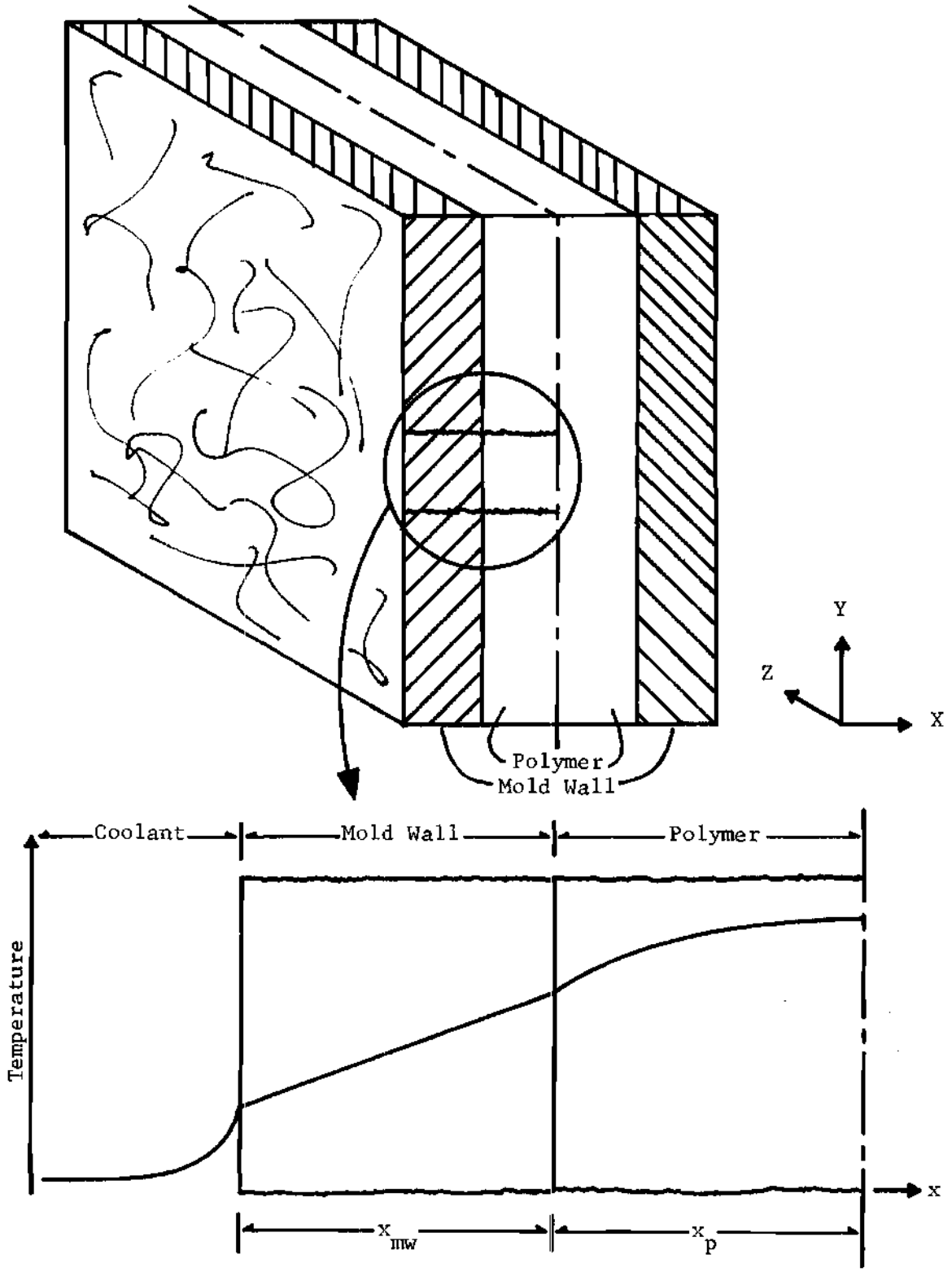

Figure 1. Typical Coolant/Mold-Wall/Polymer Arrangement

using Gurney and Lurie charts. (27) With the more highly crystalline polymers - polyolefins, polyesters, and polyamides - which possess high latent heats of crystallization, solution of the transient heat conduction equation is significantly complicated by the highly nonlinear heat generation term due to the temperature dependency of crystallization.

Initial attempts at solving heat conduction problems involving these highly crystalline polymers ignored completely the kinetic aspects of crystallization. Gloor (23) converted the latent heat to an equivalent temperature through rearrangement of the enthalpy-temperature curve; thus his specific heat-temperature curve exhibits a linear profile over the phase transition temperature range. See Figure 2. Kenig and Kamal (43) replaced the latent heat with an equivalent temperature change defined as follows:

$$\Delta T = \Delta \bar{H}_c / C_p \tag{2.3}$$

where C_p is the specific heat of the polymer at the temperature under consideration. When the upper melt temperature, T_{um}, is reached, further reductions in the temperature are made in proportion to the accumulated crystalline fraction. The successive, partial delays in temperature reductions terminate at the lower melting temperature, T_{lm}, which is obtained from the following definition:

$$\Delta \bar{H}_c = \int_{T_{um}}^{T_{lm}} C_p \, dT \tag{2.4}$$

Progelhof and Throne (60) solved the transient heat conduction equation for structural foams. They chose a modified Gloor technique as shown in Figure 2. This technique assumes that the crystallization

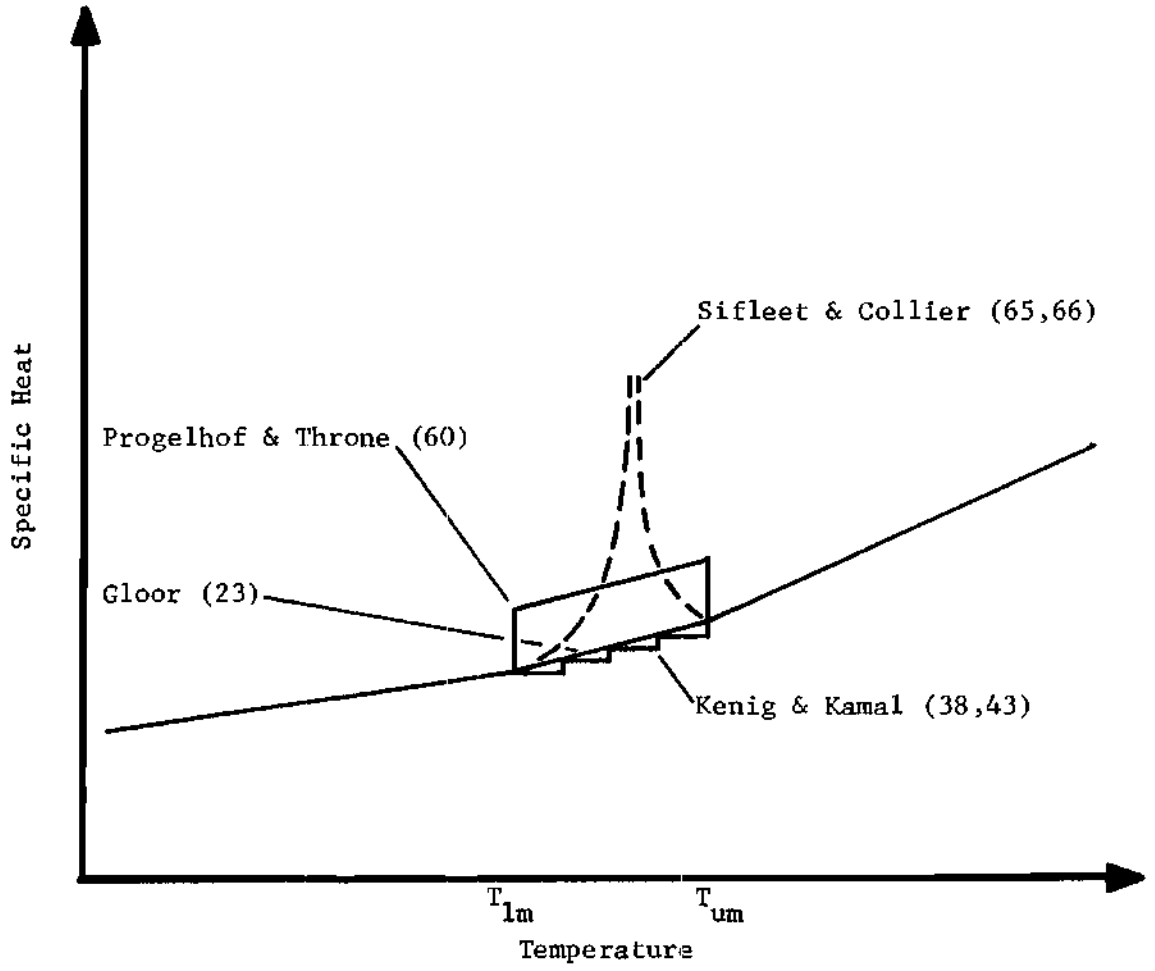

Figure 2. Summary of Techniques for Representing Latent Heat of Crystallization in Transient Heat Conduction Analysis

is directly proportional to the temperature over a short region and that the crystallization is in quasi-equilibrium. Thus the induction time is zero, and the rate of crystallization is significantly faster than the rate of heat removal causing an immediate temperature rise.

Collier and co-workers (66) are the first known to incorporate crystallization kinetics into the heat generation term of the transient heat conduction equation. In representing kinetically the crystallization phenomena, they employed the classical Avrami relation:

$$\chi = 1 - \exp(-Z_n t^n) \tag{2.5}$$

which relates the degree of crystallinity (χ) to the time (t) when crystallization began under constant temperature conditions (isothermal crystallization). Z_n is the kinetic parameter, and n is an integer function for the type crystallization and nucleation occurring. By rearranging Equation (2.5) as follows:

$$\ell n \{-\ell n(1 - \chi)\} = n \ell n\, t + \ell n\, Z_n \tag{2.6}$$

then Z_n and n may be determined from crystallization data by plotting $\ell n \{-\ell n(1 - \chi)\}$ versus ℓn t giving a straight line with a slope of n and an intercept of $\ell n\, Z_n$. But, there are three significant problems with this approach. First, using a $\ell n\ \ell n$ function of χ with respect to time imposes an apparent linear relationship. Secondly, Collier's crystallization rate constants are determined from an isothermal process. As discussed earlier, a cooling polymer has a temperature profile and thus crystallizes at different rates. Consequently, it is mandatory that several sets of isothermal rate constant data be collected so as to have

temperature dependency. And thirdly, in solution of the transient heat conduction equation, heat generation is determined from incremental changes in crystallinity (ΔX) corresponding to pre-determined incremental changes in time (Δt). (65) This approach actually corresponds to the physical process in reverse; that is, the change in crystallinity is selected and then the corresponding temperature changes are calculated.

It should now be readily apparent that none of these investigators (23,43,60,65,66) have included and/or represented the kinetics of crystallization in the classical sence - solely temperature dependent. However, the work of Collier and co-workers (65,66) clearly made the first bona fide attempt at incorporating the kinetics of polymer crystallization into the heat generation term of the heat conduction equation. But even their approach is on a macro-scale; in that, their kinetic parameters are determined by empirically fitting rate data. The consideration of stepwise mechanisms in the crystallization of polymer molecules is completely absent. Hoffman (34) has developed a model of such mechanisms and has incorporated it into the Avrami equation. Before proceeding any further, it would be prudent to review the origin and basis of the classical Avrami relation, the phenomenological aspects of polymer crystallization, and then lead into a synposis of Hoffman's crystallization model.

The Avrami Relation

The Avrami relation evolved from the theoretical and experimental work on the kinetics of phase change by Melvin Avrami. (3,4,5) His theory is developed from the experimentally supported assumptions that a new phase is nucleated by germ nuclei already existing in the current

phase. The number of germ nuclei can be affected by temperature, degree and duration of supercooling, and thermal history. These nuclei may be heterogeneities, such as foreign particles with an absorbed layer of the new phase, or crystal molecules of the new phase. During growth of the new phase, the density of germ nuclei diminishes through activation of some to growth nuclei and ingestion of others by the growing phase. (3) In any real growth process, impingement of a new region upon a second results in the cessation of growth of both in the contact region, i.e., one new phase region does not penetrate the other. The mathematical relation derived by Avrami based on the foregoing conditions is:

$$1 - \chi = \exp(-Z_n t^n) \tag{2.7}$$

where $1 - \chi$ is the fraction of the current phase not transformed; t is time since incipient phase transformation; Z_n is the kinetic rate parameter which determines the time scale of crystallization, reflects the intrinsic rate of nucleation and growth processes that control crystallization, and is extremely sensitive to temperature; and n is an integer function of the type of nucleation and crystallization occurring. (3,59) Implicit in Equation (2.7) is the assumption that the volume does not change during transformation. Because the derivation of Equation (2.7) does not consider how the transformed regions arrived at their particular shape, size, and distribution, the equation applies rigorously only to spheres when n is equal to three. (58)

Shortly, after Avrami published his work (3,4,5), Evans (21) published a similar relation founded on the laws of expanding spheres from a predetermined nuclei density and incorporated kinetically the

geometric representation of spherulitic growth as follows:

$$1 - \chi = \exp(-4/3\ \pi\ \nu_o\ G^3\ t^3) \qquad (2.8)$$

where $4/3\ \pi\ \nu_o\ G^3 \equiv Z_n$ in the Avrami relation, Equation (2.7). ν_o is the density of growth nuclei; G, the spherulitic growth rate; and t, the time since incipient crystallization. Hoffman (31,34) uses this relation as a means of introducing his theory of spherulitic growth rates of crystallizing bulk polymers through the radial growth rate parameter, G.

Crystallization

The total crystallization process depends not only upon the rate of growth of crystalline phases but also upon the number of such phases. Thus any description of phase transformation must include a discussion of the birth (primary nucleation) of such phases.

Primary Nucleation

The nucleation process may be either homogeneous or heterogeneous. Homogeneous nucleation starts randomly and proceeds sporadically within the polymer melt phase as a result of random fluctuations in molecular alignment and order initiating the crystalline phase. Heterogeneous nucleation begins with the absorption of somewhat disordered crystal layers of the new phase on the surface of inherent, randomly distributed, insoluble impurities within the melt phase. There exists sufficient evidence to indicate that in polymer crystallization, nucleation is predominately heterogeneous. (64) During isothermal crystallization, the number of growth nuclei (those germ nuclei which attain growth nuclei status by having absorbed crystal layers of the new phase) remains

constant. When the temperature is lowered, the number of growth nuclei increases, reflecting the effect that a lower free energy state activates otherwise dormant germ nuclei to growth nuclei status. These growth nuclei initiate the formation of polycrystalline aggregates which, in turn, grow in a radially symmetric pattern. These growing aggregates are termed "spherulites". (59) See Figure 3a.

Primary Crystallization

Incipient crystallization begins with lamellar type structures growing radially outward from each growth nuclei. See Figure 3b. As the lamellae grow, they reject preferentially low molecular weight and stereo-irregular (atactic conformation) components of the polymer. Thus there is a build-up of such "impure" polymer components on each lamellar growth front. Simultaneously, growing lamellae are separated from one another by layers of yet uncrystallized polymer melt composed of some "impurity" components as well as the typical, bulk melt components. See Figure 3b. Depending upon prevailing crystallization conditions and the polymer, these layers of melt either remain uncrystallized indefinitely or crystallize slowly to fill in the over-all structure. Lamellar thicknesses (200-1000 Å) are governed principally by the supercoolings at which they are grown and do not appear to be affected appreciably by changes in molecular weight. However, lamellar widths are sensitive to both supercooling and changes in molecular weight and are determined primarily by impurity segregation. Also, the frequency of noncrystallographic lamellar branching varies inversely with lamellar width. (39,40,41,42)

Radial growth of the lamellae continues in all directions until the growing spherulites impinge upon one another forming interspherulitic

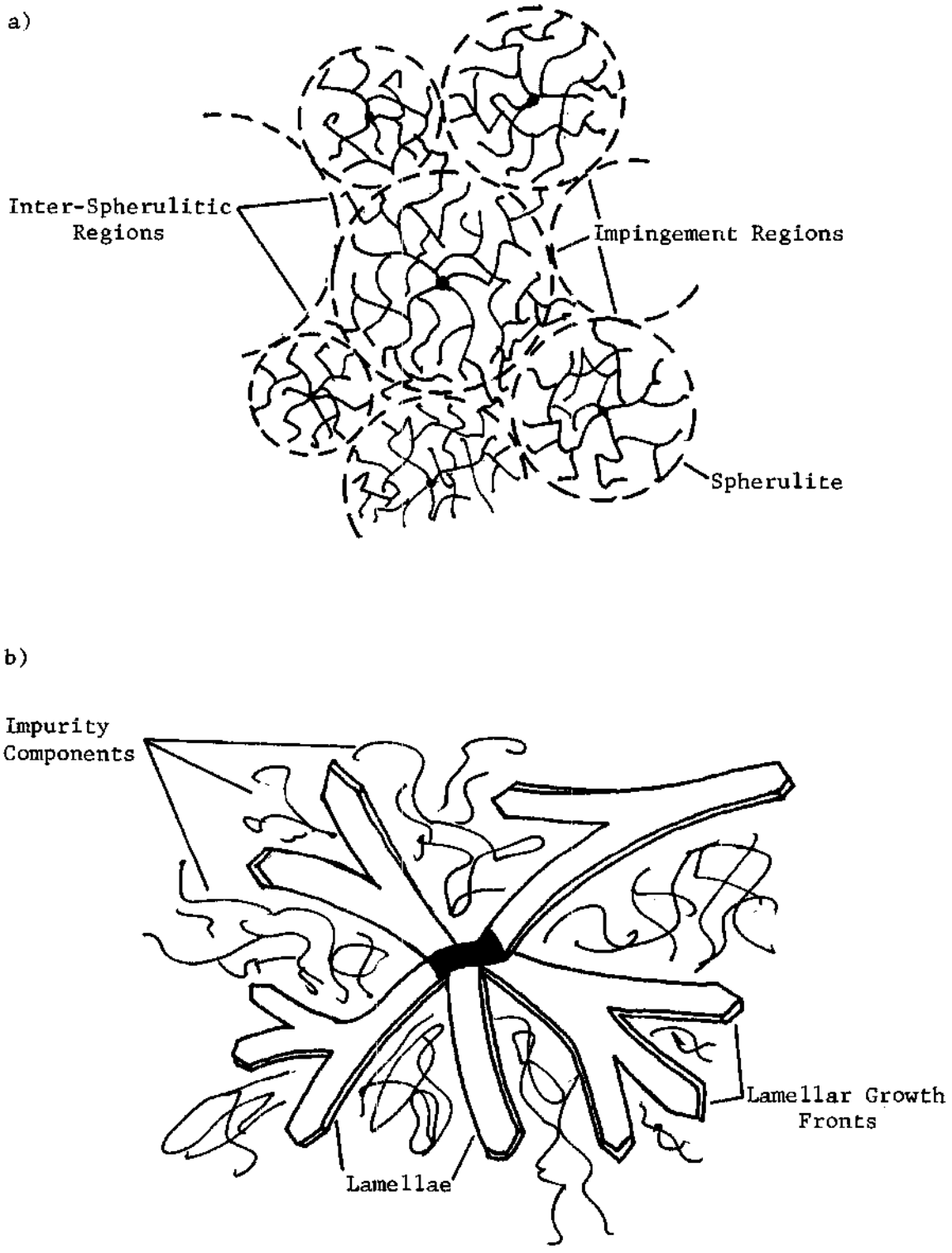

Figure 3. Morphological Features of Polymer Spherulites

regions. See Figure 3a. This phenomenon signifies the end of primary crystallization and the establishment of an extensive network of tie molecules and intercrystalline links that respectively connect adjacent lamella within a spherulite and bridge adjacent spherulites. Also, the crystallinity is approximately 50% of its ultimate value. (39,40,41,42)

Secondary Crystallization

Secondary crystallization is largely associated with inter-lamellar crystallization initiated by the melt polymer trapped between lamellae, and a continuation of the primary crystallization mode into the un-crystallized inter-spherulitic regions. The net result is a slow increase in crystallinity (39,42)

Annealing

Annealing is the thickening of lamellae; thus this phenomenon can occur during and after primary and secondary crystallization. Again, the net result is a slow increase in crystallinity.

Spherulite Growth Rates

The radial growth rates (G) of spherulites have generally been described quantitatively by equation of the form:

$$G = G_o \exp(-\Delta\Phi/kT) \exp(-\Delta F/kT) \qquad (2.9)$$

which is a simple extension of the Turnbull-Fisher expression (74) for the rates of surface nucleation. (34,41) It is assumed that the rate of lamellar growth is controlled by the rate of two-dimensional surface nucleation on the face of growing lamellae. (41,42) $\exp(-\Delta F/kT)$ may be considered as the probability that a particular polymer chain traverses

the melt/crystalline interface; $\exp(-\Delta\Phi/kT)$ represents the probability that a particular polymer chain in the immediate vicinity of a lamellar growth front crystallizes, and G_o is the inherent lamellar growth rate. ΔF is the free energy of activation of molecular chain transport, and $\Delta\Phi$ is the free energy of activation for surface nucleation of a polymer chain on a growing lamellar front. (34)

Equation (2.9) describes the temperature dependence of spherulitic growth rate as two competing processes. Opposing one another are the rate of molecular transport in the melt which increases with increasing temperature, and the rate of surface nucleation which decreases with increasing temperature. At temperatures in the neighborhood of the glass transition, the resistance to molecular transport dominates; at temperature near the melt temperature, the resistance to surface nucleation dominates. Thus, between these two extremes, the growth rate (G) passes through a maximum where the two competing processes are of comparable weight. (41)

Free Energy of Activation in Chain-Folded Polymers

It is a well accepted and experimentally proven fact that when long-chain polymer molecules crystallize on the growth front of lamellae, they do so by folding parallel to themselves across the lamellar growth front but with their molecular chain axis perpendicular to the direction of lamellar growth. See Figure 4.

Polymer molecules fold simply because at crystallization temperatures substantially below the thermodynamic melt temperature, the molecule can attain the lowest possible free energy conformation by regularly folding parallel to itself. Consider the free energy relation:

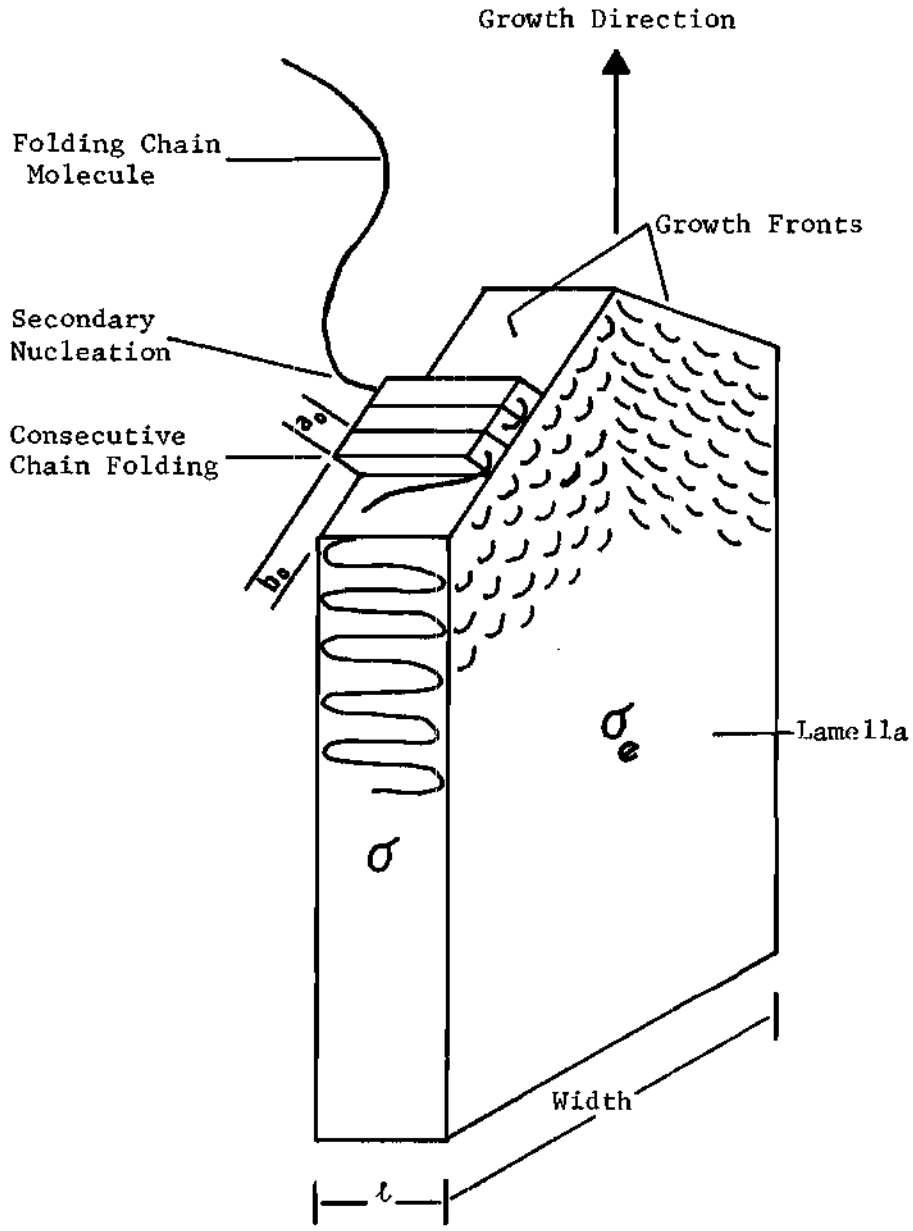

Figure 4. Typical Lamellar Growth Front

$$\Delta\bar{F} = \Delta\bar{H} - T\Delta\bar{S} \qquad (2.10)$$

where the polymer melt is the reference state. By definition, the thermodynamic melt temperature is that temperature where $\Delta\bar{F}$ is zero. At all lower temperatures, $\Delta\bar{F}$ will be negative, and the crystallizing polymer molecules will adopt a conformation for which $\Delta\bar{F}$ will be most negative under the prevailing conditions. When the temperature is substantially less than the melt temperature, the entropy contribution can be neglected relative to the enthalpy contribution. The lowest energy conformation of a single molecule in the crystalline phase is some form of a helix or a planar zigzag; because they permit the maximum amount of molecular packing within a unit cell structure. But, if a helix is forced to fold, the free energy of the molecule increases. However, if the fold is a regular fold which permits the helix or coplanar zigzag on either side of a fold to pack together in a crystallographic manner, then additional molecular interactions decrease the free energy by an amount proportional to the length of the chain. Thus, if the polymer chain molecule is long enough, the increase in energy required to make the fold is more than offset by the decrease in energy by consequence of crystallographic packing of the chain folds. Thus a single chain molecule can minimize its conformational energy by regular folding. (46) This phenomena helps explain why growing lamellae preferentially tend to reject short chain and stereo-irregular molecules during crystallization. (39,40,41)

Also, it is an experimentally observed fact that as lamellae grow radially outward from a spherulite center, they twist vaguely resembling

a twisted ribbon. The twist is thought to result from lamellae shifting structurally to permit better surface packing so as to relieve stress build-up in the plane of molecular chain folds. (31)

Now consider the pictorial model of two dimensional surface nucleation (secondary nucleation) on a lamellar growth front initiating molecular chain folding as illustrated in Figure 4. The molecular layer thickness (b_o) and width (a_o) can be derived from unit cell dimensions, and ℓ is the average chain fold length. The consecutive laying down of chain folds corresponds to growth across the substrate surface. The lateral fold surface free energy is σ, and the work required to fold the chain back parallel to itself is σ_e; thus σ_e is considerably greater than σ. Through a very rigorous development Lauritzen and Hoffman (31) define the free energy of activation for chain folding as:

$$\Delta\Phi = \frac{4b_o \sigma \sigma_e}{\Delta G_v} + 2kT - \frac{a_o \Delta G_v}{\sigma} kT \qquad (2.11)$$

where ΔG_v is the bulk free energy difference between the supercooled melt and crystalline structure and the driving force in nucleation and growth processes. At high supercoolings, Hoffman (30) defines:

$$\Delta G_v = \frac{\Delta h_c (T_m - T)}{T_m} \cdot \frac{T}{T_m} \qquad (2.12)$$

where Δh_c is the latent heat of crystallization for a perfect crystal structure. By substituting (2.12) into (2.11) and rearranging the following expression for $\Delta\Phi/kT$ (34) is obtained:

$$\frac{\Delta\Phi}{kT} = \frac{4b_o \sigma \sigma_e T_m^2}{k \Delta h_c T^2 (T_m - T)} + 2 - \frac{a_o \Delta h_c T(T_m - T)}{\sigma T_m^2} \qquad (2.13)$$

Free Energy of Activation for Molecular Transport

The principal concern is adequately accounting for the temperature dependence of molecular transport. The free energy of activation for molecular transport represents the barrier that a molecule in the supercooled melt must jump to be within the vicinity of the growing lamellar surface. To represent the temperature dependence of this molecular jump associated with viscosity, Hoffman (34) chose the well-known viscosity equation of Williams, Landel, and Ferry (WLF equation) (83,84):

$$\log(\eta/\eta_{T_g}) = -c_1 (T - T_g)/(c_2 + T - T_g) \tag{2.14}$$

The free energy of activation is defined by:

$$\Delta\bar{F} = \Delta\bar{H}_a = R \, d \, \ell n(\eta/\eta_{T_g})/d(1/T) \tag{2.15}$$

and performing the indicated differentiation on (2.14) and substituting into (2.15) gives:

$$\Delta\bar{F} = \Delta\bar{H}_a = 2.303 \, c_1 c_2 \, RT^2/(c_2 + T - T_g)^2 \tag{2.16}$$

With $2.303 \, c_1 c_2 \, R$ assuming its universal value of 4120 (22), Equation (2.16) takes its standard format as:

$$\Delta\bar{F} = \Delta\bar{H}_a = 4120 \, T^2/(c_2 + T - T_g)^2 \tag{2.17}$$

and introducing temperature dependence results in the desired expression:

$$\frac{\Delta F}{kT} = \frac{\Delta\bar{H}_a}{RT} = \frac{4120 \, T^2}{(c_2 + T - T_g)^2} \frac{1}{RT} \tag{2.18}$$

which is valid over the temperature range: $T_g \leq T \leq T_g + 100$. (83,84)

In summary, Equations (2.9), (2.13), and (2.18) formulate the basis for a quantitative study of polymer crystallization under non-isothermal conditions. In conjunction with (2.2) and (2.8), the equations aid in a study of the thermal and crystalline histories in a solidifying bulk polymer.

CHAPTER III

THEORY

The objective of this research will be the development of a method for adequately representing the kinetics of crystallization for solidifying crystalline polymers. The kinetics are needed to resolve the transient heat conduction problem arising in bulk polymer solidification. The net result will be to gain insight regarding the thermal and crystalline history through the bulk polymer slab.

The mathematical representation for the transient heat conduction process occurring within a bulk polymer will be developed first. The nonlinear, heat generation term is expressed as an enthalpic change due to the melt/solid transformation, which is dominated by the latent heat contribution from crystallization. A rigorous development of the Avrami relation for predicting crystallization follows with a discussion and critical evaluation of the conventional method of determining its kinetic parameters. Since the conventional analysis of bulk crystallization kinetics using the Avrami relation will be shown to be not completely satisfactory, an alternate approach will be developed.

Sections from Chapter II will be presented to maintain coherency.

Transient Heat Conduction

The mathematical representation for heat conduction with heat generation in a rectangular, isotropic solid is expressed by (12):

latent heat and density at 100% crystallinity respectively.

Crystallinity

Conventional Analysis

Commonly, bulk crystallization experiments are performed under isothermal conditions. Typically, a polymer sample is quenched rapidly from just above its melt temperature to a pre-determined temperature sufficient to induce a least a measureable amount of crystallization. The sample must attain this pre-determined temperature before any crystallization occurs so as to insure isothermal conditions.

Crystallinity is commonly measured through dilatometry or calorimetry. Dilatometry is the measurement of volumetric changes in materials subjected to particular conditions of temperature and pressure; thus crystallinity is defined as:

$$X = \frac{\bar{V}_m - \bar{V}}{\bar{V}_m - \bar{V}_c} \qquad (3.6)$$

where $\bar{V}$ is the specific volume at a specified time (t); $\bar{V}_c$, specific volume of 100% crystalline polymer; and $\bar{V}_m$, specific volume of 100% polymer melt. (34) In calorimetry, the energy evolved from the crystallization process is recorded with time (t). In this case crystallinity is defined as:

$$X = \Delta\bar{H}/\Delta\bar{H}_c \qquad (3.7)$$

where $\Delta\bar{H}$ is the accumulative energy evolved with time, and $\Delta\bar{H}_c$ is the latent heat of a 100% crystalline polymer. Plotting crystallinity (X) as a function of $\ln$ t results in sigmoidal curves. See Figure 5 and note only the general format for the present.

$$\frac{\partial T}{\partial t} = \alpha \left[\frac{\partial^2 T}{\partial x^2} + \frac{\partial^2 T}{\partial y^2} + \frac{\partial^2 T}{\partial z^2} \right] + \frac{Q}{\rho C_p} \tag{3.1}$$

In Equation (3.1), thermal conductivity is assumed to be constant. By assuming a rectangular geometry thin in the x-direction, heat transfer principally in the x-direction, and constant volume, Equation (3.1) reduces to the nonlinear, parabolic differential equation:

$$\frac{\partial T}{\partial t} = \alpha \frac{\partial^2 T}{\partial x^2} + \frac{Q}{\rho C_p} \tag{3.2}$$

with:

$$\rho = \frac{X}{X_w} \rho_c + \frac{X_w - X}{X_w} \rho_m \tag{3.3}$$

$$C_p = \frac{X}{X_w} C_{p_c}(T) + \frac{X_w - X}{X_w} C_{p_m}(T) \tag{3.4}$$

where Q is the heat generation via polymer crystallization and is time and position dependent; X, the degree of crystallinity; X_w, the maximum attainable degree of crystallinity; ρ, the density; C_p, the specific heat; and subscripts c and m denote the crystalline and melt phases respectively. Equation (3.2) is highly nonlinear and not readily amenable to an analytical solution. Thus, it must be solved through numerical techniques which are developed in Appendix A.

Heat Generation

The rate of heat generation (cal/cm^3/sec) within a cooling polymer can be expressed as follows:

$$Q = \rho_c \Delta \bar{H}_c \frac{dX}{dt} \tag{3.5}$$

where dX/dt is the change in crystallinity with time; $\Delta \bar{H}_c$ and ρ_c, the

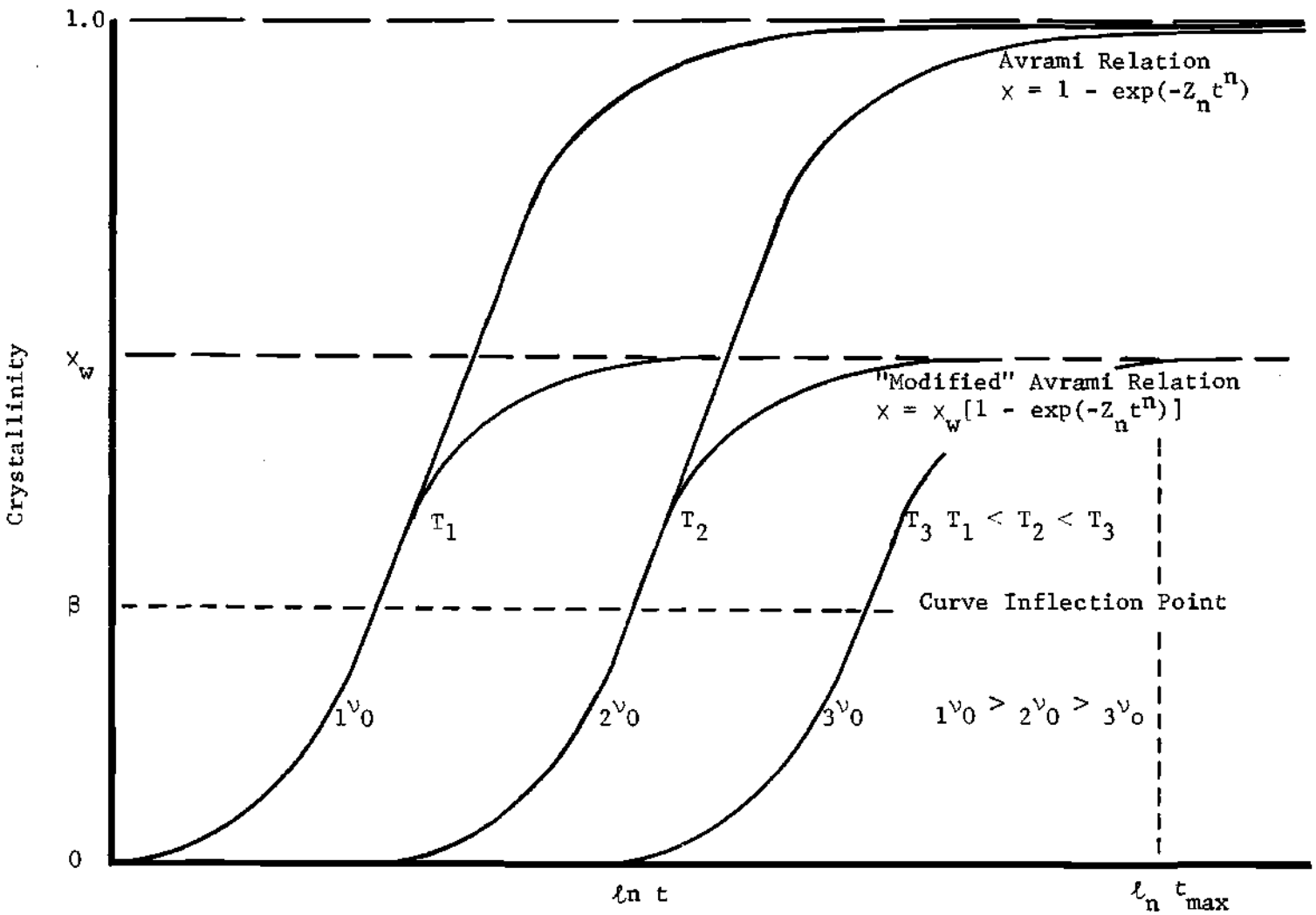

Figure 5. Typical Bulk Crystallization Isotherms

The Avrami Relation

The Avrami relation (3,4,5):

$$X = 1 - \exp(-Z_n t^n) \tag{3.8}$$

applies to randomly distributed, growing spheres which coalesce and approach 100% crystallinity so that $X \rightarrow 1$ as $t \rightarrow \infty$. However, the relation is not valid after the spheres impinge. In reality, no polymer can attain 100% crystallinity because of inherent imperfections within the polymer. Thus a polymer crystallizes to a lesser degree, X_w. The Avrami relation, Equation (3.8), is "modified" as follows:

$$X = X_w[1 - \exp(-Z_n t^n)] \tag{3.9}$$

so that $X \rightarrow X_w$ as $t \rightarrow \infty$. See Figure 5.

In analyzing bulk crystallization isotherms, heterogeneous nucleation can be assumed thereby defining a corresponding nuclei density (ν_o). (33) In Figure 5, stage 1 is predominately primary crystallization from the baseline to the curve inflection point where $dX/d(\ell n\ t)$ is at a maximum. At the inflection point, significant impingement of spherulites occurs causing a decrease in spherulite growth rate, which is reflected by a decrease in curve slope. Stage 2 is predominately secondary crystallization with massive impingement of spherulites occurring. Crystallinity approaches a maximum within a reasonable time span (t_{max}). After stage 2, additional crystallization occurs over a time span of several orders of magnitude greater than the total time span across stages 1 and 2.

The "modified" Avrami relation, Equation (3.9), has been used empirically to fit stages 1 and 2 of a bulk crystallization isotherm

through variations in n. Typically, an Avrami isotherm for which n is 3 fits the early portions of stage 1 to just beyond the infection point. Generally, after stage 1 progressively smaller values of n are necessary to fit the experimental data. (41)

Two principal problems exist with this isothermal scheme for determining the kinetic parameters of the "modified" Avrami relation. First, when a bulk solid is cooled, a temperature gradient exists through the solid and varies with time. Since the crystallization kinetic process is temperature dependent, then the kinetics of crystallization vary accordingly through the bulk polymer. When an isothermal technique is used to determine values of kinetic parameters, those values are useful only when a point within the bulk polymer is momentarily at that particular temperature. Thus, enough isotherms must be run so as to determine adequately the temperature dependence of the kinetic parameters.

Secondly, the empirical curve fit of the "modified" Avrami relation to bulk crystallization isotherms is independent of any mechanisms of polymer crystallization. Defining Z_n in Equation (3.9) equal to $4/3\ \pi\ \nu_o\ G^n$ based on the work of Evans (21), where G is the spherulite radial growth rate, it is possible to calculate the spherulite size from the Avrami relation. However, no data has been found to date comparing experimental to calculated spherulite diameters once the "modified" Avrami relation has been empirically fitted to a bulk crystallization isotherm.

The "modified" Avrami equation used in this kinetic study is Equation (3.9) and is repeated here for convenience:

$$\chi = \chi_w[1 - \exp(-Z_n t^n)] \tag{3.9}$$

By assuming heterogeneous nucleation and spherulitic growth of crystalline regions, n is necessarily set to 3. To account for the temperature dependence of crystallization kinetics, Hoffman (33) uses the definition of Z_n developed independently by Evans (21) as:

$$Z_n = \frac{4}{3} \pi \nu_o G^n \tag{3.10}$$

and then incorporates his growth rate expression for polymer crystallization by molecular chain-folding and transport mechanisms through (31,33,34):

$$G = G_o \exp(-\Delta\Phi/kT) \exp(-\Delta F/kT) \tag{3.11}$$

where:

$$G_o = b_o k T/h \tag{3.12}$$

$$\frac{\Delta\Phi}{kT} = \frac{4 b_o \sigma \sigma_e T_m^2}{k \Delta h_c T^2 (T_m - T)} + 2 - \frac{a_o \Delta h_c T (T_m - T)}{\sigma T_m^2} \tag{3.13}$$

and:

$$\frac{\Delta F}{kT} = \frac{4120T}{(c_2 + T - T_g)^2} \frac{1}{RT} \tag{3.14}$$

which is valid over the temperature range: $T_g \leq T \leq T_g + 100$; and for $T \geq T_g + 100$, T is set to $T_g + 100$ and substituted as follows:

$$\frac{\Delta F}{kT} = \frac{4120(T_g + 100)}{(c_2 + 100)^2} \frac{1}{RT} \tag{3.15}$$

Equations (3.2,3.5,3.9-15) are sufficient to define the one-dimensional, transient heat conduction equation with heat generation through polymer crystallization utilizing a kinetic expression. The

immediate problem now is to derive dX/dt in Equation (3.5) which is done in Appendix B.

Because of the problems associated with using isothermal techniques to determine the kinetic parameters, and the conventional analysis of bulk crystallization isotherms in terms of the "modified" Avrami relation, a scheme independent of the "modified" Avrami relation will be developed, but it will still be based on Hoffman's growth rate expression, Equation (3.11).

The Volumetric Growth Relation

Several assumptions applied in the analysis of bulk crystallization isotherms using the "modified" Avrami relation also formulate the basis for developing a new relation for predicting crystallinity: 1) heterogeneous nucleation, 2) spherulitic growth of crystalline phases, and 3) crystallization by Hoffman's growth rate expression.

Since a spherulite is comprised of melt/crystalline forms of the polymer, then the rate of energy evolved is directly proportional to the rate of spherulite growth and degree of crystallinity. As spherulites grow and expand volumetrically, the accumulation of energy evolved is directly proportional to the amount of crystallization having occurred (primary crystallization). Upon the impingement of spherulites, growth is restricted to the remaining regions of polymer melt, and the rate of growth by primary crystallization decreases, causing a decline in the rate of energy evolved (secondary crystallization). After crystallization of these regions, growth subsides, and crystallization decreases to a very slow rate (annealing). This crystallization behavior generates a thermogram profile as shown in Figure 6.

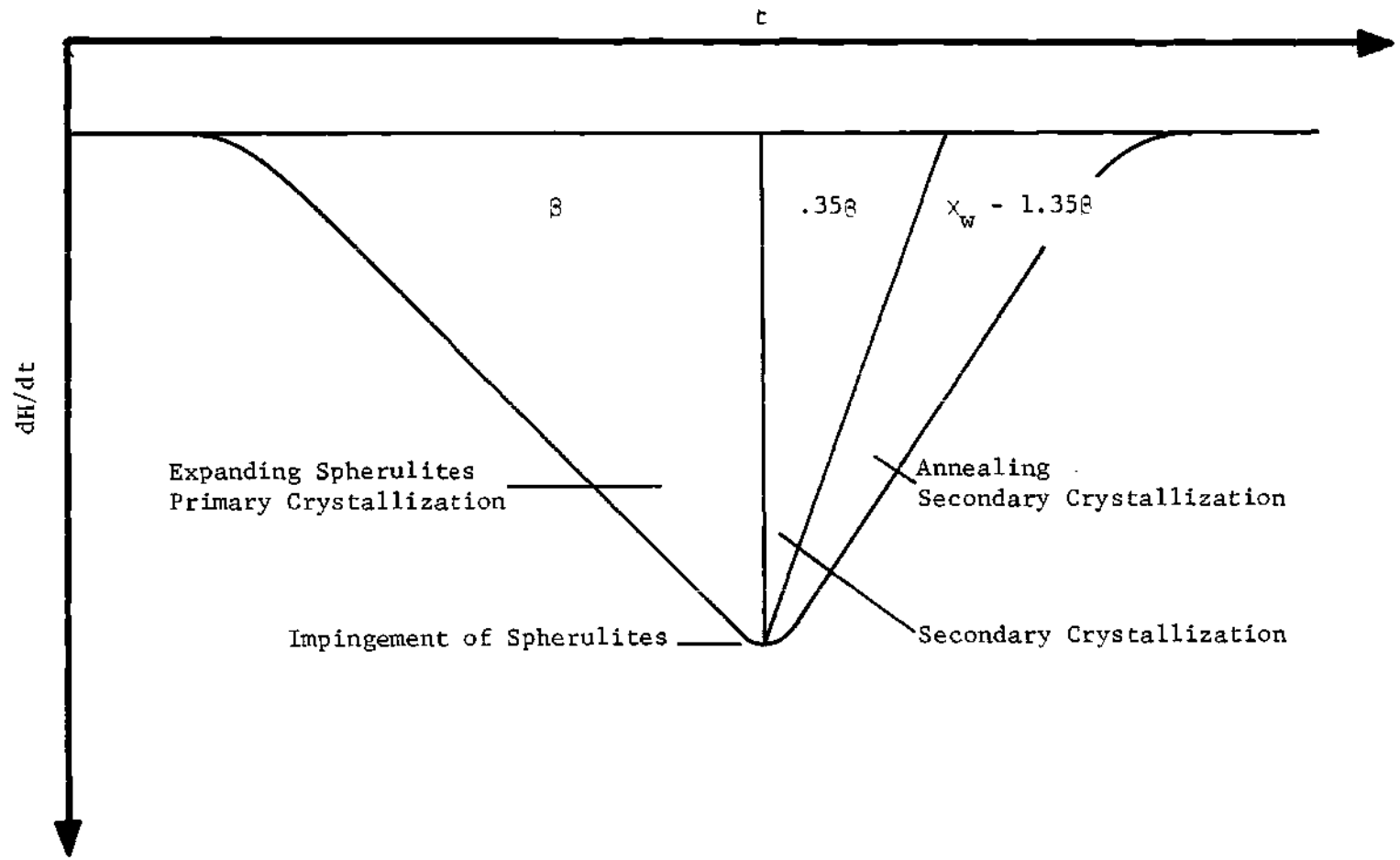

Figure 6. Typical Non-Isothermal Crystallization Thermogram

Assuming all spherulites are "born" simultaneously (heterogeneous nucleation), are uniformly distributed (ν_o), and grow at a common rate (G); then upon impingement, all spherulites are uniform in size and assume more likely than not a cell structure with the maximum packing efficiency. A face-centered cubic (FCC) structure (78) permits the maximum packing efficiency (74%) and has an inter-spherulitic volume (occupied by polymer melt) uniform in shape, size, and distribution. See Figure 7a. Upon impingement, the spherulites continue to grow into the inter-spherulitic volumes, crystallizing the residual polymer melt. Assuming that crystallization is in proportion with the volumetric growth of spherulites, then the amount of crystallization occurring in the inter-spherulite region is $(26/74)\beta$ where β is the total amount of crystallization that occurred up to the moment of impingement of spherulites. See Figure 6. During and after spherulite growth, additional crystallization $[\chi_w - (1 + 26/74)\beta]$ occurs at a much slower rate. According to Keith and Paddin (41,42), this is the crystallization of polymer melt trapped between neighboring lamellae and the thickening of lamellae. These phenomena can only occur within the spherulitic phase.

The problem now is to calculate the rate of volumetric growth into the inter-spherulitic volumes using Hoffman's growth rate expression, Equation (3.11). Consider the FCC structure in Figure 7a and extract the hemi-spherical element shown in Figure 7b in two dimensions. By rotating about the indicated axis, the triangular element AIKA generates a regular cone (a cone with its altitude perpendicular to its base). The rotation of shape ABCDA generates a cone with a spherically dished bottom which closely represents one of the six inter-spherulitic volumes

a)

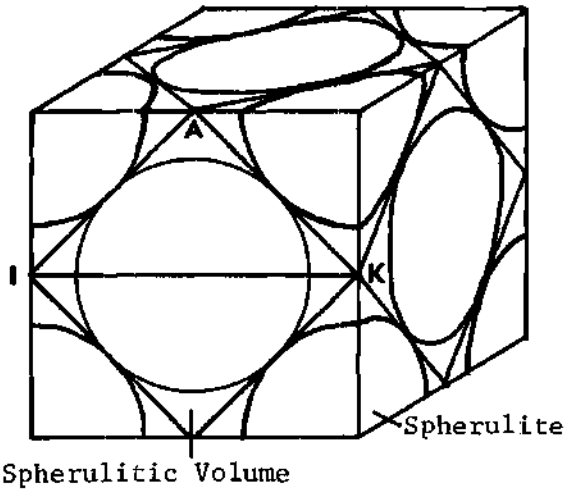

b)

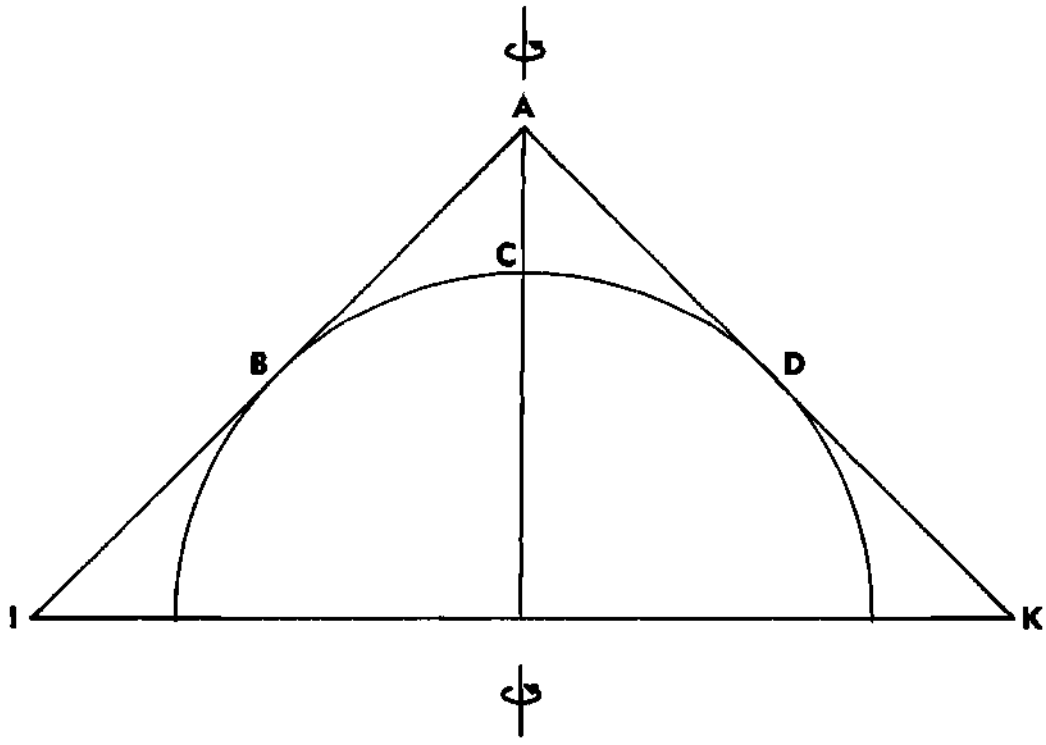

Figure 7. Face-Centered Cubic Structure

associated with each spherulite in a FCC configuration. The spherulite impingement radius is r_i, and r_m is the maximum radial growth of the spherulites required to fill the inter-spherulitic volume. For a radial growth $r(0 \leq r \leq r_m)$, there corresponds a volume $V(0 \leq V \leq V_m)$ which has a degree of crystallinity (χ) defined as:

$$\chi = \chi_w(V/V_m) \tag{3.16}$$

where V_m is the volume of a spherulite at impingement plus the volume of six inter-spherulitic volumes associated with each spherulite. The derivation of crystalline volume V as a function radial growth r is given in Appendix C. Equation (3.16) is incorporated into the heat generation expression, Equation (3.5), as follows:

$$Q \doteq \rho_c \, \Delta\bar{H}_c \, \frac{\Delta\chi}{\Delta t} \tag{3.17}$$

In summary, Equation (3.16) is sufficient to represent the concept of the volumetric growth model for analysis of non-isothermal crystallization isotherms as shown in Figure 6.

CHAPTER IV

PLAN AND PROCEDURE

A cooling polymer has a temperature profile, and if crystallization is occurring, it does so at different rates through the polymer. Therefore, it is reasonable to expect that the degree of crystallinity and morphology are not uniform through the polymer and vary with time. Crystallization is an exothermic process, and monitoring the rate of energy evolved would be measuring indirectly the rate of crystallization. Monitoring the rate of energy evolved under non-isothermal conditions would simulate the cooling phenomenon occurring within a bulk polymer. Mathematically, this can be expressed as:

$$\frac{dq}{dt} = F[T(t)] \qquad (4.1)$$

where dq/dt is rate of energy evolved or absorbed, and T(t) is the programmed rate of temperature change with time (t). Analytically, this approach is analogous to differential thermal analysis.

Differential scanning calorimetry (DSC) has gained wide acceptance in the thermal analysis of polymers because quantitative as well as qualitative information can be produced. Typically, thermodynamic properties such as latent heats of transition, heats of reactions, and heat capacities can be evaluated quantitatively. Furthermore, kinetic data such as crystalliaation rates can also be assessed quantitatively. In DSC, as the temperature is programmed, the sample and its reference

are continuously maintained at the same temperature. When the sample absorbs or evolves energy, more or less energy is required by the sample to maintain it at the same temperature as the reference. It is this differential amount of energy (dq/dt), automatically and continuously varied according to the energy requirements of the sample, which is the output in DSC. Thus, the DSC records the rate of energy absorbed or evolved as a function of temperature, Equation (4.1). Consequently, for a linear time base recorder, a peak represents the energy of transition. This characteristic makes the DSC ideal for a quantitative study of polymer crystallization kinetics under isothermal and non-isothermal conditions. The DSC can simulate cooling and crystallization patterns within the bulk polymer simply by varying the scan speed (degrees/time) at which the sample is cooled. Identification and calibration of the DSC used in this study is given in Chapter V, Instrumentation and Equipment, and Appendix D, Calibration of the Differential Scanning Calorimeter, respectively.

The technique followed in this research of analyzing DSC cooling scans in order to resolve the non-isothermal crystallization kinetics of polymers, and at the same time provide a basis for heat conduction analysis during bulk polymer solidification has not been previously reported. Gornick (24,25) has reported a relatively similar approach based on differential thermal analysis (DTA). In DTA, a temperature difference (ΔT) between a sample and reference is monitored during cooling as a function of time. By using a modified version of the Avrami relation, Equation (3.8), and incorporating a modified version of Hoffman's growth rate relation, Equation (3.11), Gornick calculates the temperature of the polymer during the cooling process induced by low scan speeds. Also,

he calculates the degree of crystallinity (χ) under isothermal conditions but does not substantiate his predictions with experimental values. His primary objective was to calculate experimental DTA thermograms and not to consider polymer morphology and crystallinity and their inter-relationship, and associated transient heat conduction as in this study.

Plan

The objective of this work is the development of a generalized method for adequately representing the crystallization phenomena in solidifying crystalline polymers. In order to develop a method based on a general theory of polymer crystallization which is independent of any particular polymer, two polymers from each of three groups are utilized in this study. Polyethylene and polypropylene represent the polyolefins; two polyethylene terephthalates, polyesters; and Nylon 6 and Nylon 66, polyamides. Thus, a particular polymer identifies itself only through its thermal and physical properties.

A cooling polymer has a temperature profile which varies with time, the thermal driving force expressed through (T_m-T) will have a corresponding profile. This driving force governs the principal phenomenological aspects of polymer crystallization - primary nucleation, secondary nucleation, and spherulitic growth rate. It necessarily follows that these phenomena will have a profile which also vary with time.

When a polymer fills a mold cavity, it is above its melt point. Polymer in contact with the much cooler mold walls quenches immediately, and through heat conduction, cools the inner regions of the polymer. Thus the polymer cools at different rates with respect to thickness -

rapidly at the wall/polymer interface and slowly at the centerline of the slab. This rate of cooling directly effects the temperature profile, and consequently the thermal driving force (T_m-T), which in turn effects the phenomenological aspects of crystallization. Thus, the more important parameter is cooling rate and how it varys through the polymer with cooling time.

By crystallizing samples of a polymer on a DSC at different scan speeds, the effects of scan speed on incipient, impingement, and final crystallization temperatures, and crystallinity (β and χ_w) can be observed. Microtoming crystallized samples and observing them under light microscopy permits observation of how scan speed effects the size and consequently the population (ν_o) of spherulites. These data are sufficient to make a quantitative study of polymer crystallization kinetics. The detailed procedure on how such data were collected follows.

Experimental Procedure

Polymer Samples

Polymer samples used in this study are clean, general-use homopolymers free of any nucleating agents and plasticizers. The samples are identified in Table 1.

Sample Preparation

For the polyolefins, high density polyethylene (HDPE) and polypropylene (PP) were available in the powder and pellet form respectively. HDPE and PP samples were melted between clean, quarter-inch thick glass plates heated in an electric oven under 30 inches Hg vacuum to prevent oxidization. Paper inserts were placed between the plates to control film thickness. After melting, the glass plates were clamped in a bench

Table 1. Identification of Polymer Samples

Group	Polymer	Trade Name	Manufacturer
Polyolefins	High Density Polyethylene	Marlex^{R} 6050	Phillips Petroleum
	Isotactic Polypropylene	Marlex^{R} HGZ-050-02	Phillips Petroleum
Polyester	Poly(ethylene terephthalate)	Mylar^{R} 700S	DuPont
	Poly(ethylene terephthalate)	Experimental Grade mw $\cong$ 34,500	Monsanto
Polyamides	Polycaprolactam, Nylon 6	Plaskon^{R} mw = 15,000-20,000	Allied Chemical
	Poly(hexamethylene adipamide) Nylon 66	Zytel$_{R}$ 101	DuPont

vise and allowed to cool under ambient conditions.

The vacuum oven could not reach a temperature sufficient to melt the polyester and polyamide samples. Fortunately, the Mylar 700S was received in film form, and samples were punched out as needed. Monsanto's poly(ethylene terephthalate) (PET) and the nylons were dissolved in appropriate solvents in an attempt to make films. Four gram samples of each nylon were dissolved in 50 ml. of 90% formic acid over moderate heat (80°C). The acid was allowed to evaporate leaving a film of nylon. Similarly, five gram samples of PET were dissolved in 50 ml m-cresol and 50 ml o-chlorophenol over heat (150°C). The solvents were allowed to evaporate leaving films of PET. Samples were punched from each film and crystallized at 40°/minute. Analysis of the DSC crystallization trace indicated that significant amounts of the solvents were still present by functioning as nucleating agents. Microscopic examination of these samples revealed extremely small spherulites with barely distinguishable boundaries. This phenomenon is indicative of massive nucleation. Thus the attempt to make solvent cast films was abandoned in favor of melting single pellets in the DSC sample assembly. The pan/holder assembly is always covered during operation and purged with dry nitrogen to prevent oxidation or combustion of the sample.

Sample Weighing

All samples for a particular polymer were weighed to within 1.0 mg of each other so as to minimize any effects weight variation may have on data consistency. The particular sample weights selected were based on a compromise between small sample weights to minimize thermal lags and large sample weights to achieve bulk spherulitic growth. A

typical sample weight was 15 mg.

Crystallization

Each polymer sample was heated to 10° above its melt temperature and held for 5 minutes in order to erase any previous history of crystallization and ensure that subsequent nucleation would be predominately heterogeneous. (75) Then, each sample was cooled to 10° below the crystallization temperature range and immediately re-melted at 20°/minute to 10° above its melt temperature.

Immediate re-melting of a freshly crystallized sample suppresses any post crystallization (annealing) which is difficult to measure because it occurs so slowly and in minute amounts. Re-melting at 20°/minutes suppresses any crystallization of the polymer melt which did not crystallize during the cooling operation. This procedure is repeated twice producing three crystallization and two melt traces for each polymer sample crystallized at a particular scan speed. The initial melting is not recorded because the sample is not in intimate contact with the sample pan. Comparison of crystallization traces gives insight to any hysteresis effects. The area under each trace was measured with a planimeter clockwise and counter clockwise around the trace boundary to within a 1% spread between the two measurements. Through the appropriate conversion factor, area was converted to $\Delta\bar{H}$ from which the degree of crystallinity (χ) was calculated, knowing $\Delta\bar{H}_c$, as follows:

$$\chi = \Delta\bar{H}/\Delta\bar{H}_c \qquad (4.1)$$

Non-Isothermal Crystallization. Crystallization thermograms were run on each polymer at six scan speeds: 1.25, 2.5, 5, 10, 20 and 40°/minute.

In addition to measuring the thermogram areas, the incipient, peak, and post crystallization temperatures were recorded.

Isothermal Crystallization. At least one isothermal crystallization thermograms was run on each polymer. The selection of isothermal crystallization temperatures was limited by the thermal response and sensitivity of the DSC/sample system. It was necessary to select crystallization temperatures for which temperature equilibrium could be attained before crystallization commenced. Also, crystallization temperatures could not be selected when the rate of heat evoluation due to crystallization was not detectable at the most sensitive scale on the DSC. Consequently only a narrow range of crystallization rates can be monitored isothermally.

Microtoming

Microtoming is the science of very thin sectioning of specimens for microscopic observation. Each crystallized polymer sample was cut in half; one half was saved for density measurement; the other half is prepared for microtoming. Each sample is placed in a regular size Beem capsule acquired from Ernest F. Fullam, Inc., Schenectady, N.Y. An epoxy cement was used to fill the capsule and allowed to dry for 24 hours at ambient conditions. Then the Beem capsule was cut away leaving an epoxy stud with the polymer sample mounted in the pyramidal end. The stud was pre-shaped using a sharp glass knife. Then, thin sectioning (4μ) was performed with a diamond knife. At least four specimens were cut from each polymer sample. Since the glass transition point of the polyolefins is below ambient temperature, these polymer samples were frozen in liquid nitrogen before being microtomed. The polyesters and polyamides have glass transitions well above ambient temperature and therefore could be

sectioned without freezing.

The microtomed specimens were mounted on standard micro-slides, and sealed with Fisher Permount[R] and a micro-slide cover glass. Clothes-pins were used to clamp the slide and cover glass together during drying of the Permount[R] to prevent rippling of the specimens.

Light Microscopy

Each slide was examined under a microscopy (with crossed polarizers), and several pictures per slide were taken using a very fine grain 35mm film. Prints (8x10) were made from the 35mm film using very fine grain paper. The objective was to acquire large pictures of the spherulites in sharp detail, particularly around their boundaries, in order to measure their size and population.

Stereology

Stereology is the study of the structure of matter in three dimensions at the microscopic level, based on the examination of two-dimensional sections through the material. (76) Because of morphological differences between the six polymers, different techniques were employed to measure spherulite size and population. These techniques are explained in Appendix E.

Density Measurement

Density gradient columns have been widely used as a rapid means of determining the density of solids. The density gradient technique is the mixing of two completely miscible fluids of different density in varying concentrations. Its basis is a column of liquid mixture with a linear density gradient. The technique depends upon the hydrostatic equilibrium between a solid specimen and a liquid mixture of identical

density. Glass floats of known density are used as calibration standards. (81)

Specimens must be free of voids, foreign matter, and very rough surfaces. Also, specimens should be thoroughly wetted in some solution saved from the column before depositing into the column. (81)

It is necessary that the two column fluids be as inert as possible with respect to the specimens and that their density range extend beyond that of the specimens. For the polymers studied, a toluene and carbon tetrachloride liquid system is the only ASTM standard which satisfies both criteria. (2) The columns were constructed according to standard procedure so as to yield a linear density gradient. (2,73,81)

Computational Procedure

All computer programs are written using the same variable nomenclature as in the derivation of the models in Chapter III and Appendices A, B, and C. The program language is FORTRAN V. The thermal and physical properties for each polymer are tabulated in Appendix F with appropriate explanations as to their origin.

Crystallization Models

Two crystallization models are programmed; the only difference is how the degree of crystallinity is calculated - from the "modified" Avrami relation or the volumetric growth relation.

Both programs employ Hoffman's growth rate relation. The immediate problem is to determine for each polymer crystallization thermogram what value of the c_2 parameter in the WLF relation is necessary to yield an accumulated spherulitic diameter at the peak crystallization temperature equal to the impingement spherulite diameter measured through quantitative

stereology. Using this c_2 value, the degree of crystallinity is calculated using both models.

With the "modified" Avrami relation, it is desired to know if the calculated degree of crystallinity (β) at the peak crystallization temperature corresponds to the experimental value under isothermal and non-isothermal conditions. Also, does the predicted maximum degree of crystallinity (χ_w) correspond to the experimental value for a particular value of n where n may vary from 3 down to 1? For isothermal simulations, the degree of crystallinity is calculated by two methods; one is the incremental integration of the differentiated form of the "modified" Avrami relation, and the other is a direct calculation from the "modified" Avrami relation:

$$\chi = \chi_w[1 - \exp(-4/3\ \pi\ \nu_o\ G^n t^n)] \qquad (4\text{-}1)$$

If the isothermal simulation matches the experimental results, this will be conclusive evidence that the differentiated form of the "modified" Avrami relation is correct. Likewise, if the non-isothermal simulations do not match the experimental results, this will be conclusive evidence that one can not differentiate the relation and apply it on an incremental basis with temperature dependent, fundamental parameters.

With the volumetric growth model, simulations will correspond with experimental results; because it is inherent in the derivation of the model.

Transient Heat Conduction Model

The heat transfer model will be executed for all the polymers using both crystallization models. These simulations will be performed

for conditions which are typical for injection molding. Also, the impact of assuming rate dependent parameters versus rate independent parameters on the transient temperature and crystallinity profiles will be illustrated.

CHAPTER V

EQUIPMENT AND INSTRUMENTATION

Sample Weighing

All polymer samples were weighed on a CAHN RG Automatic Electrobalance^{R} manufactured by the CAHN Instrument Company, Paramount, California.

The balance was operated in conjunction with a Hewlett-Packard, Moseley Autograf X-Y Recorder, Model 7001AR.

The overall system accuracy is $\pm$0.01 mg for typical sample weights of 15 mg.

Calorimetry

All crystallization and melt operations of polymer samples were run on a Differential Scanning Calorimeter, Model DSC-1B, manufactured by the Perkin-Elmer Corporation, Norwalk, Connecticut. The instruction manual does not explain the temperature calibration procedure for heating or cooling modes of operation, how to correct for the thermal lag of the sample holder, or how to check for compatibility between the DSC and the recorder. These problems are considered in detail in Appendix D.

The calorimeter was operated in conjunction with a Hewlett-Packard, Moseley Autograf X-Y Recorder, Model 7001AR.

Microtoming

All thin sectioning was performed on a SORVALL^{R} MT2-B "Porter

Blum" Ultra-Microtome manufactured by the Ivan Sorvall, Inc., Norwalk, Connecticut. All thin sectioning was done according to standard techniques. (71) A procedure developed by Hester (29) for freezing polymer specimens was used in sectioning the polyolefins.

Light Microscopy

All microtomed specimens were observed under a Bausch & Lomb Dynoptic Polarizing Microscope with polarizers crossed.

Photomicrographs were taken of selected specimens using a CanonQL FT 35mm camera. A Canon Lens Mount Converter, Type A was used to adapt the camera to the microscope eye piece. A Canon Booster light meter was used to determine the exposure times for such unusually low light intensities.

The objective in taking photomicrographs of polymer specimens is to acquire ultimately prints of high resolution of spherulites and their boundaries. This is necessary for accurate measurement of their size and population through quantitative stereology. The desired results were obtained by using Kodak SO-410, photomicrographic, monochromic, 35mm, black and white, ASA 160 film (68) and Kodabromide, F4, printing paper for 8x10 enlargements.

Densitometry

The density gradient columns are Borosilicate glass columns manufactured by the SGA Scientific, Inc., Bloomfield, New Jersey. The glass density floats used for calibration were made to ASTM D1505 criteria and are accurate to $\pm$0.0002 gm/cc.

Computations

All computer programs were executed on a UNIVAC 1108 computer system.

CHAPTER VI

RESULTS AND DISCUSSION OF RESULTS

The objective of this research is the development of a method for adequately representing the kinetics of crystallization for solidifying crystalline polymers. The kinetics of crystallization is embedded in the heat generation part of the transient heat conduction process occurring during bulk polymer solidification. The method begins with the representation of heat generation through an enthalpic energy expression for phase change where the latent heat portion is dominant. Its contribution is governed by changes in crystallinity developed through a kinetic expression. This expression is based on two previously developed relations, the "modified" Avrami relation and the volumetric growth relation, both of which incorporate a spherulite growth rate expression. This expression is comprised of three functions: 1) an inherent instantaneous growth rate, 2) a probability of molecular crystallization, and 3) a probability of molecular transport. Embedded within the probability of molecular crystallization is the thermal driving force for crystallization (T_m-T) or supercooling. How the supercooling varies through the polymer during cooling is of primary importance as discussed in Chapter IV. The probability of molecular transport represents the mobility of polymer chain molecules which is necessary for spherulitic growth. This probability is represented through the classical WLF equation. The c_2 parameter within the WLF equation has been determined by the size of the spherulites at their

impingement. This c_2 parameter is the only variable adjusted to fit the experimental data.

By crystallizing samples of a polymer at different scan speeds on the DSC, the effect of cooling rate on crystallization temperatures and crystallinity, can be determined. Microtoming crystallized samples and observing them by light microscopy permits observation of how scan speeds effects spherulite size.

Experimental results are presented independent of any particular polymer so as to promote the concept of a single, generallized method for adequately representing the crystallization phenomena in solidifying crystalline polymers. However, qualifying explanations regarding phenomenological aspects for a particular polymer will be made where appropriate.

Calorimetry Experimental Data

Non-isothermal crystallization thermograms were run at six scan speeds: 1.25, 2.5, 5, 10, 20, and 40°/minute. Also, at least one isothermal crystallization thermogram was run on each polymer. Each polymer sample was melted and crystallized three times to study any hysteresis effects.

Hysteresis effects imposed by repeatedly melting and crystallizing a sample proved to be minimal, and usually the effects were within experimental error of temperature and thermogram area measurements. The most significant effect was the general trend of continuously lowering the final crystallization temperature (T_F) by 1-5° per cycle. This would normally have the tendency of increasing the area under a thermogram and correspondingly increasing the total degree of crystallinity (X_w). But

within experimental error for calculating X_w, such a corresponding trend was not reflected in the crystallinity data. Because hysteresis effects were minimal, only the thermal data for the last crystallization and melt thermograms for each polymer are tabulated as a function of cooling scan speed in Appendix F.

Analysis of such data for each polymer shows that increasing the cooling scan speed has the general effect of lowering the crystallization temperatures (T_i, T_{peak}, and T_F), particularly the final temperature, T_F. This trend is to be expected. Since crystal growth is time and temperature dependent and as the cooling scan speed increases, less time is spent at any particular temperature, and thus less cumulative growth can occur even though the growth rates at lower temperatures are usually greater. This feature explains the gradual decrease in the incipient crystallization temperature (T_i). The decrease in T_i with increasing scan speed is more significant in poly(ethylene terephthalate) (PET) due to its comparatively slow crystallization kinetics.

Greater reductions in the peak and final temperatures (T_{peak} and T_F respectively) occur because additional phenomena also influence these temperatures. With polyethylene, it is readily evident from the crystallization thermograms, by the presence of their long tails, that possible significant amounts of annealing are occurring during non-isothermal crystallizations. The tail becomes longer with increasing scan speed. This phenomenon significantly lowers T_F and increases the area under the thermogram. This increase in area is reflected by the increase in crystallinity with scan speed. This phenomenon is not common to the other polymers studied.

Explanation of the temperature behavior for the other polymers requires analysis of their growth rate behavior. For polypropylene, there is a gradual deceleration in spherulitic growth rate around the peak temperature (T_{peak}) for 10°/minute and greater with larger cooling scan speeds. The same is true for poly(ethylene terephthalate), but it is compounded furthermore by very slow kinetics. Also, at 40°/minute, the crystallization temperatures in the neighborhood of T_F are within the range of the WLF equation ($T_g \leq T \leq T_g + 100$) which accounts for the increase in resistance for molecular transport. This suppresses the growth and crystallization rates even more and causes additional lowering of T_F.

The behavior of the crystallization temperature recorded for both nylons can be explained in the same manner as for PET.

Theoretically, crystallinity should decrease with increasing cooling scan speed because there is less time for crystalline perfection to occur. Because of the combined effects of secondary crystallization and annealing occurring after the cooling thermogram peak point, which indicates spherulite impingement, the baseline is sometimes difficult to establish as accurately as desired. This difficulty affects the accuracy of the final crystallization temperature (T_F) and the area under the thermogram. The latter correspondingly effects the crystallinity determination. This difficulty in distinguishing the culmination of crystallization helps to explain the general lack of a distinct trend in crystallinity as determined from the crystallization data. This is particularly the situation with high density polyethylene. Crystallinity as determined from melt data is more consistent and follows the theoretical

trend with only a few exceptions at the low cooling scan speeds.

Densitometry Data

At this point it is not possible to say which set of crystallinity data (crystallization or melt) is more accurate. However, a comparison of crystallinity data calculated from density measurements should provide some insight. Densitometry data for each polymer are tabulated in Appendix G. A comparison of calculated crystallinity from thermal and density measurements as a function of sample cooling scan speed are shown in Figures 8, 9, and 10 for the polyolefins, polyesters, and polyamides respectively.

Such comparison shows that crystallinity calculated from melt thermograms and densitometry data correlate well over the whole range of scan speed. Also, crystallinity tends towards a specific or ultimate value with increasing scan speed. This indicates that at a very high cooling rates, characteristic of bulk polymer samples solidifying in an injection molding process, these polymers will attain an ultimate degree of crystallinity which will probably be uniform with sample thickness.

An alternative determination of crystallinity can be obtained through X-ray analysis, but considerable data are required. Also, larger sample sizes are required than could be crystallized under controlled conditions on the calorimeter. Since the only purpose in measuring crystallinity by an a alternate method was to determine which set of thermal crystallinity data is more representative, which densitometry analysis adequately resolves, analysis by X-ray diffraction was not considered essential and therefore was not performed.

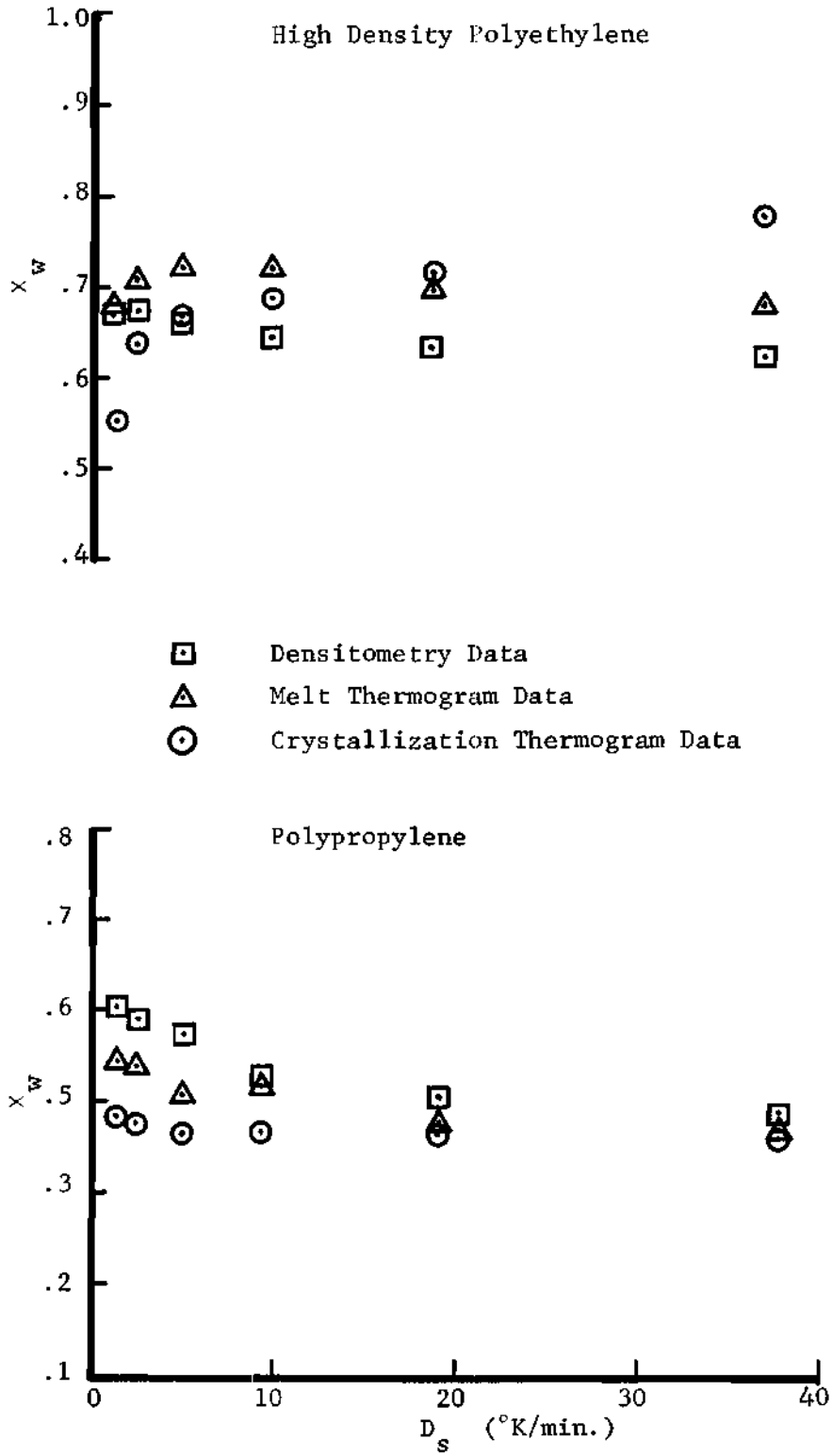

Figure 8. Crystallinity (X_w) as a Function of Sample Scan Speed (D_s): Polyolefins

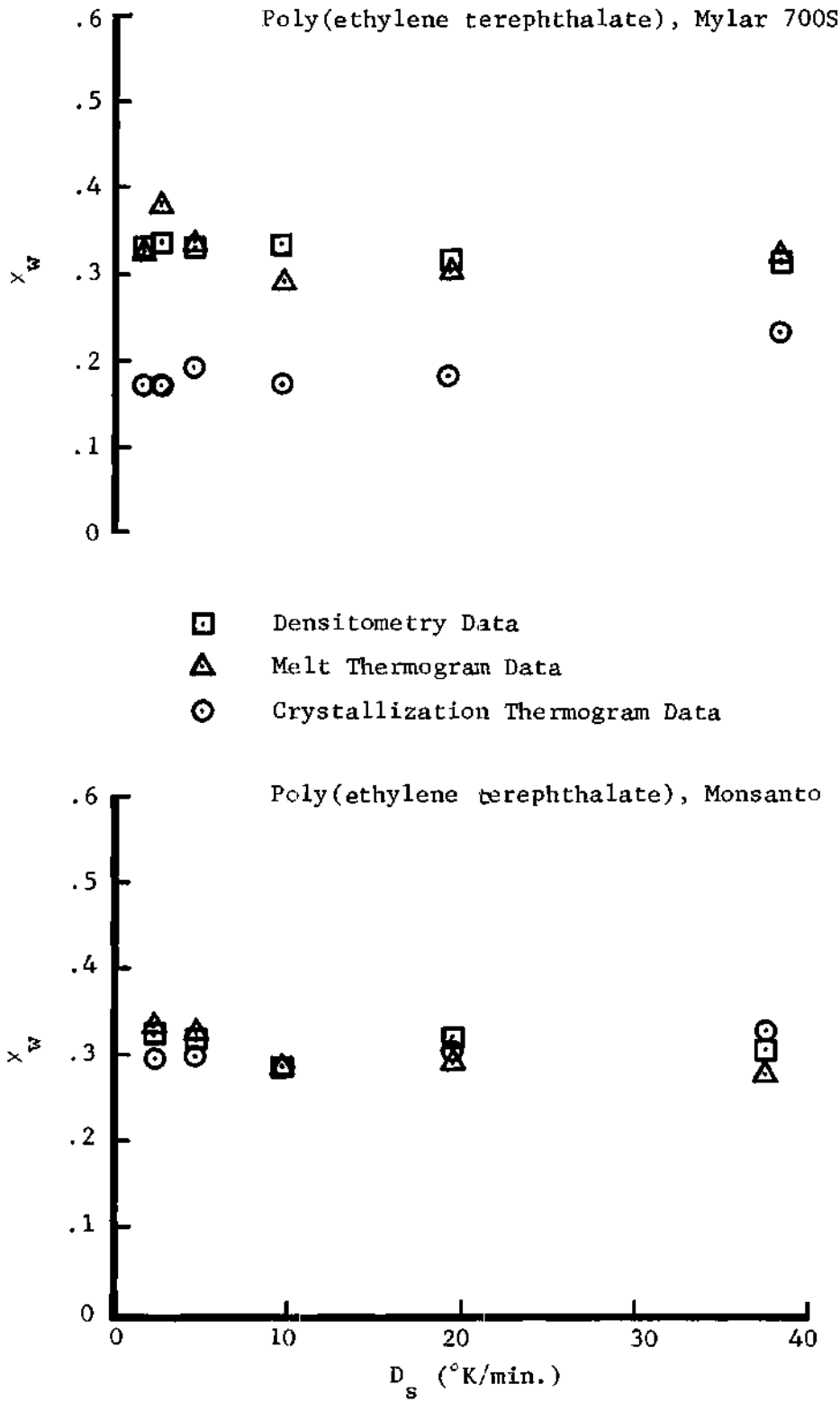

Figure 9. Crystallinity (X_w) as a Function of Sample Scan Speed (D_s): Polyesters

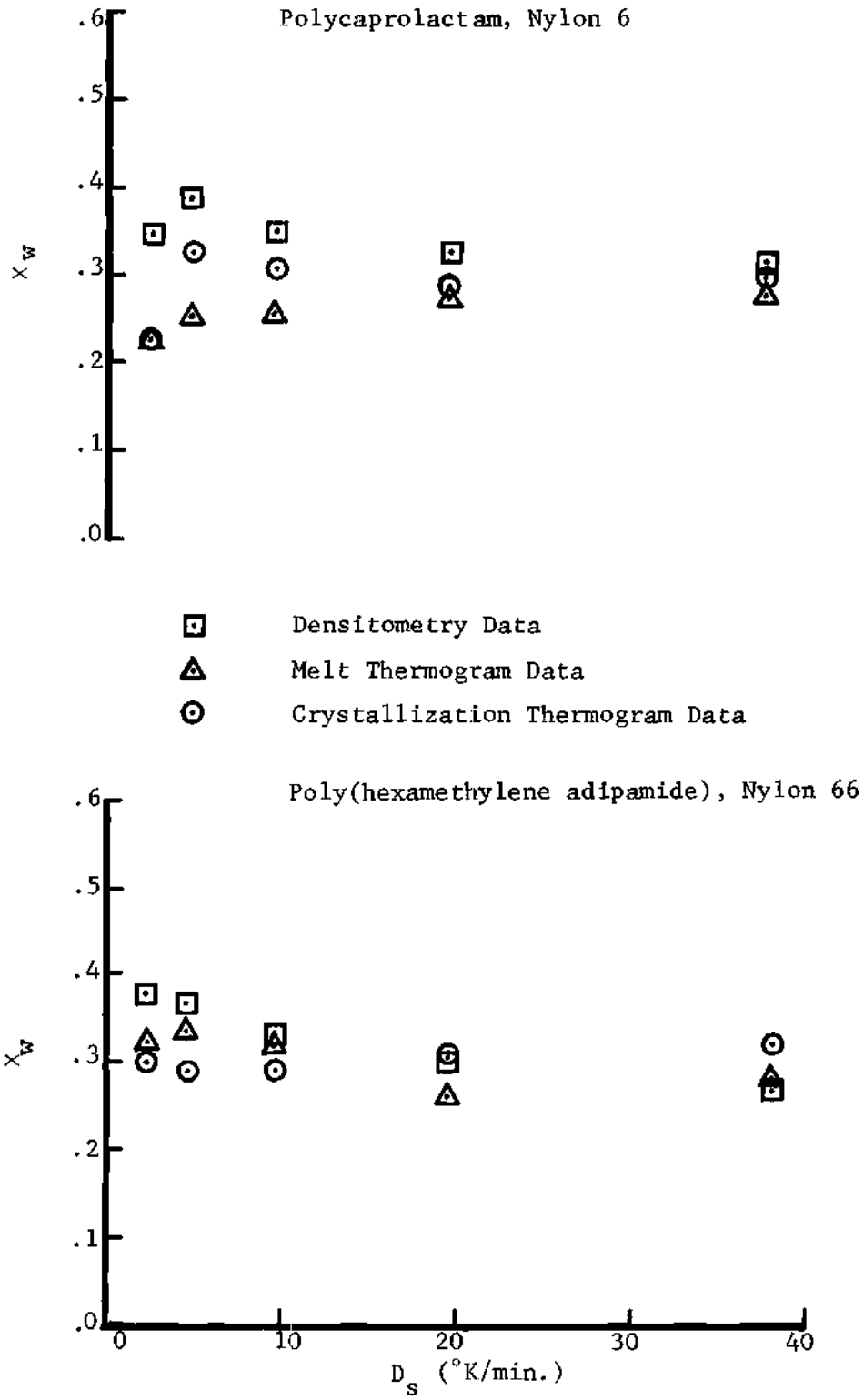

Figure 10. Crystallinity (X_w) as a Function of Sample Scan Speed (D_s): Polyamides

Thus, in the computer simulations to follow, crystallinity (x_w) calculated from melt thermogram data will be used. These data are plotted as a function of sample cooling scan speed for each polymer in Figures 11 through 16.

Stereology Data

The diameter (D_i) of spherulites at impingement was measured according to the procedure outlined in Appendix E. The results are tabulated in Appendix H and are shown graphically as a function of sample cooling scan speed in Figure 11 through 16.

With the exception of Mylar 700S, spherulite impingement diameters (D_i) decreases with increasing scan speed. Based on the nucleation theory by Turnbull and Fisher (74), the supercooling (T_m-T) determines the number of germ nuclei which attain growth nuclei status. At low degrees of supercooling (concommitant with low scan speeds), the thermal driving force is low and consequently fewer number of growth nuclei exist than at higher degrees of supercooling (concommitant with high scan speeds) where the thermal driving force is greater. The greater the number of growth nuclei the smaller is the volume that each growth nuclei must fill through spherical growth to create a space-filling, contiguous system of spherulites. Consequently, the size of the spherulites decreases with their increasing number which increases with cooling scan speed. Thus spherulite impingement diameters (D_i) should and generally do decrease with increasing scan speed.

Mylar 700S was received in the film form which implies a high degree of deformation occurred in producing the film. This deformation may not have been completely relieved during the repeated melt/crystallization

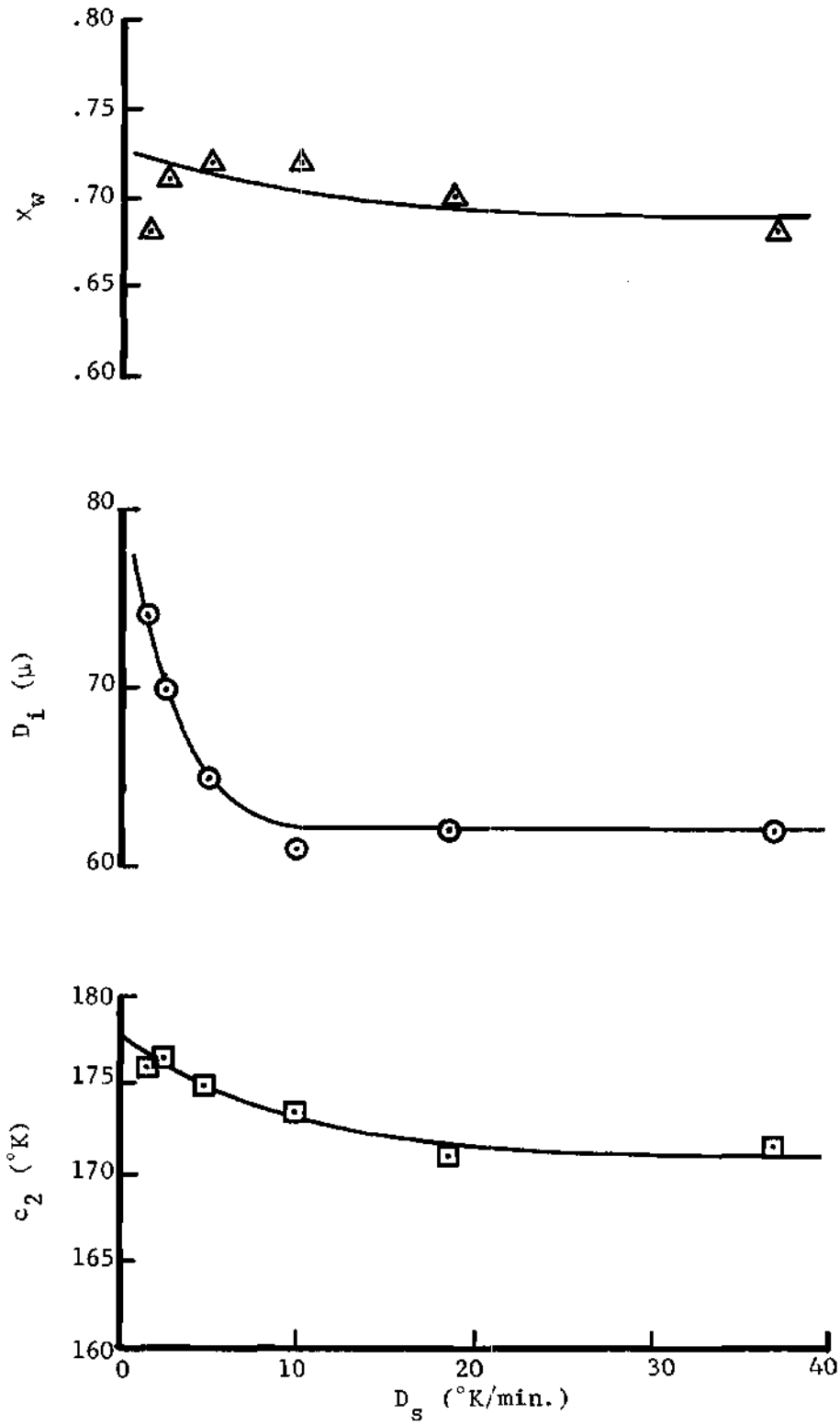

Figure 11. Crystallinity (X_w), Spherulite Diameter (D_i), and WLF Parameter (c_2) as a Function of Sample Scan Speed (D_s): Polyethylene

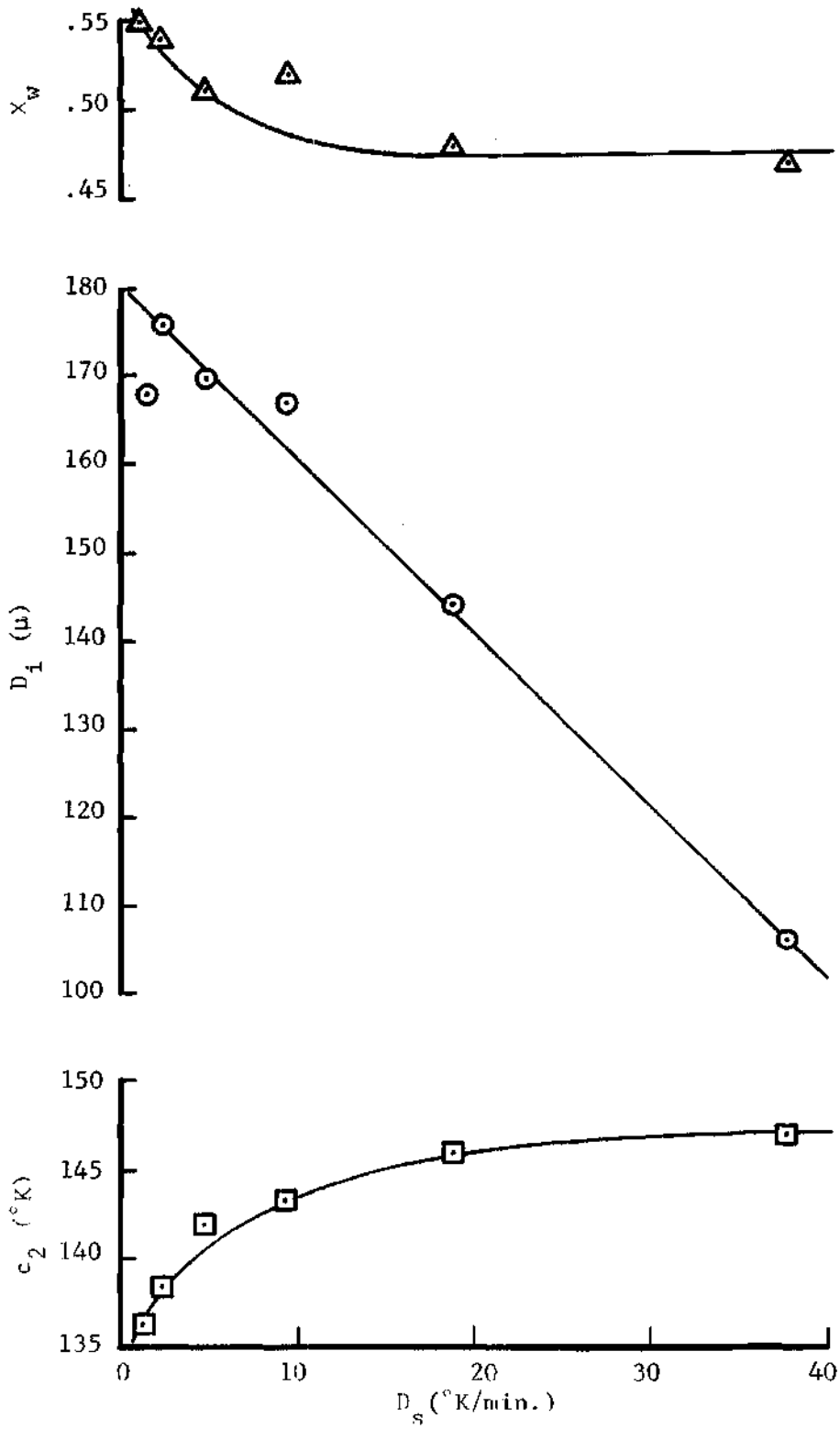

Figure 12. Crystallinity (X_w), Spherulite Diameter (D_i), and WLF Parameter (c_2) as a Function of Sample Scan Speed (D_s): Polypropylene

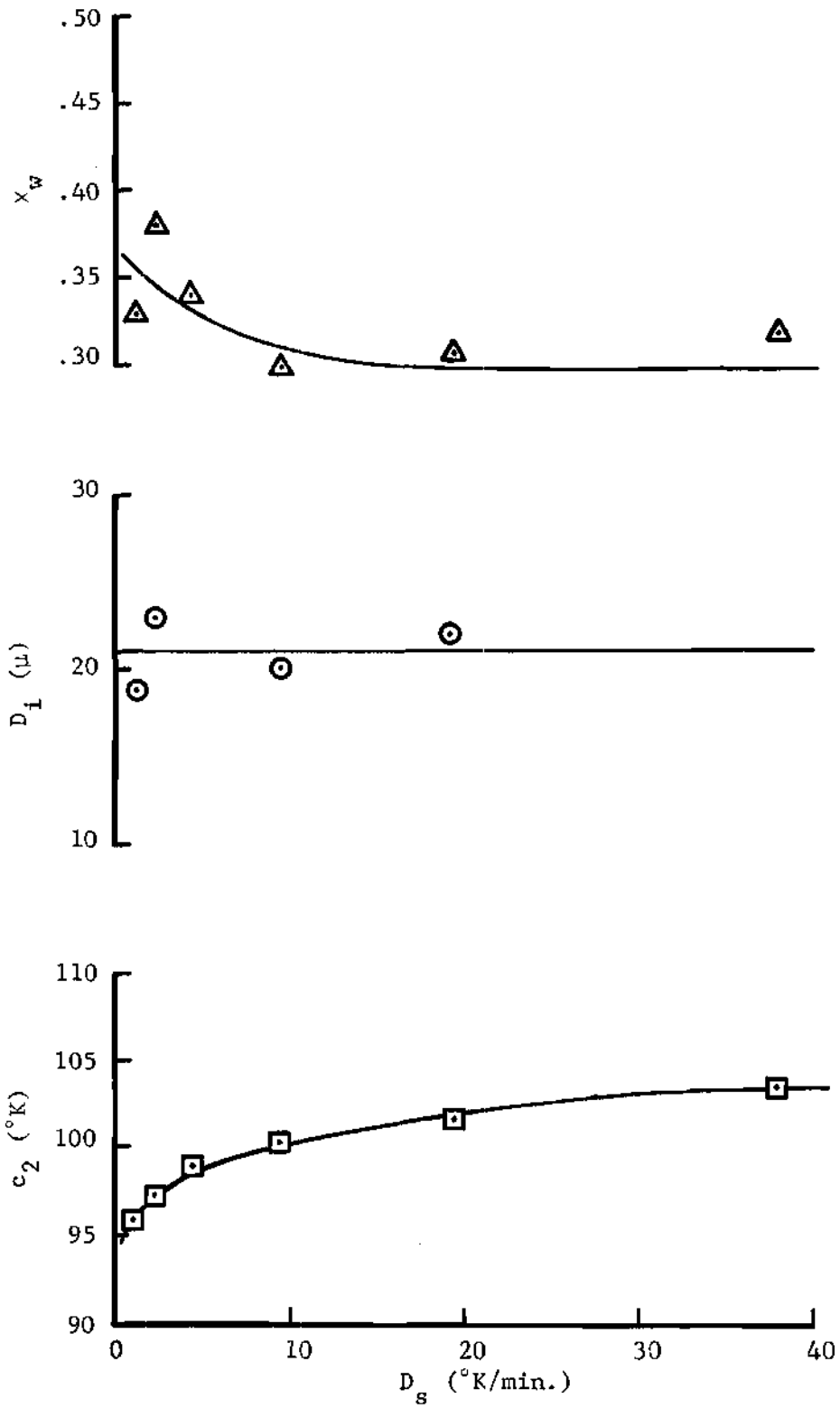

Figure 13. Crystallinity (x_w), Spherulite Diameter (D_i), and WLF Parameter (c_2) as a Function of Sample Scan Speed (D_s): Poly(ethylene terephthalate), Mylar 700S

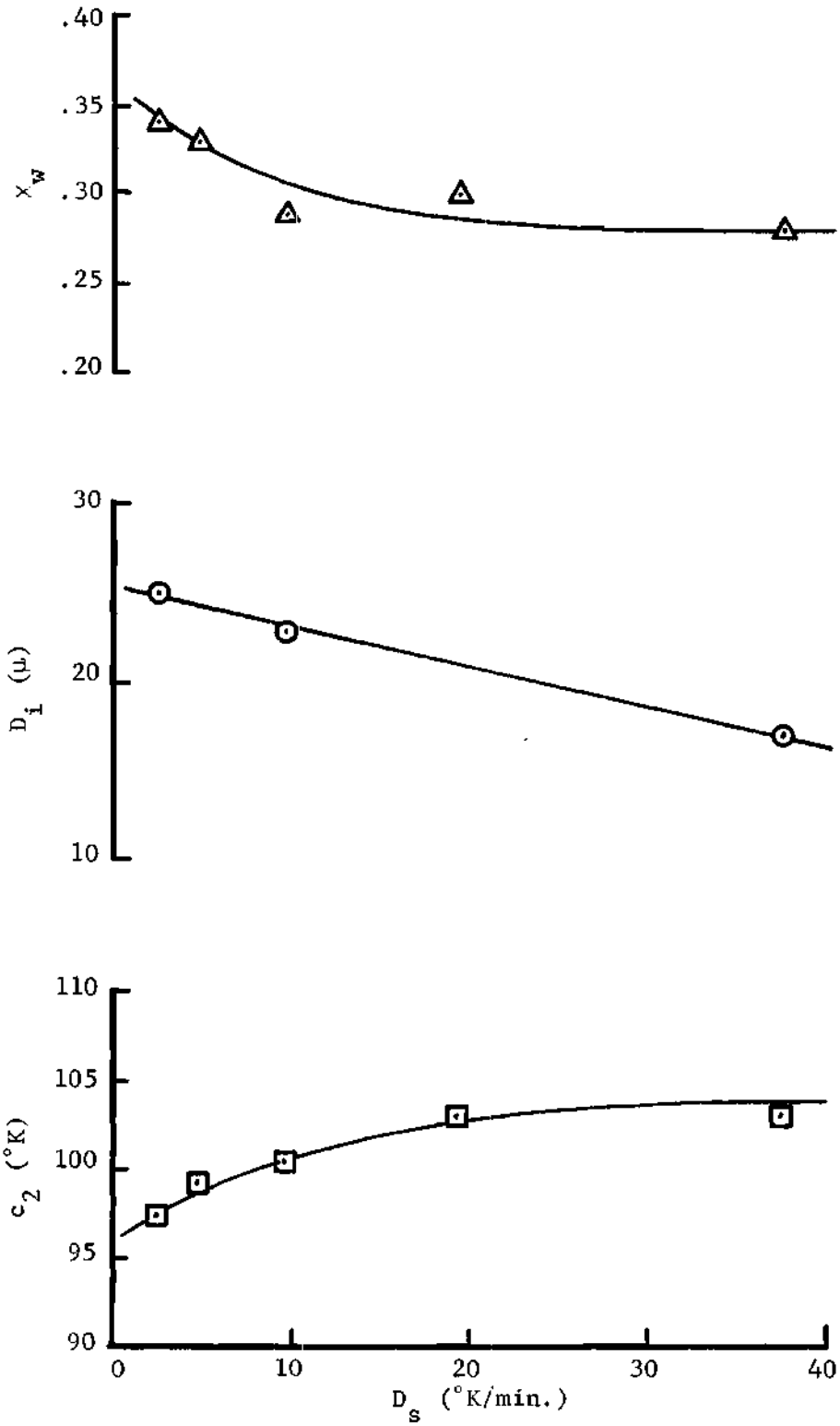

Figure 14. Crystallinity (x_w), Spherulite Diameter (D_i), and WLF Parameter (c_2) as a Function of Sample Scan Speed (D_s): Poly(ethylene terephthalate), Monsanto

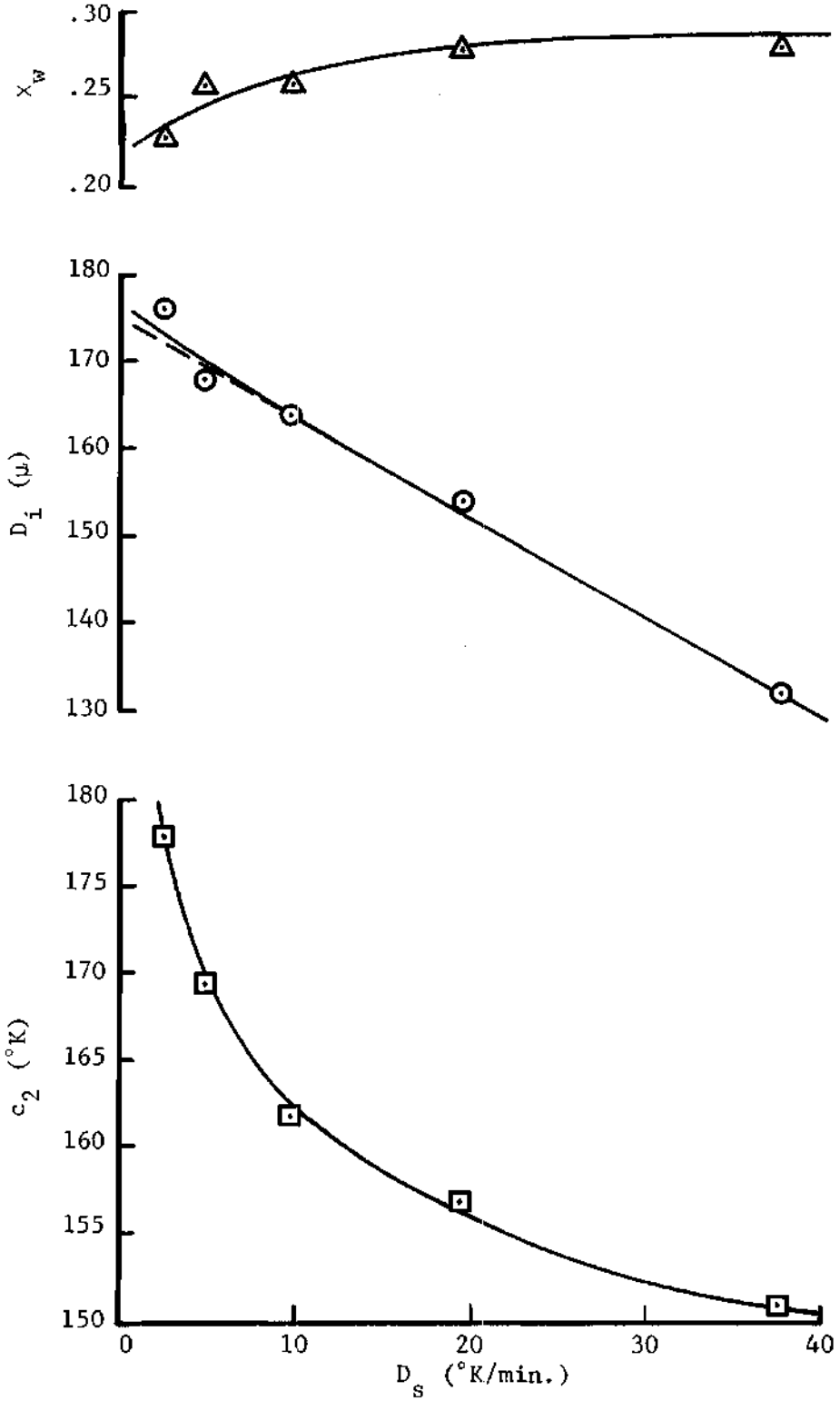

Figure 15. Crystallinity (X_w), Spherulite Diameter (D_i), and WLF Parameter (c_2) as a Function of Sample Scan Speed (D_s): Polycaprolactam, Nylon 6

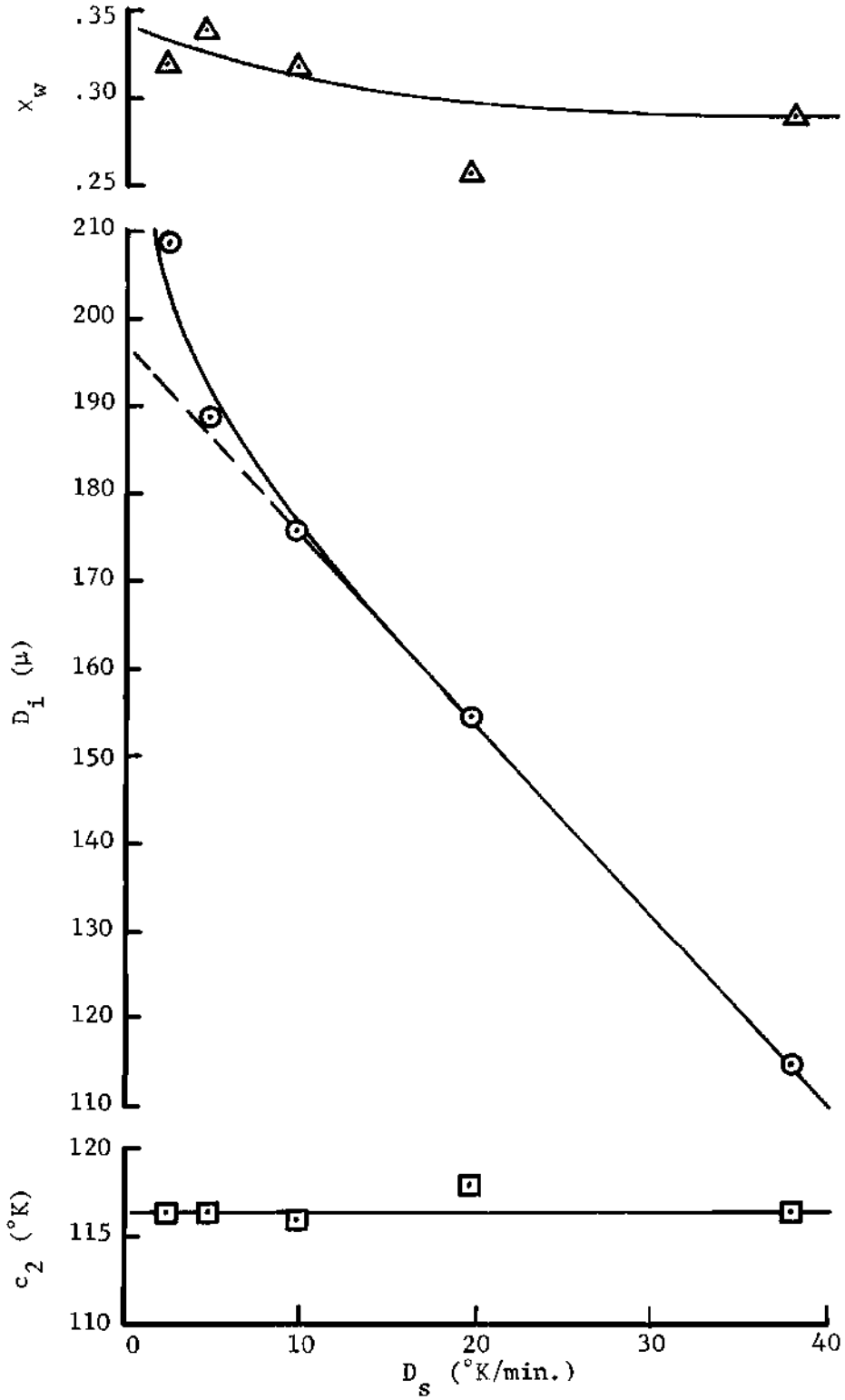

Figure 16. Crystallinity (x_w), Spherulite Diameter (D_i), and WLF Parameter (c_2) as a Function of Sample Scan Speed (D_s): Poly(hexamethylene adipamide), Nylon 66

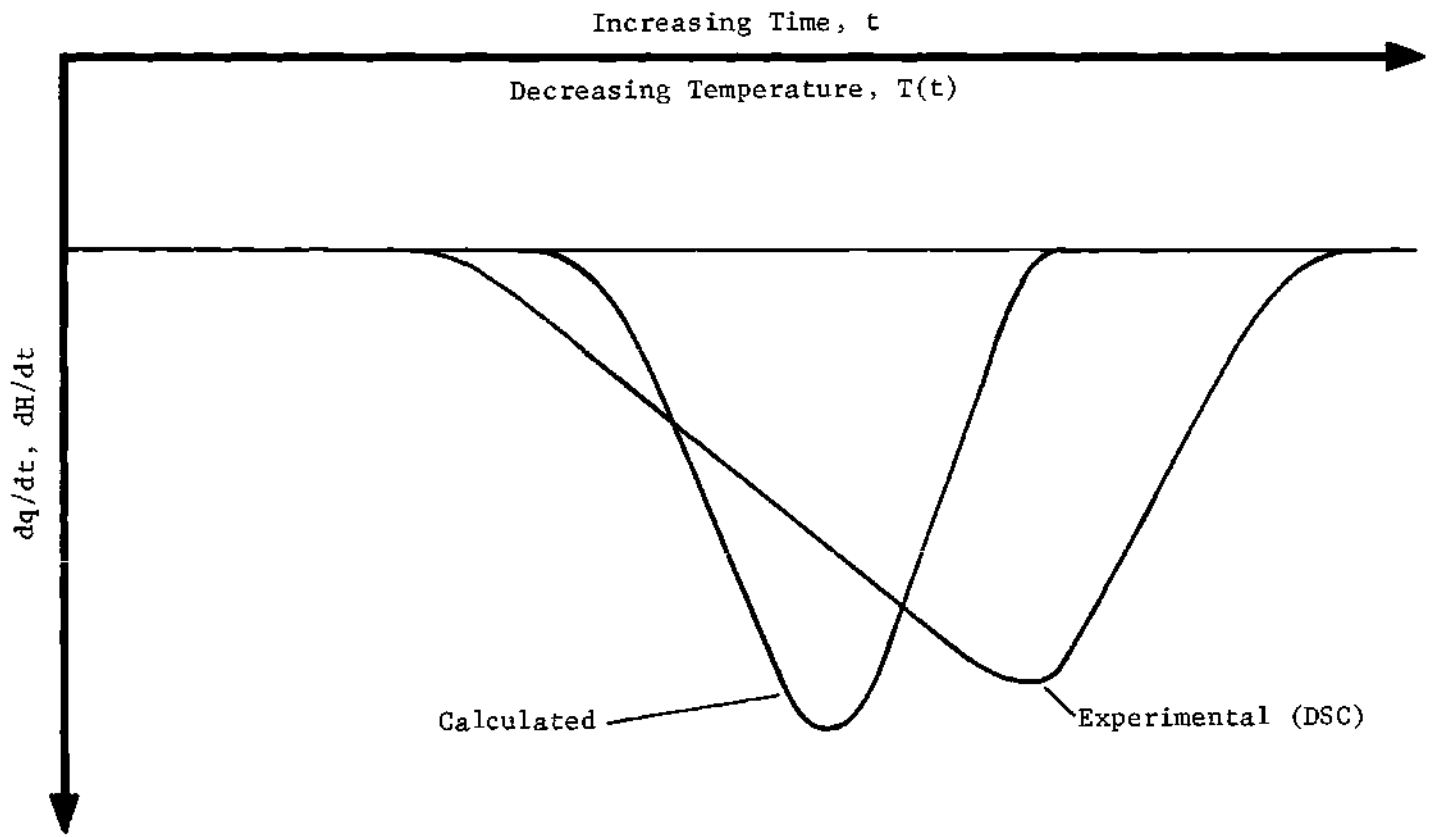

Figure 17. Comparison of Typical Calculated and Experimental Crystallization Thermograms

cycles in the process of collecting crystallization data. Along with the possible presence of unknown additives, such as nucleating agents, these two factors could possibly control the size of spherulites under any solidification conditions. Only limited data on spherulite diameters for both samples of poly(ethylene terephthalate) could be collected because of the general lack of distinct spherulites and their boundaries. However, the data does agree quite well with that collected by Watkins. (79) Also, the size of spherulite diameters for high density polyethylene measured in this study agree quite well with similar data collected by Hester. (29)

Crystallization Models

A computer program was written simulating the isothermal and non-isothermal crystallization of polymer samples. The degree of crystallinity was calculated from the two relations derived in Chapter III: the "modified" Avrami relation and the volumetric growth relation. A listing of each program is contained in Appendix K.

The thermal and physical property data for each polymer necessary to execute the programs are tabulated in Appendix I. The experimental crystallization thermogram data (D_s, T_i, T_{peak}, and T_F) and melt thermogram data (χ_w) for each polymer necessary to execute the programs are tabulated in Appendix F.

The only parameter still to be determined is c_2 within the WLF equation. This equation representing molecular transport is temperature dependent and strongly influences the ultimate size of the spherulites. As discussed earlier, the growth rate expression is a product of three functions. The first two are based on the theory of kinetics and thermo-

dynamics of polymer crystallization respectively. All parameters embedded within these two functions are either physical constants or have already been determined and are tabulated in Appendix I. Thus c_2 must be determined by matching the cumulative growth with impingement spherulite diameter.

For a given polymer crystallized at a particular scan speed (0 to 40°/minute), the value of c_2 was adjusted until the accumulated growth predicted by Equation (3.11) is equivalent to the spherulite impingement diameter, $\Sigma[G(T,c_2)]\Delta t \doteq D_i$, between thermodynamic melt and crystallization peak temperatures, T_m and T_{peak} respectively.

The "Modified" Avrami Relation

Isothermal Crystallization Simulations. Isothermal simulations were run first in order to check the incremental integration of the differentiated form of the "modified" Avrami relation derived in Appendix A against its analytical form, Equation (3.9). It should be apparent that these two forms are mathematically equivalent. The Avrami exponent (n) was set equal to three over the whole crystallization range, and the time increment (Δt) was initially set to one second.

Once the appropriate value for c_2 was determined, values of crystallinity calculated by both forms of the "modified" Avrami relation agreed exactly to four significant figures. This was the case for all isothermal simulations run on all polymers studied. This indicates that the differentiated form of the "modified" Avrami relation is correct, and the one second time interval is sufficiently small to permit accurate incremental integration.

The calculated degree of crystallinity to the peak point (β) agreed

quite well with its corresponding experimental value. Consult the zero scan speed entries in Tables 2, 3, and 4 for polyolefins, polyesters, and polyamides respectively. The experimental values of β are taken from Appendix F. Again note, this agreement holds for all isothermal simulations for all polymers studied.

The calculated maximum degree of crystallinity (X_w) would not, and consequently did not, match its corresponding experimental value; because the Avrami exponent (n) was set to three. As discussed in Chapter III, the Avrami relation, Equation (3.9), has no significant meaning for values of n other than three when heterogeneously nucleated, spherulitic growth is occurring as was the case for all polymers examined.

The values determined for c_2 are also tabulated under zero scan speed in Tables 2, 3, and 4.

Non-Isothermal Crystallization Simulations. Now, knowing that the differentiated form of the "modified" Avrami relation is correct, the non-isothermal crystallization simulations were run.

The value of c_2 was determined by exactly the same procedure as for the isothermal simulations. Values for c_2 are tabulated as a function of sample cooling scan speed for each polymer group in Tables 2, 3, and 4. These values are typical of those reported by Ferry for similar polymers. (22) As c_2 increases, the activation energy for molecular flow decreases. (51) This phenomenon causes an increase in growth rate which was observed in the computations of the growth rate expression. Also tabulated are the values of crystallinity calculated to the peak point (β). Comparison with experimental values of β shows a marked difference, except for polypropylene which is believed to be more coincedental than

Table 2. Crystallinity (β) and WLF Parameter (c_2) Values: Polyolefins

High Density Polyethylene				Polypropylene			
		β				β	
D_s (°K/min)	c_2 (°K)	Expt.	Calc.	D_s (°K/min)	c_2 (°K)	Expt.	Calc.
1.25	176.	.29	.66	1.21	136.5	.32	.32
2.41	176.5	.33	.70	2.44	138.5	.35	.35
4.89	175.	.33	.76	4.90	142.	.35	.36
9.74	173.5	.33	.70	9.30	143.5	.34	.33
18.7	171.	.34	.67	18.8	146.	.34	.32
36.9	171.5	.39	.65	37.6	147.	.30	.22
0. (395)	167.5	.24	.28	0. (395)	144.	.28	.24

Table 3. Crystallinity (β) and WLF Parameter (c_2) Values: Polyesters*

Mylar 700S				Monsanto Grade			
		β				β	
D_s (°K/min)	c_2 (°K)	Expt.	Calc.	D_s (°K/min)	c_2 (°K)	Expt.	Calc.
1.23	96.	.09	.01				
2.45	97.5	.10	.01	2.46	97.5	.15	.01
4.64	99.	.11	.01	4.80	99.25	.13	.01
9.68	100.5	.11	.01	9.70	100.5	.12	-.02
19.1	101.75	.10	.01	19.2	103.	.14	-.01
38.1	103.5	.12	-.05	37.5	103.	.13	-.07
0. (492)	101.5	.13	.16	0. (492)	103.5	.11	.13
0. (482)	102.75	.13	.12	0. (482)	103.75	.10	.10

*Poly(ethylene terephthalate)

Table 4. Crystallinity (β) and WLF Parameter (c_2) Values: Polyamides

Nylon 6*				Nylon 66**			
		β				β	
D_s (°K/min)	c_2 (°K)	Expt.	Calc.	D_s (°K/min)	c_2 (°K)	Expt.	Calc.
2.41	178.	.13	.22	2.50	116.5	.19	.19
4.82	169.5	.22	.22	5.00	116.5	.19	.16
9.54	162.	.19	.22	9.80	116.	.18	.10
19.4	157.	.19	.22	19.5	118.	.20	.08
37.4	151.	.19	.19	38.1	116.5	.16	.04
0. (462)	191.5	.11	.10	0. (512)	120.75	.11	.14

*Polycaprolactam

**Poly(hexamethylene adipamide)

anything else. It should be immediately apparent that the non-isothermal simulations do not match the experimental results; this is conclusive evidence that one can not differentiate somewhat empirical relation and apply it on an incremental basis with temperature dependent, fundamental parameters.

Analysis of computer print-outs revealed that the calculated rate of energy evolved, Equation (3.5), during non-isothermal crystallization consistently peaked earlier in time (or at higher temperatures) when compared to a DSC crystallization thermogram. See Figure 17. Also, the calculated thermograms were narrower than their corresponding experimental thermograms.

As discussed in Chapter III, the Avrami exponent (n) should normally assume decreasing values (3→1) after the peak point to represent the secondary crystallization and annealing phenomena. But, since the primary crystallization phenomenon does not even match for the appropriate exponent value of 3, adjusting n would be meaningless.

In conclusion, the "modified" Avrami relation is not an adequate relation for calculating the changes in crystallinity with time under non-isothermal conditions.

The Volumetric Growth Relation

The isothermal and non-isothermal crystallization simulations were re-run using the volumetric growth relation derived in Chapter III. The same c_2 values tabulated in Tables 2, 3, and 4 were used; because the growth rate expression, Equation (3.11), is common to both and embedded within each relation predicting crystallinity. The same experimental and thermal/physical data from Appendices F and I respectively was used

again.

For all simulations of isothermal and non-isothermal crystallizations, the volumetric growth relation predicted the total degree of crystallinity (χ_w) at the maximum spherulite growth ($D_m = \sqrt{2}\ D_i$) which is inherent in the derivation of the relation. The validity of the relation is substantiated by the fact that the crystallization temperature at which χ_w and D_m occur is within the experimental error of the final crystallization temperature (T_F) reported in Appendix F. This was the case of polypropylene, the polyesters, and polyamides. As discussed earlier, the occurrence of considerable annealing in polyethylene caused the final crystallization temperature to be well below the temperature computed to correspond with maximum spherulite growth.

The validity of the relation is further substantiated by the fact that the heat generation rate, Equation (3.17), did not become significant until the polymer supercooled to a temperature within experimental error of the incipient crystallization temperature (T_i) tabulated in Appendix F. Also, the heat generation rate peaked in magnitude at a temperature within experimental error of the peak crystallization temperature (T_{peak}) tabulated in Appendix F. These phenomena were the case for all polymers studied.

Based on these results, the volumetric growth relation was used to predict changes in crystallinity with time within the heat generation term, Equation (3.17), of the transient heat conduction expression, Equation (3.2).

Transient Heat Conduction Model

The objective of this work has been the development of a method for adequately representing the crystallization phenomena occurring within solidifying polymers. The purpose is to be able to predict the thermal and crystalline histories occurring within a polymer during solidification. This was accomplished by programming the transient heat conduction relation. Equation (3.2) and its solution algorithm are given in Appendix A.

The WLF parameter c_2 tabulated in Tables 2, 3, and 4 were plotted as a function of sample scan speed in Figures 11 through 16. Now, Figures 11 through 16 show total crystallinity (χ_w), impingement diameter (D_i), and the WLF parameter (c_2) as a function of sample scan speed. Typical polymer cooling rates during solidification in an injection molding process are substantially greater than 40°/minute. (50) The inscribed curves aid in showing trends towards ultimate values for χ_w, D_i, and c_2 at higher scan speeds. Values for χ_w and c_2 were selected for each polymer and are tabulated in Appendix J along with other pertinent data necessary for execution of the heat conduction program. Linear functions of impingement diameter (D_i) with scan speed were determined and programmed for each polymer. These are given in Appendix K, Computer Programs.

Cooling and crystallinity curves were generated for each polymer for typical injection molding conditions. A typical coolant temperature (T_c) and heat transfer coefficient (h_i) are 100°F (310°K) and 100 Btu/hr/ft^2/°F (0.01357 cal/sec/cm^2/°K) respectively. (38,50) A typical mold wall thickness (Δx_{mw}) and thermal conductivity (k_{mw}) are one inch (2.54 cm) and 27 Btu·ft/hr/ft^2/°F (0.1117 cal·cm/sec/cm^2/°K) respectively.

(38,50,57) Typically, molded parts are ejected from the die once they have cooled sufficiently to prevent deformation. (50) The best source of information for the ejection temperature is the crystallization thermogram data tabulated for each polymer in Appendix F. The final crystallization temperature (T_F) is the temperature at which significant heat evolution due to crystallization ceases. Thus, the temperature (T_F) is the best criterion for determining when to eject a molded part. So as to prevent any deformation through the molded part, the ejection time is programmed to occur when the mid-plane temperature of the molded part is at or below T_F recorded at 40°/minute. Cooling curves were calculated using data tabulated for each polymer in Appendices I and J.

The cooling curve predictions for each polymer are shown in Figures 18 through 23 for 1/4 inch thick polymer slabs. Defining the figure legend, zero (0) indicates the zero-plane for the mold wall/polymer interface; 1/4, the 1/4 plane of the polymer slab; 1/2, the 1/2 plane, or mid-plane, of the polymer slab; T_m, the polymer thermodynamic melt temperature; and T_c, the coolant temperature. The general shape of these curves has been noted before (65), but they were generated based on curved-fitted, isothermal crystallinity data. The deficiencies with this approach and application were discussed in Chapter II.

Corresponding crystallinity curves for each polymer are shown in Figures 24 through 29. The 0, 1/4, and 1/2 legends are the same as before with the addition that X_w denotes the maximum attainable degree of crystallinity. For any particular polymer where there is a temperature plateau or spike in the cooling curve, there is a corresponding significant increase in crystallinity (X) at the same cooling time for the 1/4 and 1/2 planes.

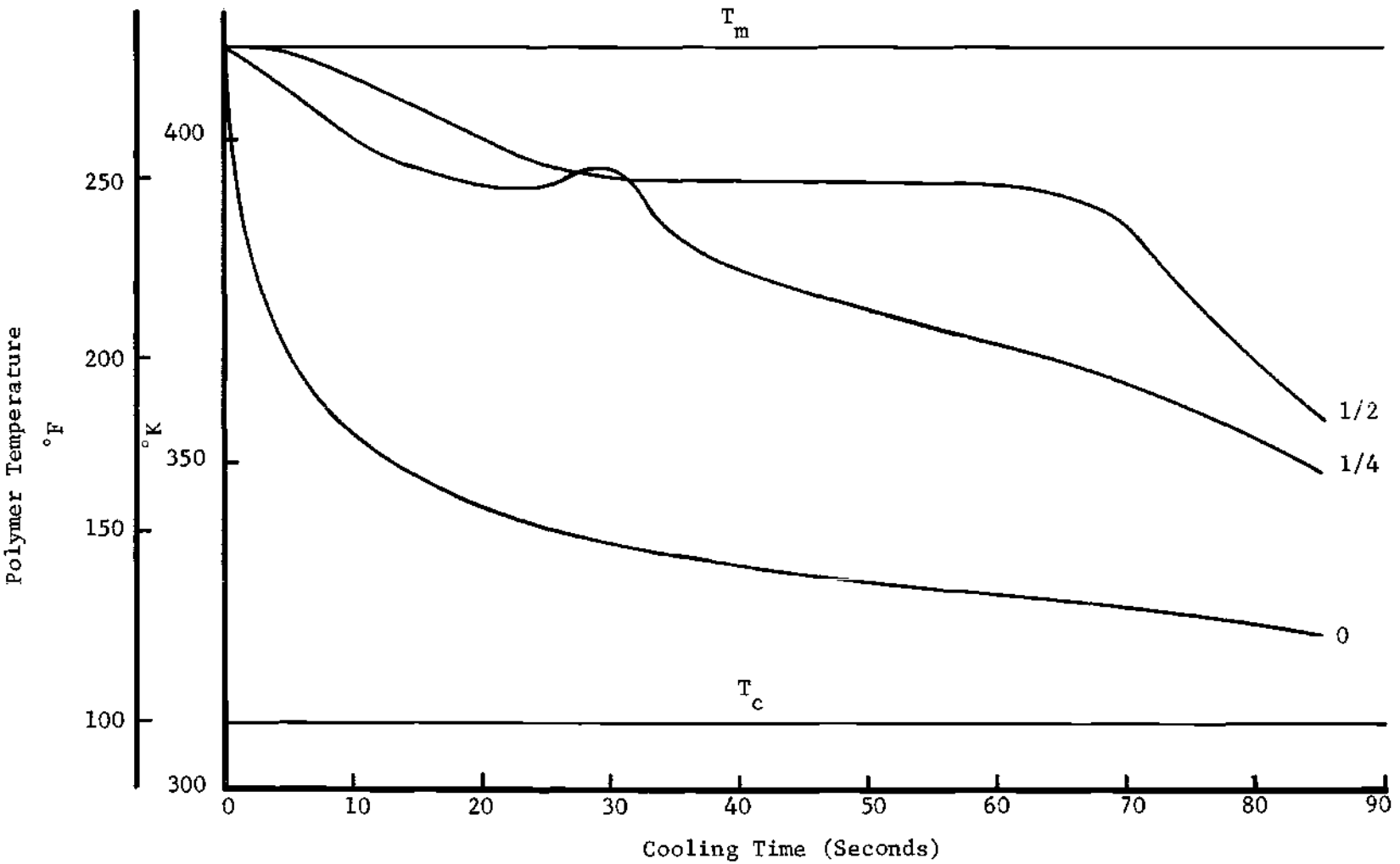

Figure 18. Cooling Curves for High Density Polyethylene

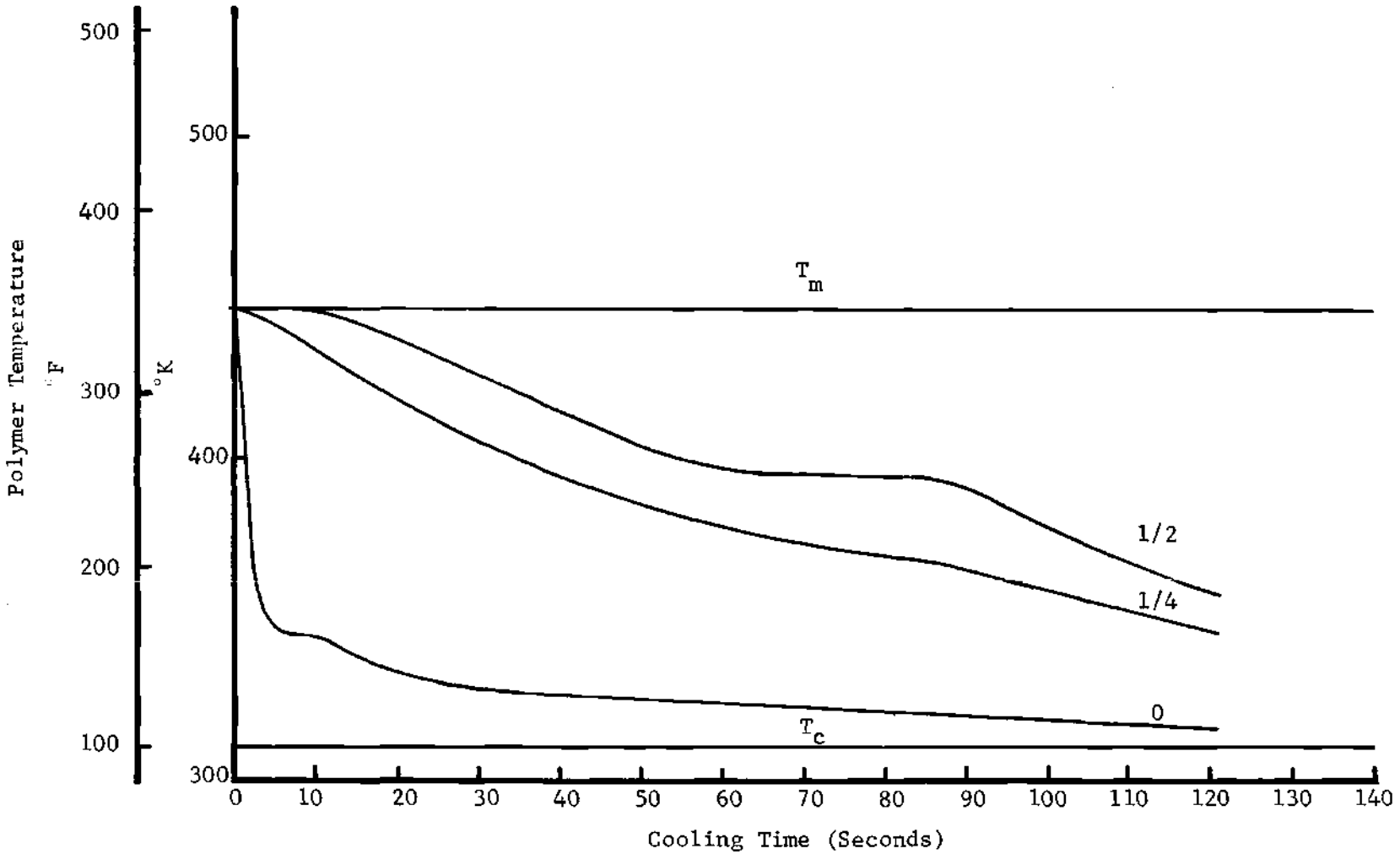

Figure 19. Cooling Curve for Polypropylene

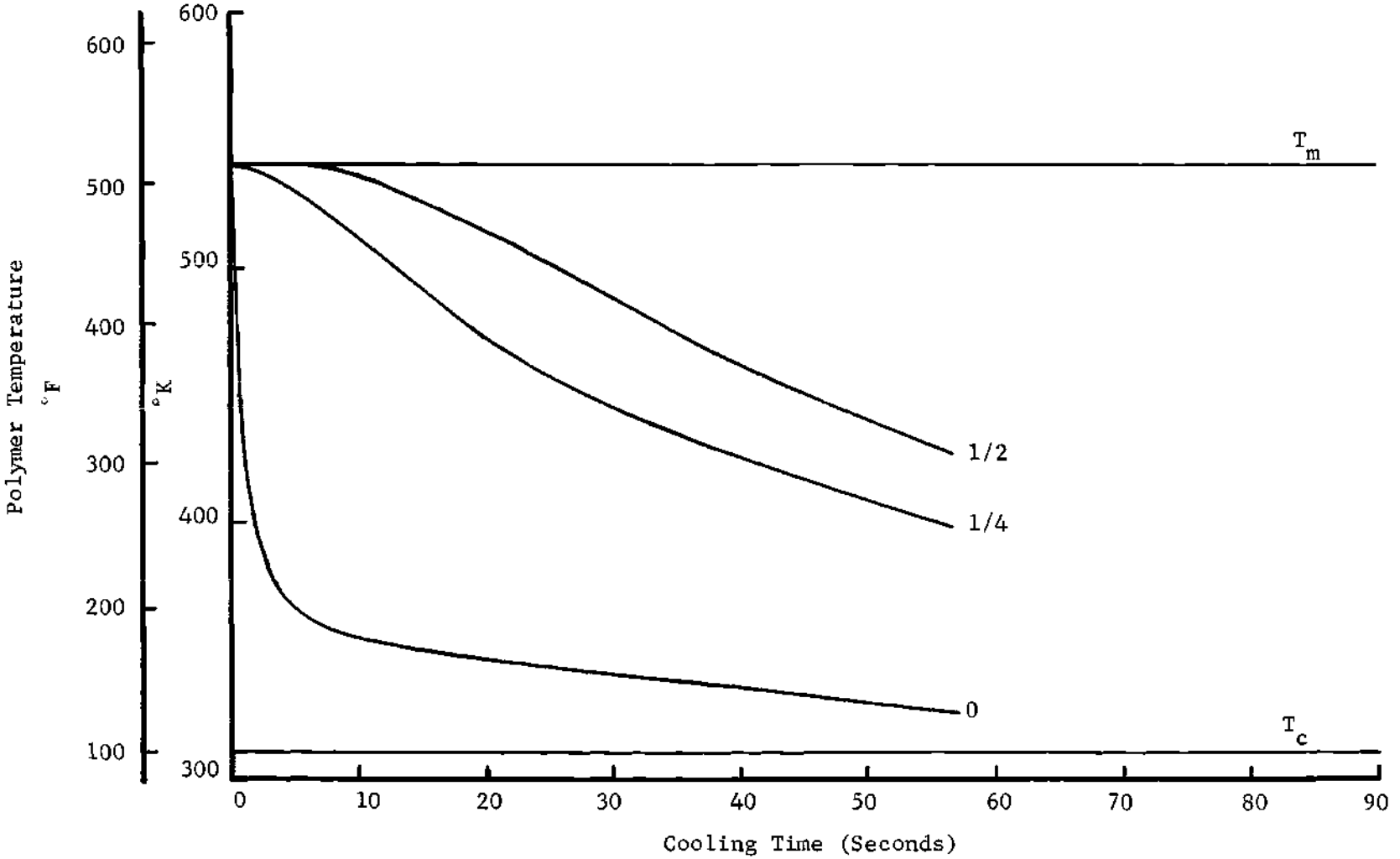

Figure 20. Cooling Curves for Poly(ethlyene terephthalate), Mylar 700S

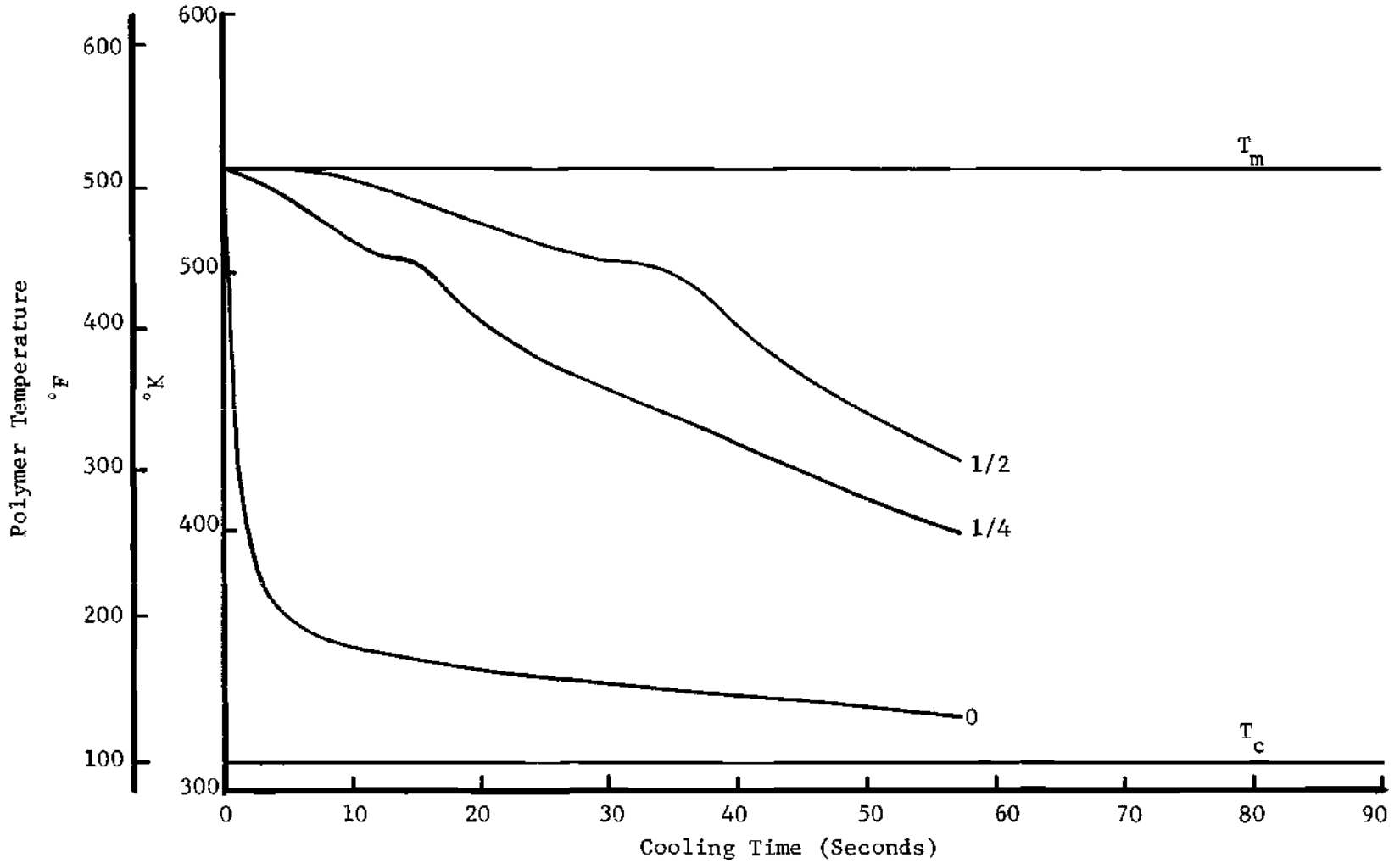

Figure 21. Cooling Curves for Poly(ethylene terephthalate), Monsanto

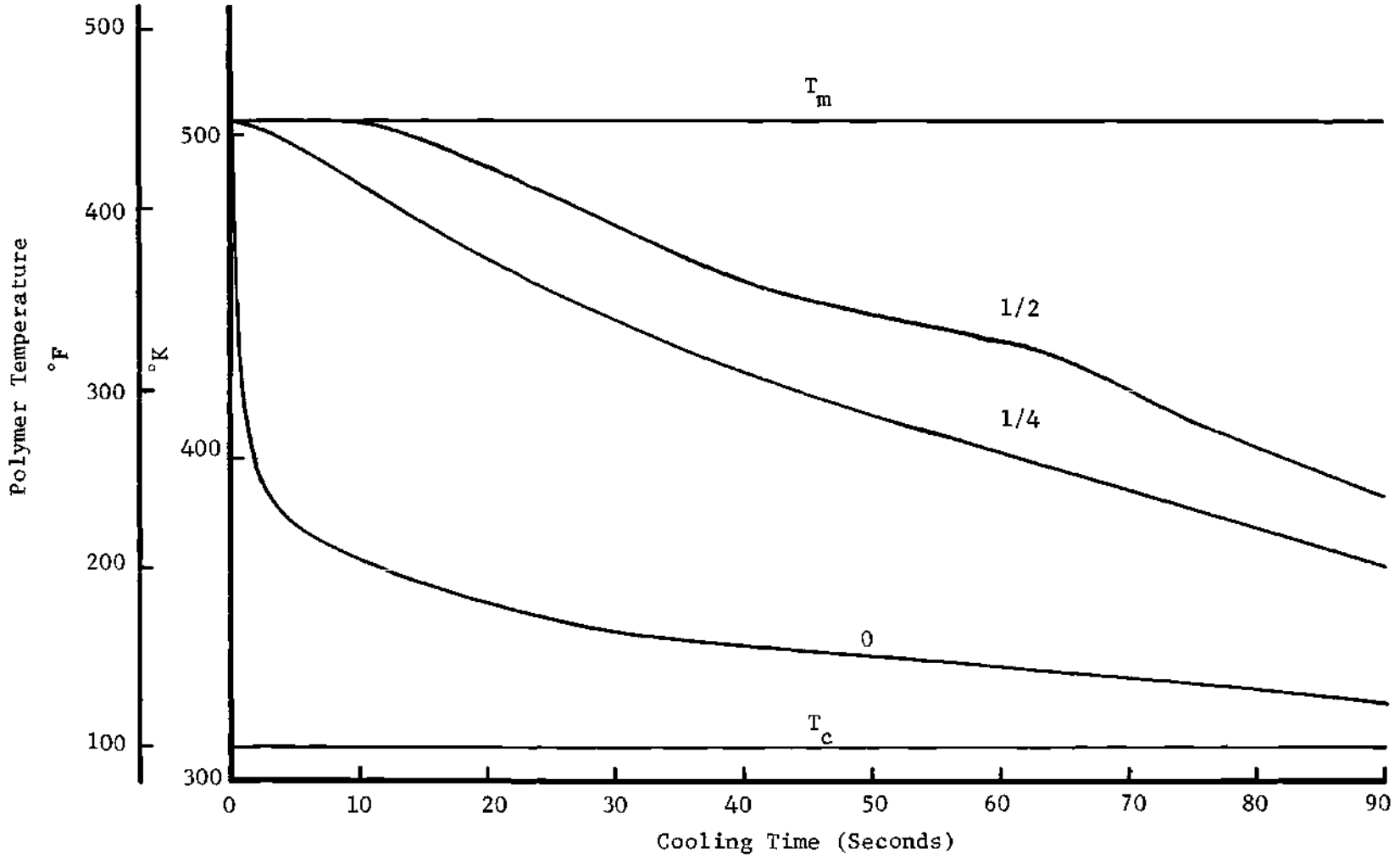

Figure 22. Cooling Curves for Polycaprolactam, Nylon 6

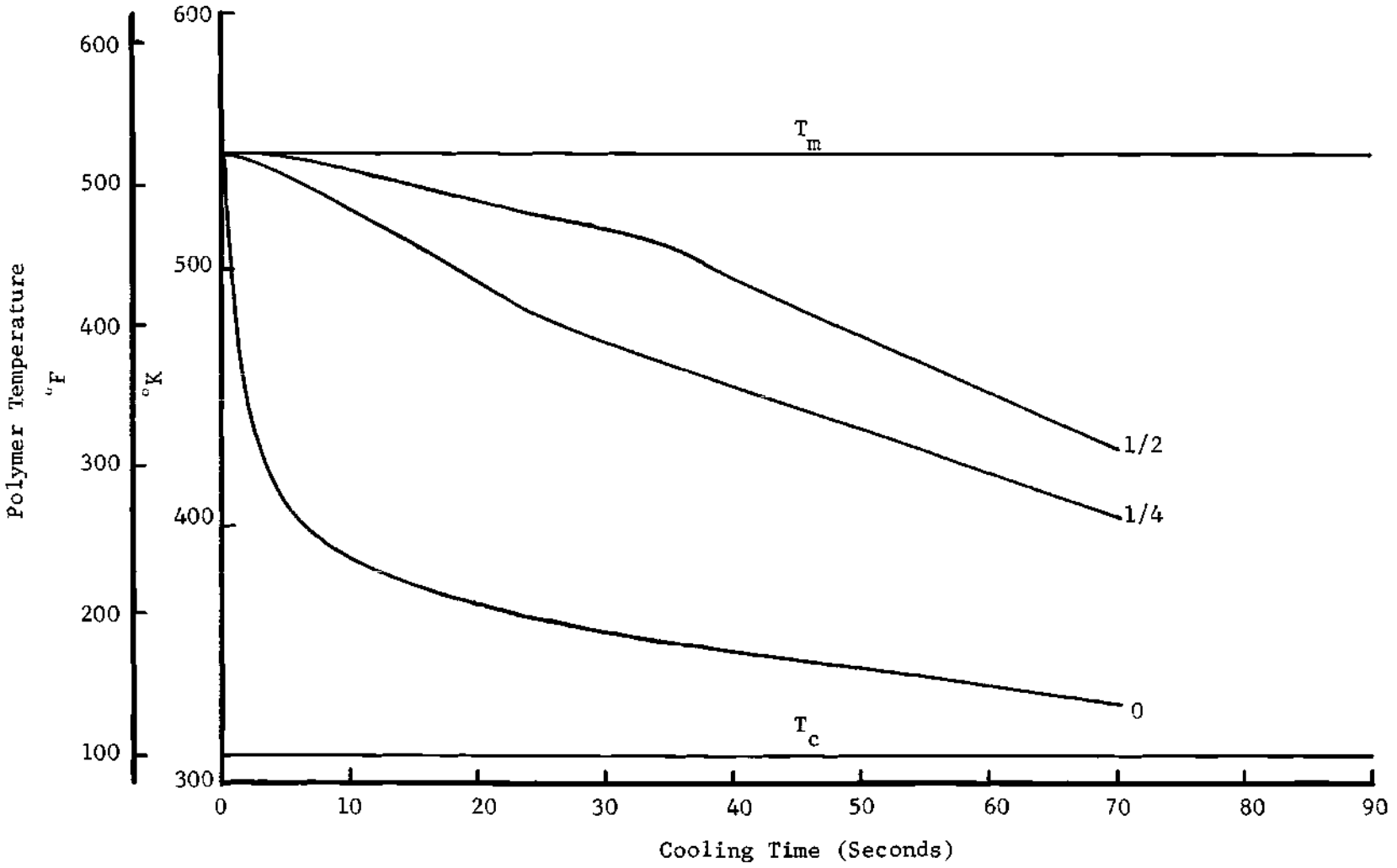

Figure 23. Cooling Curves for Poly(hexamethylene adipamide), Nylon 66

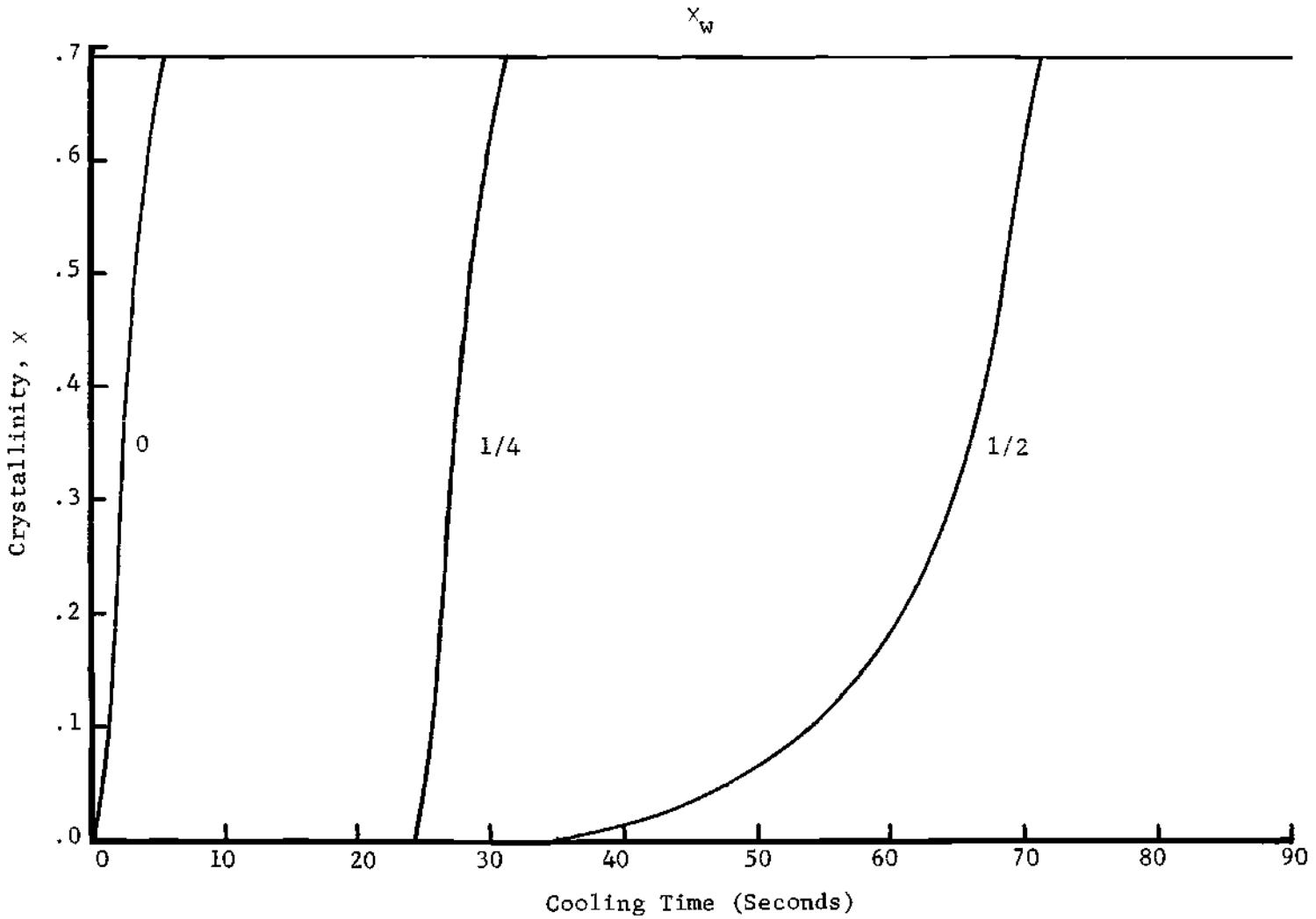

Figure 24. Crystallinity Curves for High Density Polyethylene

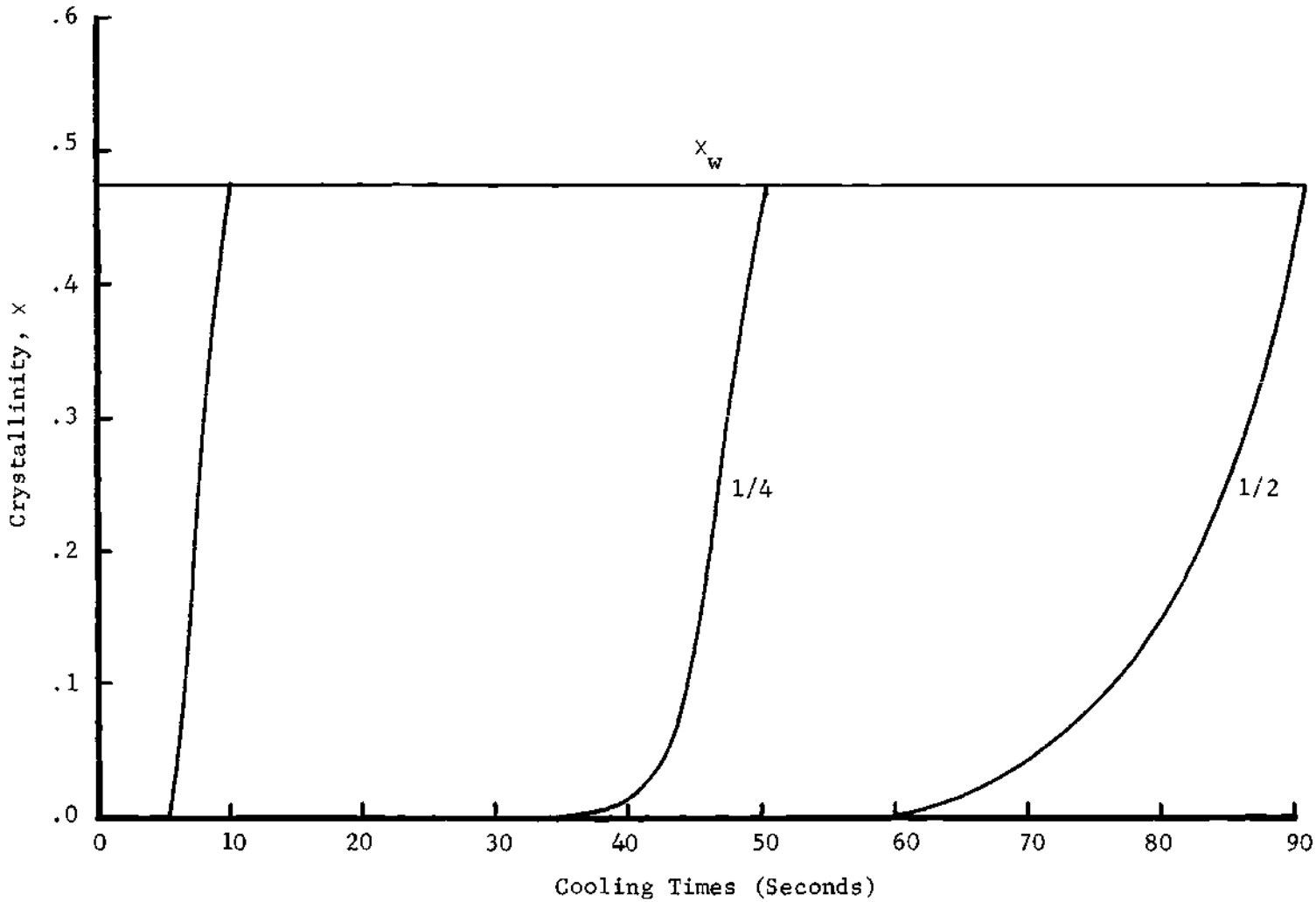

Figure 25. Crystallinity Curves for Polypropylene

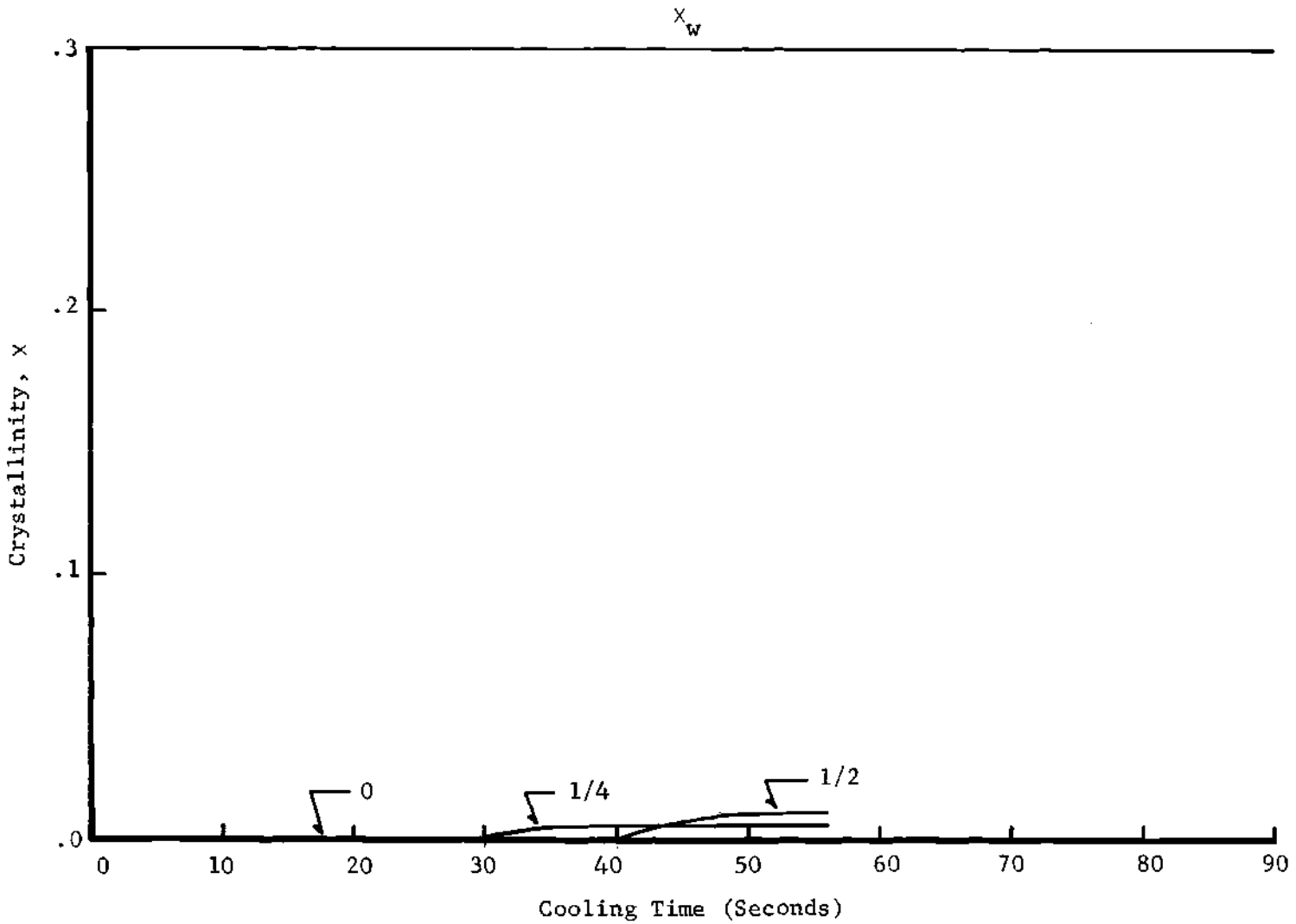

Figure 26. Crystallinity Curves for Poly(ethylene terephthalate), Mylar 700S

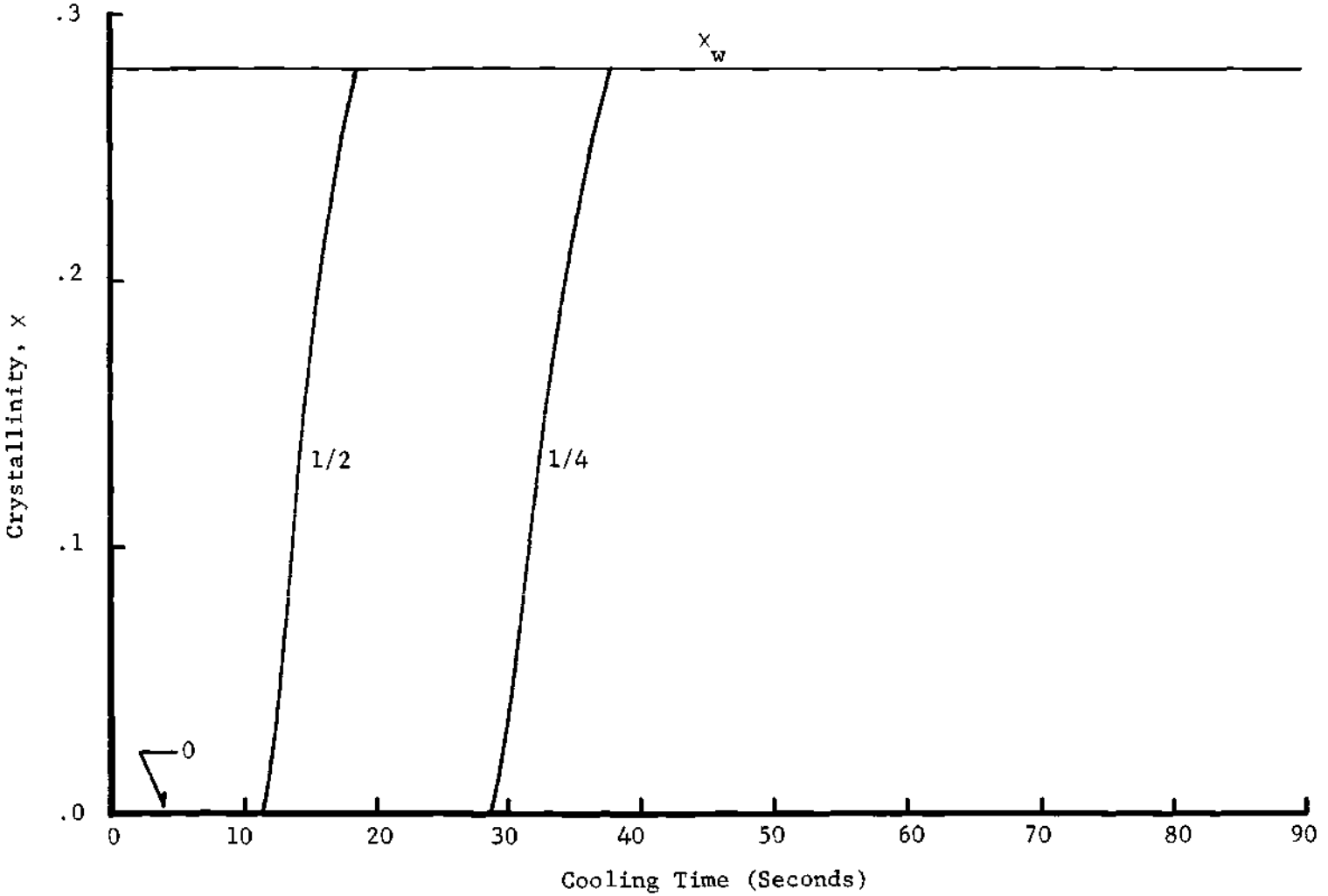

Figure 27. Crystallinity Curves for Poly(ethylene terephthalate), Monsanto

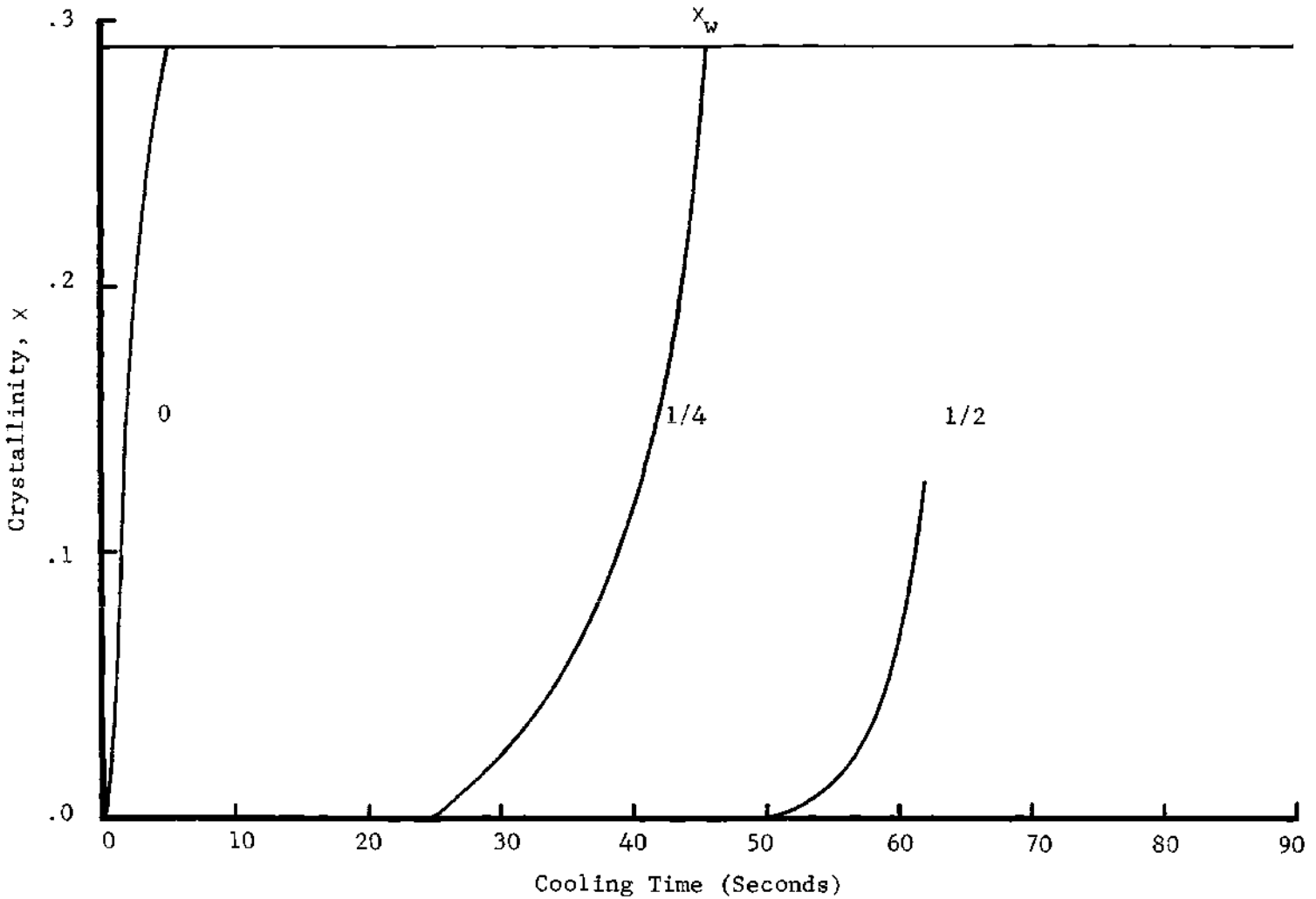

Figure 28. Crystallinity Curves for Polycaprolactam, Nylon 6

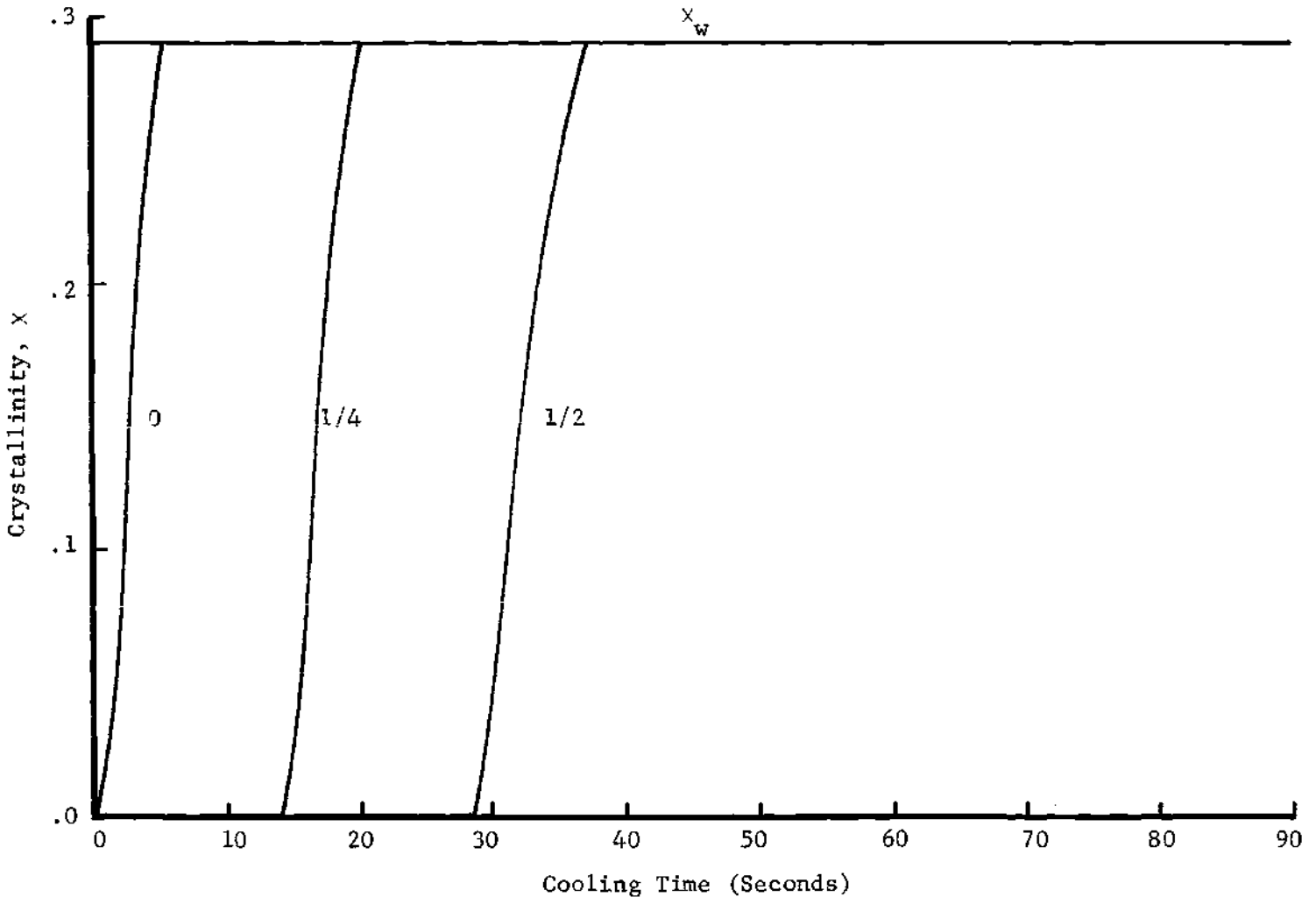

Figure 29. Crystallinity Curves for Poly(hexamethylene adipamide), Nylon 66

This is particularly evident for polyethylene and polypropylene.

The behavior of the crystallinity curves can be explained through spherulite size and typical, calculated growth rates given in Table 5. For polyethylene, the impingement diameter (D_i) is not a function of scan speed above 10^c/minute. Refer back to Figure 11. Once spherulitic growth is initiated, it proceeds at 1-10 μ/second; thus it only takes 5-10 seconds of cooling time to attain the maximum growth ($\sqrt{2}\ D_i$) to yield the maximum crystallinity. The delayed response at the 1/2 plane is due to the high temperature plateau up to 70 seconds (see Figure 18) causing a low thermal driving force (T_m-T) and consequently a low growth rate. The same general explanation applies to polypropylene.

The principal explanation for the behavior of poly(ethylene terephthalate) is that is possesses a very low growth rate. For Mylar 700S, the problem is compounded by the fact that nucleation density is not a function of cooling rate. Refer back to Figure 13. Because of the method by which the volumetric growth relation calculates crystallinity, $[X = X_w(V(D)/V_m(D_i)]$, and with the very low growth rate, the crystallinity inherently can not attain a significant value. The explanation for the behavior of the Monsanto grade, where nucleation density is a function of cooling rate, is analogous with that given for polyethylene and polypropylene at the 1/4 and 1/2 planes. For the zero plane (mold wall/polymer interface), the temperature drop is sudden and very large (see Figure 21) resulting in a temperature near the glass transition (353°K). It is characteristic of the WLF equation, Equation (3.14), within the growth rate expression, Equation (3.11), that at the glass transition, the energy required for molecular transport of polymer chain molecules

Table 5. Variations of Spherulite Diameter Through Polymer Slab

Polymer	Spherulite Diameter, D_i (μ) Reference Plane			Spherulite Growth Rate (μ/sec)
	0	1/4	1/2	
High Density Polyethylene	62	62	62	1-10
Polypropylene	1	18	30	1
Poly(ethylene terephthalate)				
Mylar 700S	~0	1	1	≤.1
Monsanto Grade	~0	1	1	≤.1
Polycaprolactam, Nylon 6	1	30	20	1
Poly(hexamethylene adipamide) Nylon 66	1	1	1	1

approaches infinity. Therefore, the growth rate becomes very small ($\sim .01\,\mu$/sec.); and consequently, an activated growth nuclei can not grow to any appreciable size.

Explanation of the crystallinity curves for Nylon 6 and 66 are analogous with that for polyethylene and polypropylene. In the case of Nylon 6, crystallization, and hence spherulite growth, had not been completed at the 1/2 plane before its temperature fell below the ejection temperature.

This concludes the presentation and discussion of results.

CHAPTER VII

CONCLUSIONS

To resolve the transient heat conduction phenomena occurring during the solidification of bulk polymers, it is necessary to adequately incorpate the crystallization kinetics and properly account for the associated latent heat contributions.

Historically, changes in crystallinity have been expressed through the "modified" Avrami kinetic relation which incorporates a kinetic rate term through which a growth rate expression was introduced. As with all kinetic relations, experimental data are necessary to determine pertinent kinetic parameters. It has been proven experimentally that with kinetic parameters determined from non-isothermal data, the "modified" Avrami relation can not be used to adequately describe the crystallization kinetics under non-isothermal conditions. Even in the differentiated form, the "modified" Avrami relation can not be applied on an incremental basis because of its temperature dependent, fundamental parameters.

Using the same growth rate expression, an alternate relation, the volumetric growth relation, was defined for predicting changes in crystallinity. The kinetic parameters can be determined from two data points collected under isothermal and non-isothermal cooling conditions: 1) the average size of the spherulites at impingement, and 2) the associated time and temperature at impingement. For simulations of isothermal and non-isothermal crystallizations, the volumetric growth relation predicted the correct degree of crystallinity at the appropriate

temperature based solely on the crystallization kinetics.

By incoporating the volumetric growth relation into the heat generation term of the transient heat conduction expression, its solution gave time-temperature-position profiles of cooling temperature and crystallinity characteristic of cooled, injected molded parts. Additional data, maximum degree of crystallinity and final crystallization temperature, was collected from the same non-isothermal experiments from which the kinetic parameters were derived. This additional data was incorporated in the analysis of transient heat conduction in order to predict the ultimate degree of crystallinity and the cessation of crystallization.

Since six crystalline polymers have been analyzed successfully using a general procedure and the volumetric growth relation, this implies that the procedure and the growth relation might be general.

CHAPTER VIII

RECOMMENDATIONS

The most obvious area for future research is to study the variations in morphological structure through injection molded slabs of the polymers studied in this research. If significant differences do occur, it will probably be due to the method of selecting spherulite impingement diameter as a function of sample scan speed. This may necessitate formulation of an alternate scheme.

Another immediate application of this general approach of determining the crystallization kinetics under non-isothermal conditions is to rewrite the nonlinear, transient heat conduction expression in a crylindrical coordinate system. This would represent the radial cooling phenomena occurring in the wire coating extrusion process. Thus the length of the take-off system can be determined from the time to cool the extrudate.

From a more scientific approach, it would be most interesting to study the variation in crystallization kinetics for various molecular weight ranges for a particular virgin polymer. The WLF parameters (c_1, c_2, T_g) will probably have to be adjusted and should follow a consistent trend with molecular weight.

Similarly, it would be equally interesting and quite worthwhile to study the effects that known amounts of nucleation agents would have on crystallization kinetics for a polymer with a particular molecular weight range. The c_2 parameter, once determined for the virgin polymer to be nucleated, should not be changed. Adjustment of the crystallization

kinetics should be accomplished through incorporation of another probability term in growth rate expression.

To fully reflect processing environments, the model should be extended to include the effects of pressure and shear on crystallization kinetics. Also the model would benefit by incorporating volumetric changes due to crystallization and precise measurements of heat capacity and thermal conductivity as a function of temperature.

APPENDIX A

SOLUTION OF NONLINEAR HEAT CONDUCTION PROBLEM

The conventional procedure for solving a partial differential equation (PDE) is by approximation of a derivative via finite difference methods. However, with a nonlinear, parabolic PDE, the problems of convergence and stability are critical. (1) Sifleet (65) did a rigorous study on the best means of solving Equation (3.2) which is repeated here for convenience:

$$\frac{\partial T}{\partial t} = \alpha \frac{\partial^2 T}{\partial x^2} + \frac{Q}{\rho C_p} \qquad \text{(A-1)}$$

The Crank-Nicolson method (14) is an explicit-implicit hybrid of finite difference techniques. The application of this technique follows (11) with reference to the space-time grid in Figure 30 :

$$\frac{\partial T}{\partial t} \doteq \frac{T_{i,j+1} - T_{i,j}}{\Delta t} \qquad \text{(A-2)}$$

$$\frac{\partial^2 T}{\partial x^2} \doteq \frac{1}{2}\left[\delta_x^2 T_{i,j+1} + \delta_x^2 T_{i,j}\right] \qquad \text{(A-3)}$$

where δ_x is the central-difference operator defined as:

$$\delta_x T_{i,j+1} = \frac{T_{i+1/2,j} - T_{i-1/2,j}}{\Delta x}$$

whence:

$$\delta_x^2 T_{i,j} = \frac{T_{i-1,j} - 2T_{ij} + T_{i+1,j}}{(\Delta x)^2} \qquad \text{(A-4)}$$

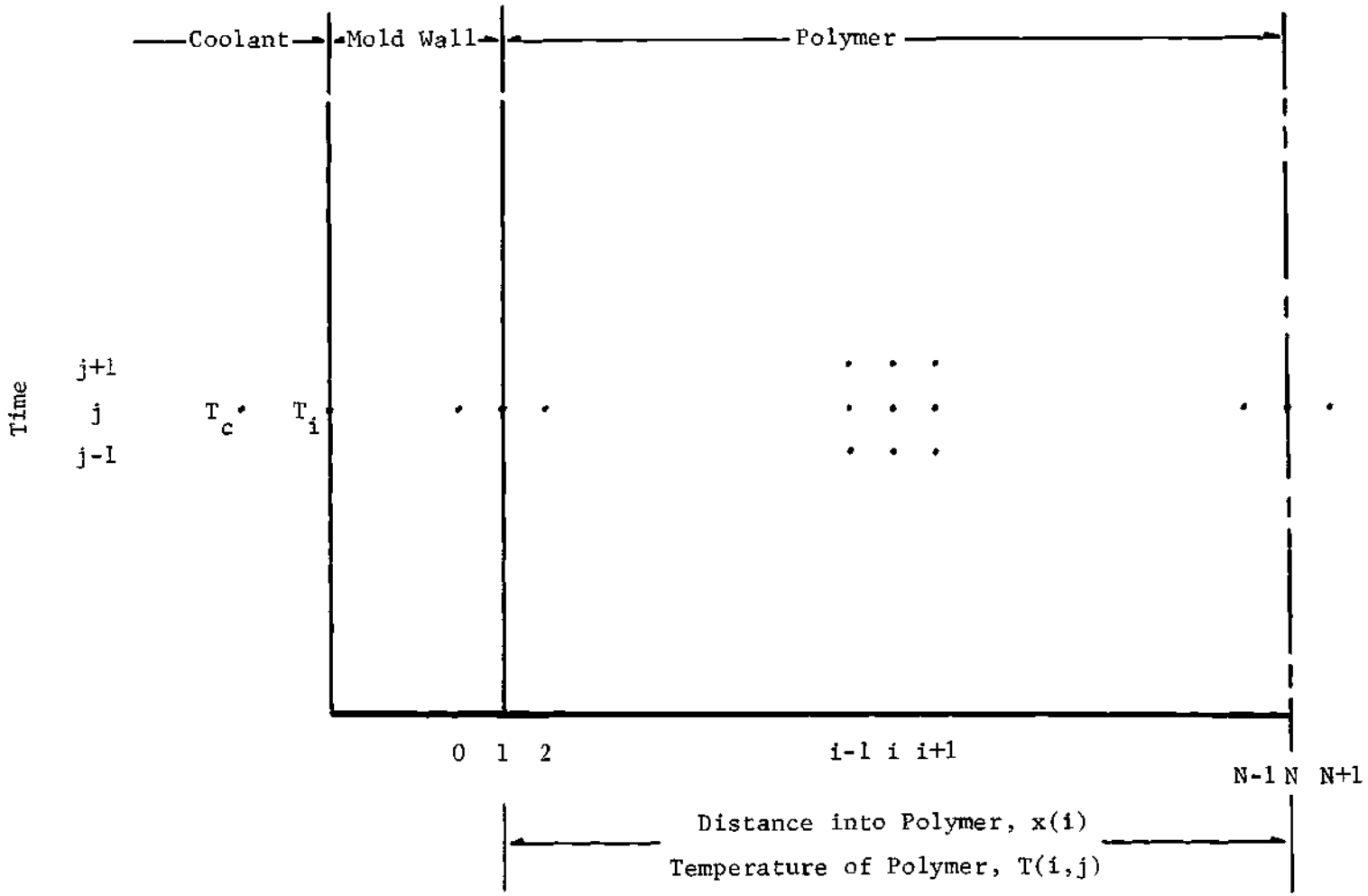

Figure 30. Space-Time Grid

By substituting (A-4) into (A-3) and the results along with (A-2) into (A-1), gives:

$$\frac{T_{i,j+1} - T_{i,j}}{\Delta t} = \frac{\alpha}{2}\left[\frac{T_{i-1,j+1} - 2T_{i,j+1} + T_{i+1,j+1}}{(\Delta x)^2} + \frac{T_{i-1,j} - 2T_{i,j} + T_{i+1,j}}{(\Delta x)^2}\right] + \frac{Q_i}{\rho C_p} \quad \text{(A-5)}$$

In Equation (A-5), three temperatures on the j+1 time row are unknown for each equation representing each node along $0 \leq x \leq x_L$. Thus, these equations must be solved simultaneously to obtain nodal temperatures $T_{i,j}$ for all values of i for a given time index, j. For a given j, a set of algebraic equations is generated by expanding on the space index i and is stable for all values of $\alpha\Delta t/(\Delta x)^2$. Rearranging Equation (A-5) by separating according to indices, gives:

$$YT_{i-1,j+1} - (2+2Y)T_{i,j+1} + YT_{i+1,j+1} =$$

$$-YT_{i-1,j} - (2-2Y)T_{i,j} - YT_{i+1,j} - 2Q_i\Delta t/\rho C_p \quad \text{(A-6)}$$

where:

$$Y = \alpha\Delta t/(\Delta x)^2 \quad \text{(A-7)}$$

Thus Equation (A-6) represents all the internal nodes of the polymer.

It is now necessary to consider the boundary conditions. Refer to Figure 30. At the center line x_N, the following equations are valid by symmetry:

$$T_{N-1,j+1} = T_{N+1,j+1} \quad \text{(A-8)}$$

$$T_{N-1,j} = T_{N+1,j} \tag{A-9}$$

Applying these conditions to Equation (A-6) and collecting terms, gives:

$$2YT_{N-1,j+1} - (2+2Y)T_{N,j+1} =$$

$$-2YT_{N-1,j} - (2-2Y)T_{N,j} - 2Q_N\Delta t/\rho C_p \tag{A-10}$$

Equation (A-10) generates the algebraic equation representing temperatures about the centerline of the polymer within the mold cavity.

Referring to Figure 30 again, consider the heat transfer at the interface and the mold wall. Heat transfer at the coolant/mold wall interface can be described by Newton's law of cooling as follows:

$$q = -h_i(T_i - T_c) \tag{A-11}$$

where the minus sign indicates heat flow is in the opposite direction of the temperature gradient. Heat transfer thru the mold wall can be described by Fourier's law of heat conduction (20) as follows:

$$q = -k_{mw}\frac{dT}{dx} \tag{A-12}$$

and assuming $k_{mw} \neq k_{mw}(T)$, the (A-12) becomes:

$$q \doteq -k_{mw}\frac{T_1 - T_i}{\Delta x_{mw}} \tag{A-13}$$

where k_{mw} is the thermal conductivity, and Δx_{mw} is the thickness of the mold wall. By conservation of energy, Equations (A-12) and (A-13) are equal:

$$-h_i(T_i - T_c) = -\frac{k_{mw}}{\Delta x_{mw}}(T_1 - T_i) \tag{A-14}$$

Re-arranging (A-14) to solve for T_1, gives:

$$T_1 = \left[1 + \frac{h_i \Delta x_{mw}}{k_{mw}}\right] T_i - \frac{h_i \Delta x_{mw}}{k_{mw}} T_p \qquad \text{(A-15)}$$

By assuming intimate contact between the mold wall and the polymer, application of Fourier's law of heat conduction (20), and conservation of energy, the following relationship across the mold wall/polymer interface is obtained (assuming quasi-steady state):

$$-k_{mw} \frac{dT}{dx}\bigg|_{mw} = -k_p \frac{dT}{dx}\bigg|_p \qquad \text{(A-16)}$$

By using a central difference definition of finite differences and substituting into (A-16), the following is obtained:

$$k_{mw} \frac{T_1 - T_i}{\Delta x_{mw}} = k_p \frac{T_2 - T_o}{2\Delta x_p} \qquad \text{(A-17)}$$

Solving for T_i gives:

$$T_i = T_1 - \frac{k_p}{k_{mw}} \frac{\Delta x_{mw}}{2\Delta x_p} (T_2 - T_o) \qquad \text{(A-18)}$$

Substitution of (A-18) into (A-15) and re-arranging gives the following:

$$\psi T_o + T_1 - \psi T_2 = T_c \qquad \text{(A-19)}$$

where:

$$\psi = \left[1 + \frac{k_{mw}}{h_i \Delta x_{mw}}\right]\left[\frac{k_p}{k_{mw}} \frac{\Delta x_{mw}}{2\Delta x_p}\right] \qquad \text{(A-20)}$$

Solving (A-19) for T_o, substituting into (A-6) for indices of $i = 1$ at j and $j+1$, and collecting coefficients of temperature variables with common subscripts, results in the following:

$$-(2+2Y+Y/\psi)T_{1,j+1} + 2YT_{2,j+1} + (Y/\psi)T_{c,j+1} =$$

$$-(2-2Y-Y/\psi)T_{1,j} - 2YT_{2,j} - (Y/\psi)T_{c,j} - 2Q_1\Delta t/\rho\, C_p \qquad \text{(A-21)}$$

Assuming that the coolant temperature (T_c) is always constant ($T_{c,j+1} = T_{c,j}$), then Equation (A-21) can be re-arranged as follows:

$$-(2+2Y+Y/\psi)T_{1,j+1} + 2YT_{2,j+1} =$$

$$-(2-2Y-Y/\psi)T_{1,j} - 2YT_{2,j} - 2(Y/\psi)T_{c,j}$$

$$- 2Q_1\Delta t/\rho\, C_p \qquad \text{(A-22)}$$

The following set of general equations represents the temperature profile from the coolant, through the mold wall, and across the polymer at any particular time:

Coolant/Mold-Wall/Polymer Interfaces

$$-(2+2Y+Y/\psi)T_{1,j+1} + 2YT_{2,j+1} =$$

$$-(2-2Y-Y/\psi)T_{1,j} - 2YT_{2,j} - 2(Y/\psi)T_{c,j}$$

$$- 2Q_1\Delta t/\rho\, C_p \qquad \text{(A-22)}$$

Polymer, Internal

$$YT_{i-1,j+1} - (2+2Y)T_{i,j+1} + YT_{i+1,j+1} =$$

$$-YT_{i-1,j} - (2-2Y)T_{i,j} - YT_{i+1,j} - 2Q_1\Delta t/\rho\, C_p \qquad \text{(A-6)}$$

Polymer, Centerline

$$2YT_{N-1,j+1} - (2+2Y)T_{N,j+1} =$$

$$-2YT_{N-1,j} - (2-2Y)T_{N,j} - 2Q_N\Delta t/\rho\, C_p \qquad \text{(A-10)}$$

Equations (A-22), (A-6), and (A-10) represent a set of N simultaneous linear equations which can be expressed as:

$$AT_{i,j+1} = CT_{i,j} + D \qquad \text{(A-23)}$$

For solution of $T_{i,j+1}$, all $T_{i,j}$ are known and C and D are matrices of coefficients. Matrices A and $T_{i,j+1}$ constitute a special class of matrices — tridiagonal matrices — which can be solved by a special algorithm. (11) To apply this algorithm, it is necessary to define a new set of coefficients as follows:

$$\left.\begin{aligned} a_1 &= 0.0 \\ a_i &= Y \\ a_N &= 2Y \end{aligned}\right\} \qquad \text{(A-24)}$$

$$\left.\begin{aligned} b_1 &= -(2+2Y+Y/\psi) \\ b_i &= -(2+2Y) \\ b_N &= -(2+2Y) \end{aligned}\right\} \qquad \text{(A-25)}$$

$$\left.\begin{aligned} c_1 &= 2Y \\ c_i &= Y \\ c_N &= 0.0 \end{aligned}\right\} \qquad \text{(A-26)}$$

$$\left.\begin{aligned} d_1 &= -(2-2Y-Y/\psi)T_{1,j-1} + 2YT_{2,j-1} - 2(Y/\psi)T_{c,j-1} - 2Q_1\Delta t/\rho\, C_p \\ d_i &= -YT_{i-1,j-1} - (2-2Y)T_{i,j-1} - YT_{i+1,j-1} - 2Q_i\Delta t/\rho\, C_p \\ d_N &= -2YT_{N-1,j-1} - (2-2Y)T_{N,j-1} - 2Q_N\Delta t/\rho\, C_p \end{aligned}\right\} \qquad \text{(A-27)}$$

Note the shift in the time index: $j+1 \rightarrow j$ and $j \rightarrow j-1$. Now, Equations

(A-22),(A-6), and (A-10) can be re-written as follows, including the shift in the time index:

$$\left.\begin{array}{c}\text{Coolant/Mold-Wall/Polymer Interfaces}\\ b_1 T_{1,j} + c_1 T_{2,j} = d_1\\ \text{Polymer, Internal}\\ a_i T_{i-1,j} + b_i T_{i,j} - c_i T_{i+1,j} = d_i\\ \text{Polymer, Centerline}\\ a_N T_{N-1,j} + b_N T_{N,j} = d_N\end{array}\right\} \quad \text{(A-28)}$$

The algorithm for solution of the tridiagonal system of Equations (A-28) follows:

$$\left.\begin{array}{l} T_N = \Gamma_N\\ T_{i,j} = \Gamma_i - \dfrac{c_i T_{i+1,j}}{\beta_i}, \; i = N-1, N-2, \ldots, 1\end{array}\right.$$

where:

$$\left.\begin{array}{l} \beta_i = b_i - \dfrac{a_i c_{i-1}}{\beta_{i-1}}\\ \Gamma_i = \dfrac{d_i - a_i \Gamma_{i-1}}{\beta_i}\end{array}\right\} \; i = 2,3,\ldots,N$$

$$\left.\begin{array}{l}\beta_1 = b_1\\ \Gamma_1 = d_1/\beta_1\end{array}\right\} \quad \text{(A-29)}$$

By using the system of Equations (A-28) representing the heat transfer phenomenon and Equations (A-29) as the solution algorithm, a solution of the heat conduction problem with heat generation can be obtained.

APPENDIX B

DIFFERENTIATION OF THE "MODIFIED" AVRAMI RELATION

Differentiating the "modified" Avrami relation (3.9) with respect to time gives:

$$\frac{dX}{dt} = X_w \exp(-Z_n t^n)\frac{d}{dt}(Z_n t^n) \tag{B-1}$$

where:

$$\frac{d(Z_n t^n)}{dt} = Z_n\, n t^{n-1} + t^n \frac{d\, Z_n}{dt} \tag{B-2}$$

Differentiation of Equation (3.11) defines:

$$\frac{d\, Z_n}{dt} = \frac{4}{3}\,\pi\,\nu_o\, nG^{n-1}\,\frac{dG}{dt} \tag{B-3}$$

with differentiation of Equation (3.12) defining:

$$\frac{dG}{dt} = G_o \exp\left(-\frac{\Delta\Phi}{kT}\right) \exp\left(-\frac{\Delta F}{kT}\right)\left[\frac{1}{G_o}\,\frac{dG_o}{dt} + \frac{d}{dt}\left(-\frac{\Delta\Phi}{kT}\right) + \frac{d}{dt}\left(-\frac{\Delta F}{kT}\right)\right] \tag{B-4}$$

and similarly from Equation (3.13):

$$\frac{d\, G_o}{dt} = \frac{b_o\, k}{h}\,\frac{dT}{dt} \tag{B-5}$$

By substituting Equations (3.12), (3.13), and (B-5) into (B-4), gives:

$$\frac{dG}{dt} = G\left[\frac{1}{T}\,\frac{dT}{dt} + \frac{d}{dt}\left(-\frac{\Delta\Phi}{kT}\right) + \frac{d}{dt}\left(-\frac{\Delta F}{kT}\right)\right] \tag{B-6}$$

Now (B-6) is substituted into (B-3) which is substituted into (B-2)

which in turn is substituted into (B-1) with minor re-arrangement gives:

$$\frac{d\chi}{dt} = \frac{4}{3}\pi\nu_o n \chi_w G^n t^n\left[\frac{1}{t} + \frac{1}{T}\frac{dT}{dt} + \frac{d}{dt}\left(-\frac{\Delta\Phi}{kT}\right) + \frac{d}{dt}\left(-\frac{\Delta F}{kT}\right)\right]\exp(-Z_n t^n) \quad \text{(B-7)}$$

Differentiation of Equation (3.14) and (3.15) for $d(-\Delta\Phi/kT)/dt$ and $d(-\Delta F/kT)/dt$ respectively follows:

$$\frac{d}{dt}\left(-\frac{\Delta\Phi}{kT}\right) = \frac{4b_o \sigma \sigma_e T_m^2}{k \Delta h_c}\left[\frac{2T_m - 3T}{T^3(T_m - T)^2}\right]\frac{dT}{dt} + \frac{a_o \Delta h_c}{\sigma T_m^2}\left[T_m - 2T\right]\frac{dT}{dt} \quad \text{(B-8)}$$

and:

$$\frac{d}{dt}\left(-\frac{\Delta F}{kT}\right) = 4120\left[\frac{2T^2 - T(c_2+T-T_g)}{(c_2+T-T_g)^3}\right]\frac{dT}{dt}\frac{1}{RT} \quad \text{(B-9)}$$

Equation (B-9) is valid only for $T_g \leq T \leq Tg+100$; for $T \geq T_g+100$, T is set to T_g+100 and substituted as follows:

$$\frac{d}{dt}\left(-\frac{\Delta F}{kT}\right) = 4120\left[\frac{2(T_g+100)^2 - (T_g+100)(c_2+100)}{(c_2+100)^3}\right]\frac{dT}{dt}\cdot\frac{1}{RT} \quad \text{(B-10)}$$

It is worth noting that the net effect of activation energy with temperature is preserved through the 1/RT term in both equations (B-9) and (B-10). At $T = T_g+100$, both equations must give the same value for $\frac{d}{dt}\left(-\frac{\Delta F}{kT}\right)$ in order to maintain a continuous function.

APPENDIX C

DERIVATION OF THE VOLUMETRIC GROWTH RELATION

Figure 7b is repeated with additional notation as Figure 31. The length of line $\overline{AK}$ is $2r_i$, and lines $\overline{AD}$ and $\overline{DK}$ equal r_i. By Pythagoreas' theorem, r_m equals $\sqrt{2}r_i$. The inter-spherulitic volume still to be filled upon impingement is calculated by subtracting the volume of spherical segment BCDB of height $\overline{CL}$ from the volume of the regular cone ABDA. It should be apparent that ΔAIKA is an isosceles triangle with sides $\overline{AI} = \overline{AK} = 2r_i$ as shown in Figure 31. Bisecting along the indicated axis of rotation generates two more isosceles triangles. Focusing on ΔAJKA, sides $\overline{AJ} = \overline{JK} = r_m$, and $\angle$AJK is a right angle. Bisecting $\angle$AJK with $\overline{JD}$, which is perpendicular to $\overline{ADK}$, sets $\angle$AJD to 45°. Now the height of a spherical segment at impingement h_i $(\overline{CL})$ can be calculated as follows:

$$h_i = r_i - r_i \cos 45^\circ \qquad \text{(C-1)}$$

and taking the cosine of 45° and rearranging gives:

$$h_i = \left(1 - \frac{\sqrt{2}}{2}\right) r_i \qquad \text{(C-2)}$$

The volume of a spherical segment at impingement (V_{si}) is calculated by standard formula (63) as:

$$V_{si} = \pi h_i^2 (3r_i - h_i)/3 \qquad \text{(C-3)}$$

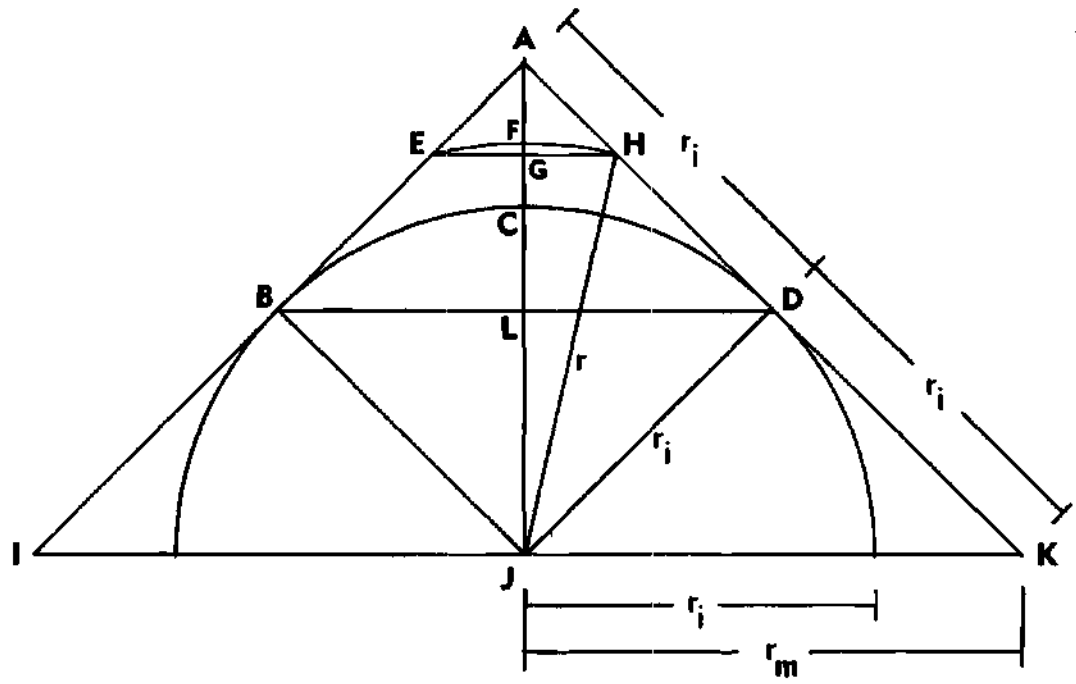

Figure 31. Face-Centered Cubic Structure

The height ($\overline{AL}$) of the regular cone ABDA is $r_m - (r_i - h_i)$. As proven earlier, ΔAJKA is an isosceles triangle. Since ΔAJKA and ΔALDA have a common angle ($\angle$JAK), two common sides ($\overline{AL}$ and $\overline{AJ}$, $\overline{AD}$ and $\overline{AK}$), and parallel opposite sides ($\overline{DL} \| \overline{JK}$), then ΔALDA is also an isosceles triangle with sides $\overline{AL}$ and $\overline{DL}$ equal. Thus the regular cone ABDA has an equivalent base radius ($\overline{DL}$) and height ($\overline{AL}$). The volume of the regular cone ABDA at impingement (V_{ci}) is calculated according to standard formula (63) as:

$$V_{ci} = \pi[r_m - (r_i - h_i)]^3/3 \qquad \text{(C-4)}$$

Now, the inter-spherulitic volume to be crystallized after impingement (V_{ii}) corresponds to the volume generated upon rotation of the planar, geometric shape ABCDA and is defined mathematically as:

$$V_{ii} = V_{ci} - V_{si} \qquad \text{(C-5)}$$

The accuracy of this technique can be determined by arbitrarily selecting some spherulite impingement radius (r_i) and calculating the total volume of four spheres comprising a FCC structure plus the volume of the twenty-four inter-spherulitic volumes within the FCC structure via Equations (C-2,C-3,C-4,C-5). The sum of these volumes is compared with the cubic volume of a FCC structure (V_{FCC}) defined as (78):

$$V_{FCC} = \left[\frac{4\ r_i}{2}\right]^3 \qquad \text{(C-6)}$$

This technique accounts for 87.5% of the volume within a FCC structure. Since the total volume of the four spheres is exact, then the 12.5% lost volume is attributable to inaccuracy in calculating the twenty-four

inter-spherulitic volumes. Since three or more solid elements with curved surfaces can not have a common tangent, a discrepency occurs in the estimated inter-spherulitic volume. This lost inter-spherulitic volume is assigned to each conical element equally.

Now it is necessary to calculate the inter-spherulitic volume at some intermediate spherulite radius, $r_i < r < r_m$. Consider the conical element AEFHA defined by spherulite radius r in Figure 31. The problem now is to calculate the height of the spherical segment h, $\overline{FG}$. As mentioned before, $\overline{JD}$ is perpendicular to $\overline{ADK}$; then, by Pythagoreas' theorem the length of $\overline{HD}$ is the square root of $(r^2 - r_i^2)$. Consequently, the length $\overline{AH}$ of cone AEHA is $(\overline{AD} - \overline{HD})$ or $(r_i - \overline{HD})$. As proven before, ΔALDA is an isosceles triangle; and by similar derivation, ΔAGHA is an isosceles triangle with $\overline{AG}$ and $\overline{HG}$ equivalent. Again by Pythagoreas' theorem, $\overline{AG}$ and $\overline{HG}$ equal $\overline{AH}/\sqrt{2}$. Continuing one step further, the height h $(\overline{FG})$ of the spherical segment volume is $\overline{AG} - (r_m - r)$. Then by substituting for $\overline{AG}$, then $\overline{AH}$, and finally for $\overline{HD}$, the height obtained is:

$$h = \frac{r_i - \sqrt{r^2 - r_i^2}}{\sqrt{2}} - (r_m - r) \qquad \text{(C-7)}$$

Now the volume of a spherical segment (V_s) is:

$$V_s = \pi h^2(3r - h)/3 \qquad \text{(C-8)}$$

The volume of cone AEHA (V_c), which has an equivalent height $(\overline{AG})$ and base radius $(\overline{HG})$ is:

$$V_c = \pi[r_m - (r - h)]^3/3 \qquad \text{(C-9)}$$

The inter-spherulitic volume (V_i) still to be crystallized corresponding

to a spherulite radius (r) is:

$$V_i = V_c - V_s \qquad \text{(C-10)}$$

Based on the preceding derivation, expressions involved in calculating inter-spherulitic volumes of polymer melt still to be crystallized are based solely on a growth radius (r) which is function of Hoffman's growth rate expression, Equation (3.1).

As discussed earlier, the degree of crystallinity is proportional to the volumetric growth of spherulites. The total volume (V_T) per spherulite to be crystallized is the volume at impingement plus the volume of six, inter-spherulitic, conical elements associated with each spherulite:

$$V_T = \frac{4}{3}\pi r_i^3 + 1.03\ (6\ V_{ii}) \qquad \text{(C-11)}$$

The 1.03 factor accounts for the 3% lost inter-spherulitic volume per spherulite arising from the calculation scheme as explained earlier. This total volume (V_T) is crystallized to a degree of crystallinity, χ_w. For pre-impingement, the volume of a spherulite (V) at radius $r(0 \leq r \leq r_m)$ is:

$$V = \frac{4}{3}\pi r^3 \qquad \text{(C-12)}$$

For post-impingement, the volume (V) is the impinged spherulite volume plus the additional volume ($V_{ii} - V_i$) corresponding to $r(r_i \leq r \leq r_m)$ as follows:

$$V = \frac{4}{3}\pi r_i^3 + 1.03[6(V_{ii} - V_i)] \qquad \text{(C-13)}$$

Thus, Equations (C-12,C-13) define the volume V in Equation (3.16).

APPENDIX D

CALIBRATION OF A DIFFERENTIAL SCANNING CALORIMETER

The differential scanning calorimeter (DSC) must be carefully calibrated in order to utilize the quantitative capabilities of the instrument. Calibration schemes must be developed for: 1) energy transferred, 2) thermal resistance (R_o), and 3) DSC dial temperatures. These calibrations are normally performed using well-characterized, standard samples of very high purity. Once the DSC has been extensively calibrated, experimental samples can be evaluated. (7,26,37,53,70)

A fully developed calibration scheme follows, including techniques for: 1) checking the compatibility of the recorder with the DSC, 2) reducing the thermal resistance (R_o), and 3) calibrating the DSC dial temperature for heating and cooling modes of operation. Finally, the application and impact of these calibration schemes on DSC heating and cooling thermograms of polymeric materials will be illustrated.

Energy Transfer Calibration

In DSC, as the temperature is programmed, the sample and reference holders, are continuously maintained at the same temperature. These holders may be held at a constant temperature or may be programmed to increase or decrease at a linear rate with respect to time. Temperature equivalence under these various modes of operation is achieved electronically. When the sample absorbs or evolves energy, more or less energy is required by the sample to maintain it at the same temperature

as the reference. It is this differential amount of energy (dq/dt), automatically and continuously varied according to the energy requirements of the sample, which is recorded as the output signal of the DSC To calibrate this signal, a conversion constant (K) is developed relating the area of a DSC thermogram to millicalories using a standard sample run at a specific DSC range, recorder range, and chart speed. In this study, a calibration sample kit (part #219-0045) purchased from the Perkin-Elmer Corp., Norwalk, Connecticut was used. The kit (37) contained samples of indium, tin, and lead certified by the U.S. National Bureau of Standards (NBS). The known latent heats of fusion (62) and weights of these standard samples were used to convert the measured thermogram area to millicalories. Conversion constants (K) should be independent of the weight and latent heat of the samples, temperature, and DSC scanning rate. (26,80)

DSC and Recorder Compatibility Check

The difference in response for a "good" and "bad" recorder is illustrated in Figure 32. An indication of poor responsiveness of the "bad" recorder is the general lack in sharpness and smoothness of the thermogram. Determination of the conversion constant as a function of scan speed provides an explicit check of the adequacy of recorder responsiveness and compatibility for use with the DSC. Figure 33 illustrates the effect of recorder responsiveness through evaluation of the conversion constant (K); the constant should be independent of scan speed. (80) With a completely compatible system, the constant should be independent of the scan speed and calibration standards used

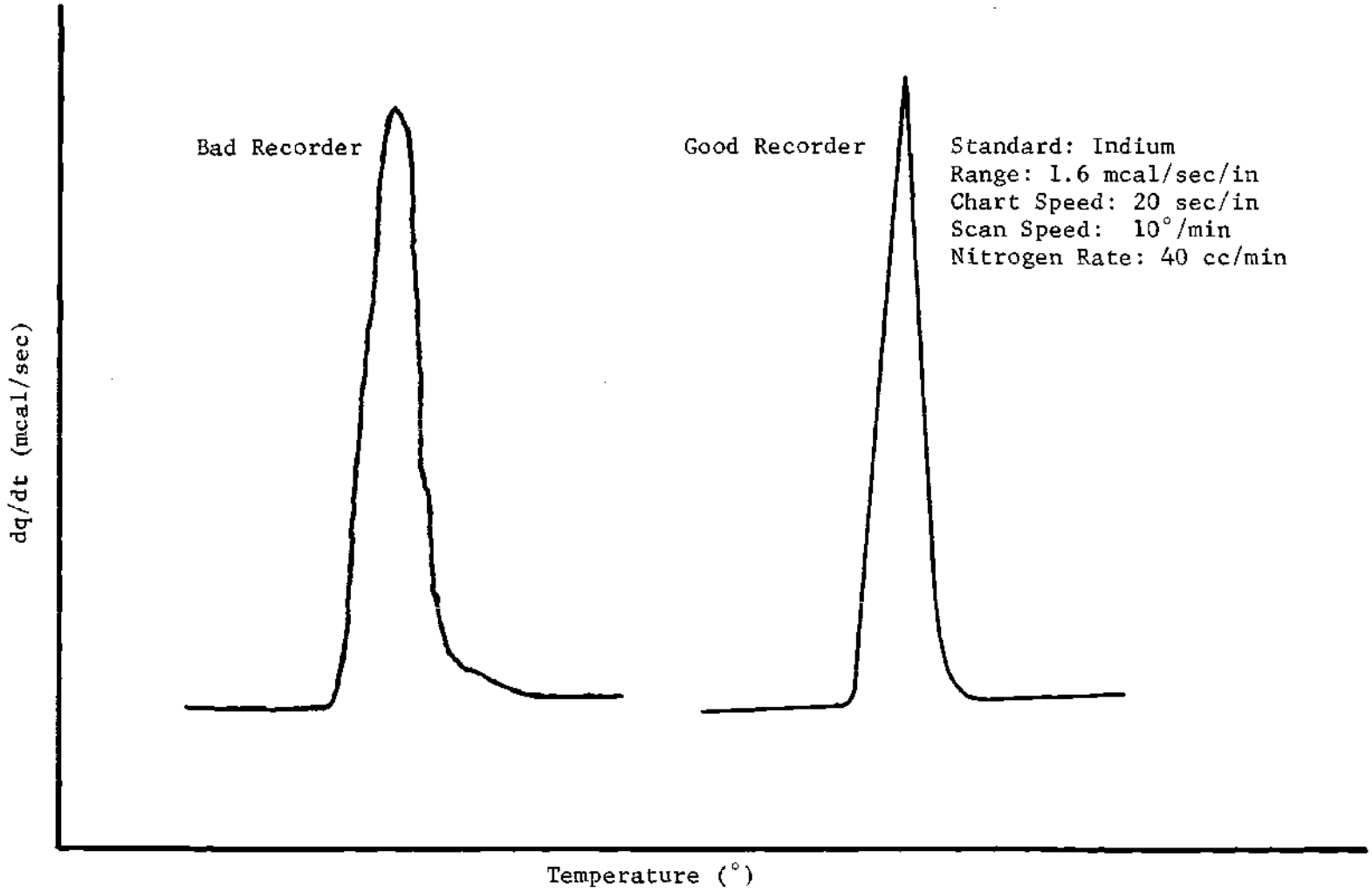

Figure 32. Effect of Recorder Responsiveness on Melt Thermograms

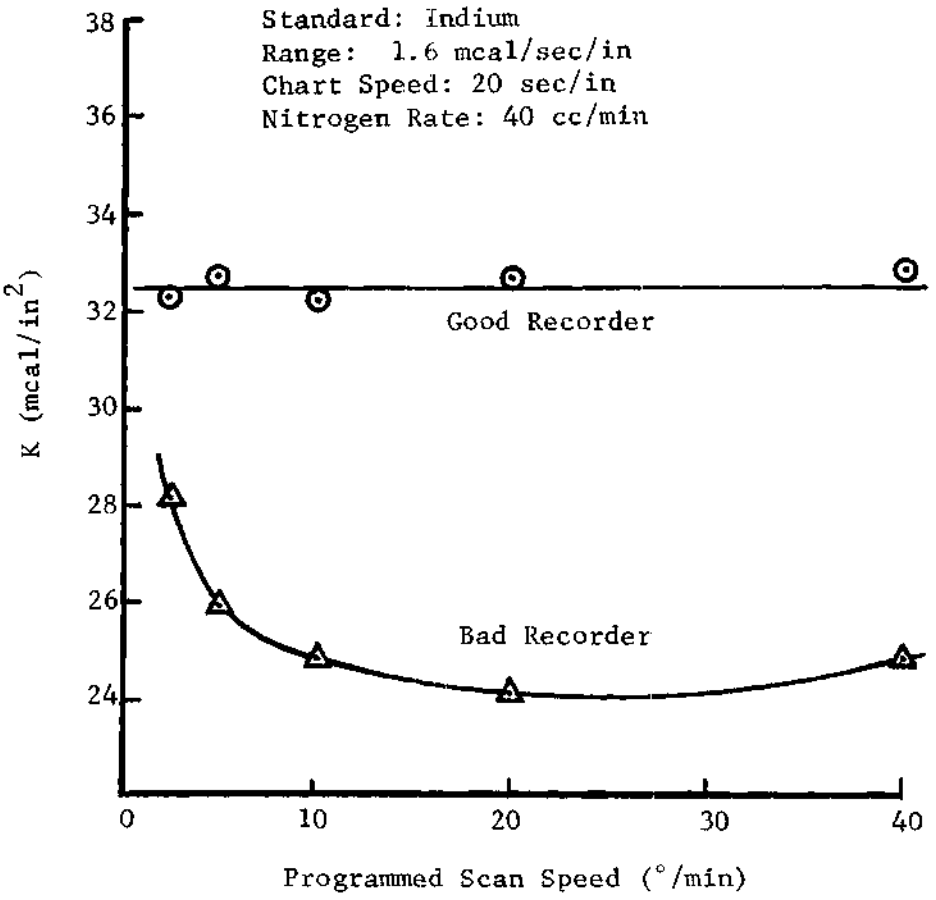

Figure 33. Effect of Recorder Responsiveness on Conversion Constant (K)

within experimental error. See Figure 34. The $\bar{K}$ values are the arithmetic averages of the constants for a particular standard. It is particularly desirable to use standards with sharp, high energy, stable transitions in order to provide a severe test of recorder responsiveness. Thus, the calibration constant provides a convenient means for checking compatibility between the DSC and recorder.

Thermal Resistance

To permit typical DSC temperature changes to occur, the size of the sample, reference, pans, and holders have all been miniaturized to reduce the thermal resistance. Despite these provisions, a measureable resistance to heat transfer between sample and holder does exist which may be expressed by Newton's law of cooling as (7,53,70):

$$\frac{dq}{dt} = \frac{T_p - T_s}{R_o + R_s} \qquad \text{(D-1)}$$

where dq/dt is the instantaneous rate of energy transfer; T_p, the DSC programmed temperature; T_s, the sample temperature; R_o, the thermal resistance between pan and holder; and R_s, the sample resistance. By using a thin sample, the sample resistance R_s will be very small compared to R_o. (56) By limiting the polymer sample sizes to less than 20 mg weight and 500 micron thickness, $R_s \ll R_o$; hence, R_o can be considered the overall thermal resistance. Equation (D-1) reduces to:

$$\frac{dq}{dt} = \frac{T_p - T_s}{R_o} \qquad \text{(D-2)}$$

As indicated by Equation (D-2), the sample and programmed temperatures can be significantly different at high rates of energy transfer

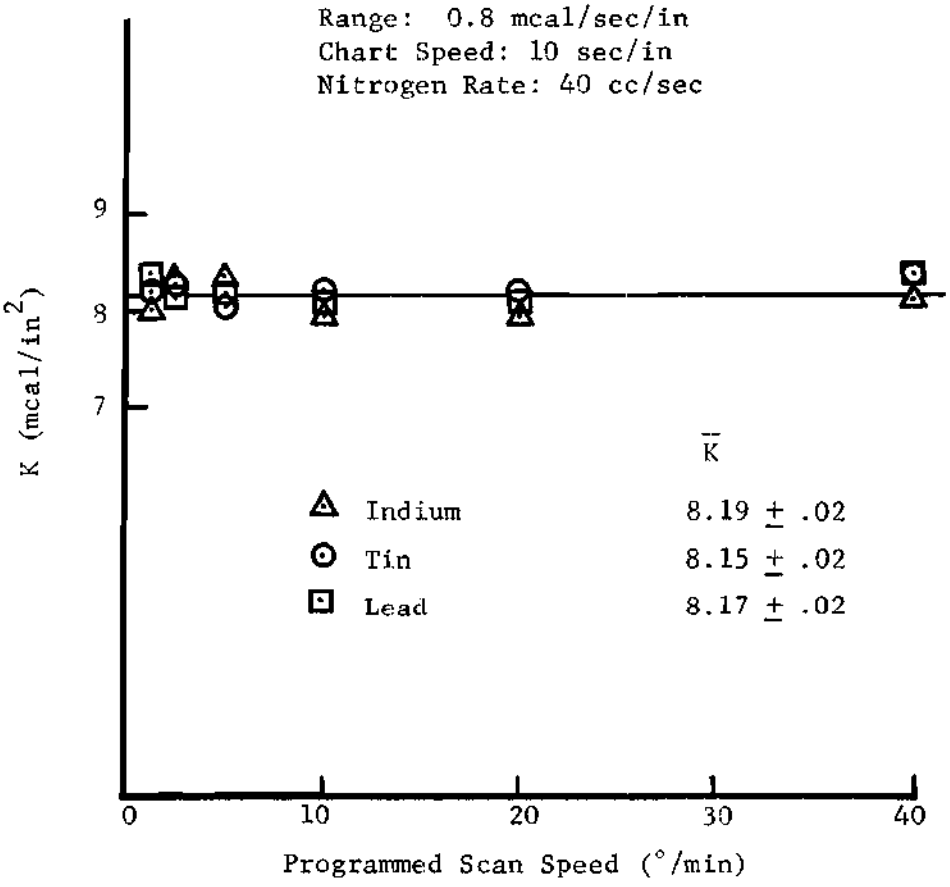

Figure 34. Conversion Constant (K) as a Function of Material Standard and Scan Speed

(dq/dt) which occur at high scan speeds (dT/dt). Differentiating Equation (D-2) with respect to time gives:

$$R_o \frac{d^2q}{dt^2} = \frac{dT_p}{dt} - \frac{dT_s}{dt} \qquad \text{(D-3)}$$

which implies that the sample scan speed (dT_s/dt) does not necessary equal the imposed, programmed scan speed (dT_p/dt). Thus to ascertain the sample temperature (T_s), the thermal resistance must be evaluated.

Evaluation of Thermal Resistance

For very pure samples with precise transition points, the sample temperature can be considered constant during its phase transition (7,70), and thus, thermal resistance is defined as:

$$R_o = \frac{dT_p/dt}{d^2q/dt^2} \qquad \text{(D-4)}$$

The procedure for evaluating R_o is illustrated in Figure 35. (70) The slope (d^2q/dt^2) is determined from the leading edge of the melt thermogram run at the slowest possible scan speed, 0.625 °/minute. For the DSC-1B utilized in this study, the thermal resistance was experimentally evaluated as 200°K sec/cal which agrees with published values. (53,56)

Reduction of Thermal Resistance

Since the sample pans are slightly crimped when the sample is encapsulated, complete contact between the pan and holder is not achieved. The resulting spaces are filled with the purge gas (dry nitrogen), a poor thermal conductor. By depositing a minute amount of a heat transfer fluid in the holder before inserting the sample or reference pans, the purge gas between the pan and holder is displaced by the fluid, and the thermal resistance is reduced. The fluid was Dow Corning^R 200 Silicone

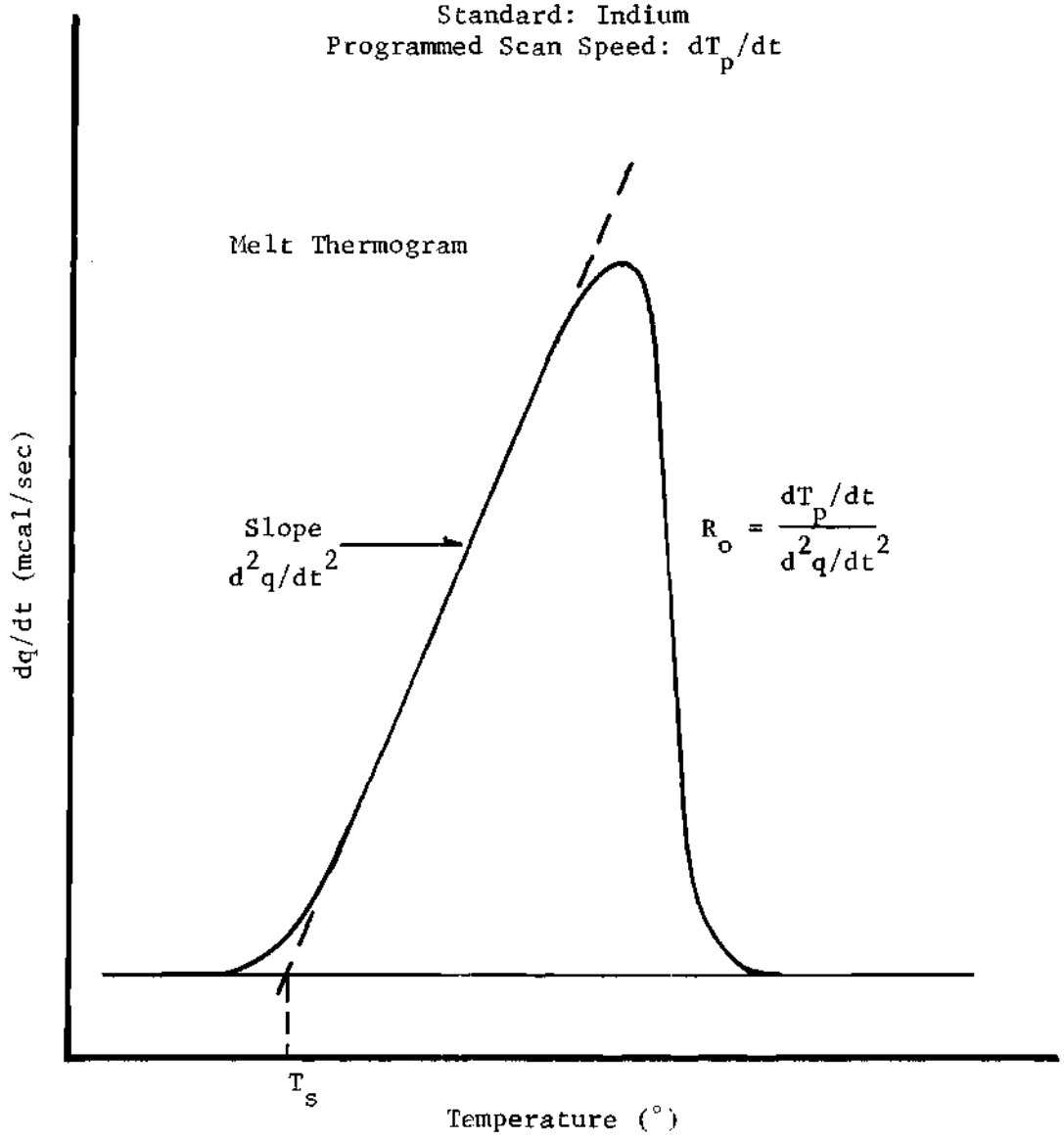

Figure 35. Evaluation of Thermal Resistance (R_o)

Fluid. Due to its high viscosity, a 25% volume solution of fluid in isopropanol was prepared to facilitate pipetting the fluid into the holders. The alcohol boils-off during the heating operation long before the transition range of the standards or polymer samples used in this study is reached. FISHERbrand^{R}, Lambda pipets (2λ, #21-157-5B) were used to do the pipetting.

Figure 36 illustrates the effect of depositing various amounts of fluid in the holders has on the thermogram of a standard indium sample. It is worth noting that no significant improvement in the thermograms was achieved for fluid volumes above 1/2 λ (1λ ≡ .001 ml.). In fact, the thermograms begin to deteriorate for fluid volumes in excess of 1.0 λ, since too much oil actually increases the overall thermal resistance. With the addition of 1/2 λ volume of fluid, the thermal resistance is reduced to 73 from 200°K sec/cal for a dry pan/holder assembly. Thus this technique of adding a heat transfer fluid can significantly improve the heat transfer characteristics of the DSC-1B.

Dial Temperature Calibration

Since the indicated dial temperature on the DSC-1B is not an explicit measurement of the true sample or holder temperature, the dial temperature must be calibrated using standard samples with precise transition temperatures. The dial temperatures must undergo two corrections: 1) correction for thermal lag between programmed and sample temperature, and 2) correction of the sample temperature to its true temperature.

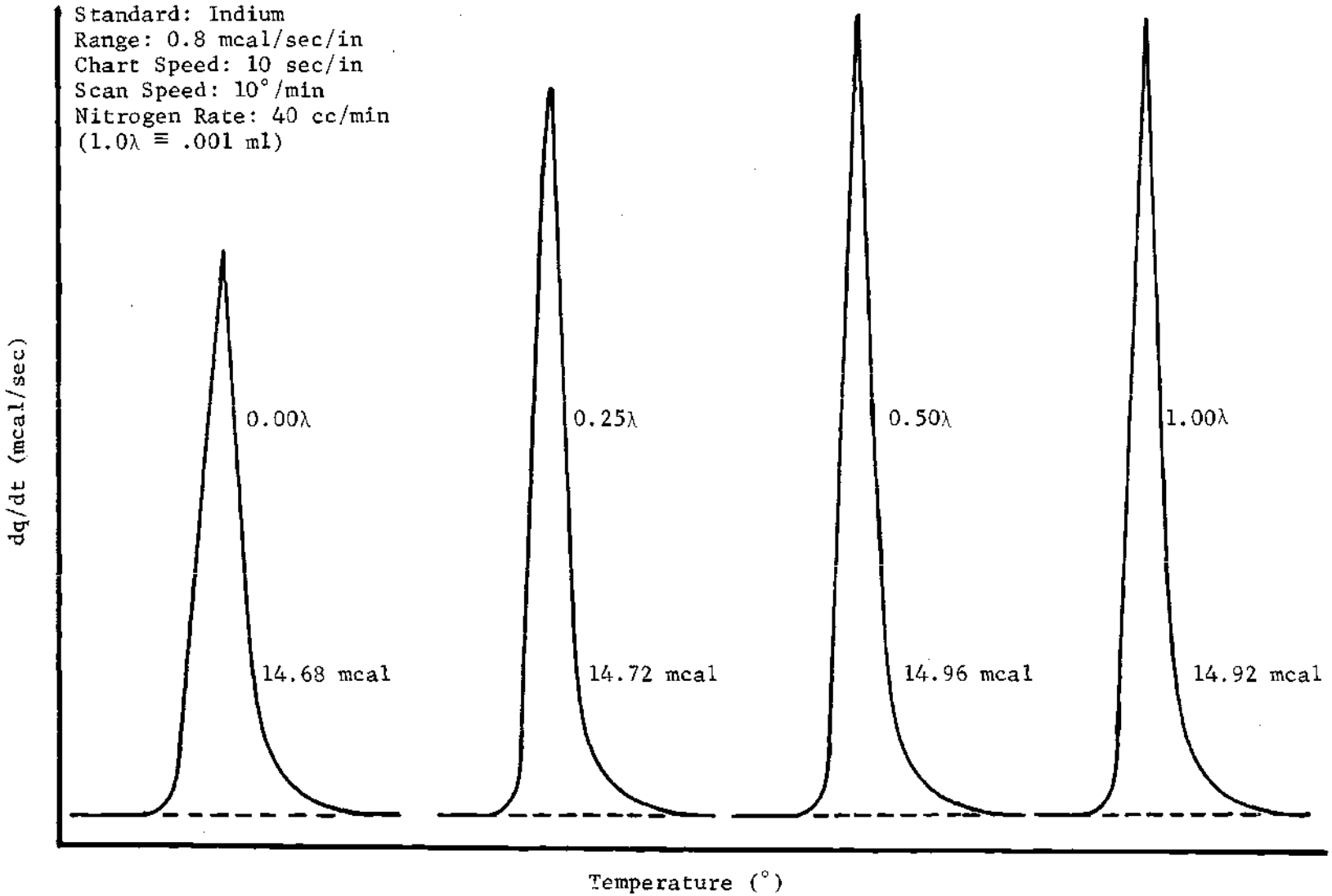

Figure 36. Effect of Heat Transfer Fluid Volumes of Thermograms

Calibration for Heating Scan Speeds

When using a high purity standard sample for dial temperature calibration purposes, the standard technique (80) for correcting for the thermal lag in melt thermograms is illustrated in Figure 37. Once R_o is determined at the slowest scan speed (0.625°/minute), as already shown in Figure 35, values of T_s at higher scan speeds can be determined. If T_s at each scan speed did not correspond to the true transition temperature (T_T) of that standard sample, it is corrected by an amount equal to their difference:

$$\Delta T = T_T - T_s \qquad \text{(D-5)}$$

Such data were collected at six scan speeds for each of the three standards: indium, tin, and lead. Graphs of correction temperature (ΔT) verses programmed sample scan speed for indium, tin, and lead are shown in Figures 38, 39, and 40 respectively as "Calibration for Heating". A set of correction curves for various heating scan speeds is shown in Figure 41. This dependence of temperature correction on scan speed has not been generally noted before.

Calibration for Cooling Scan Speeds

Calibration of the dial temperature for various cooling scan speeds is basically the same approach as just outlined for heating scan speeds. However, in the calibration procedure, the supercooling required to induce solidification must be considered. Since the kinetics of solidification of very high purity samples is very fast, once solidification is initiated it is virtually instantaneous, resulting in a cooling thermogram with the

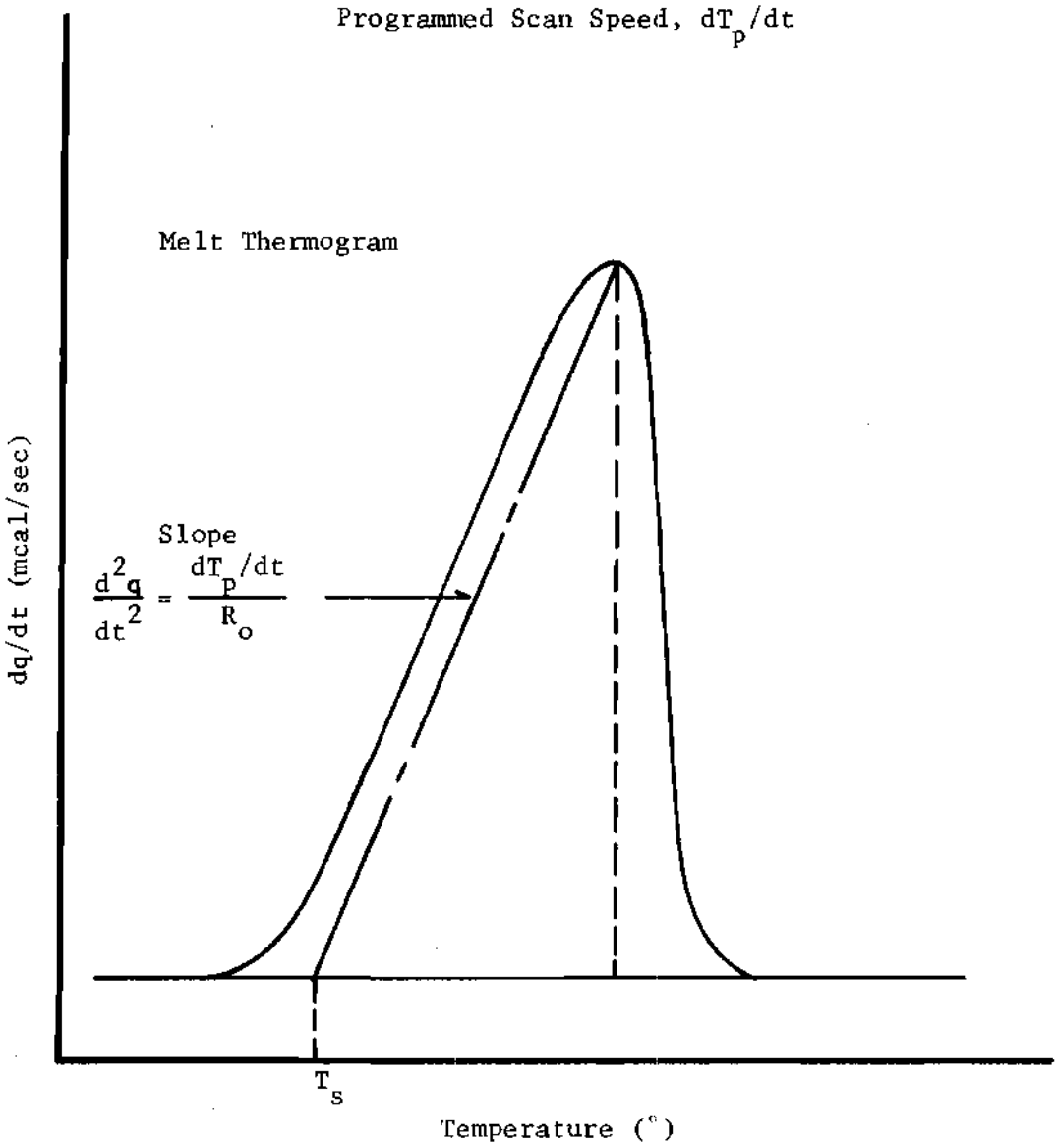

Figure 37. Determination of Standard Sample Temperature

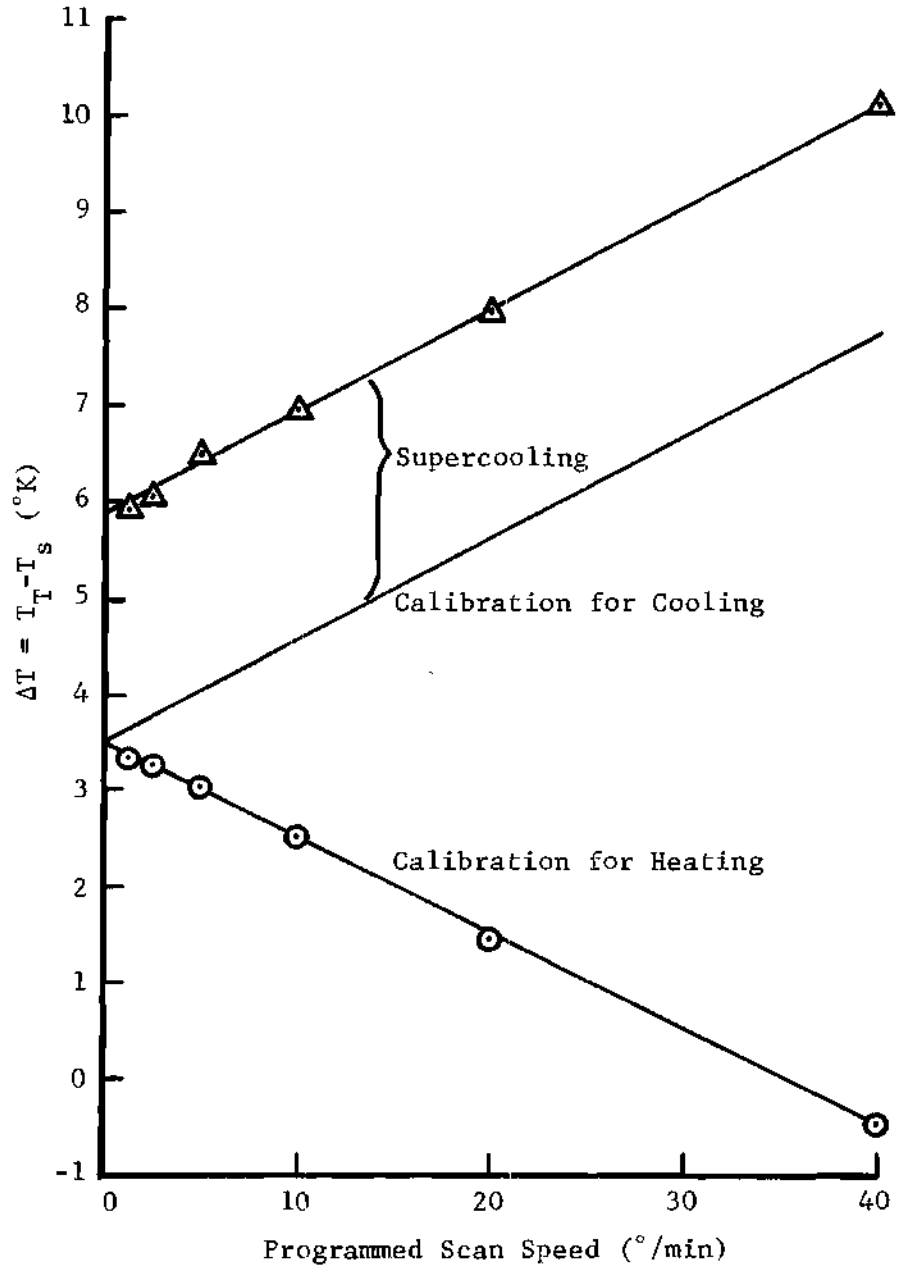

Figure 38. Calibration of Standard Sample Temperature at Indium Transition

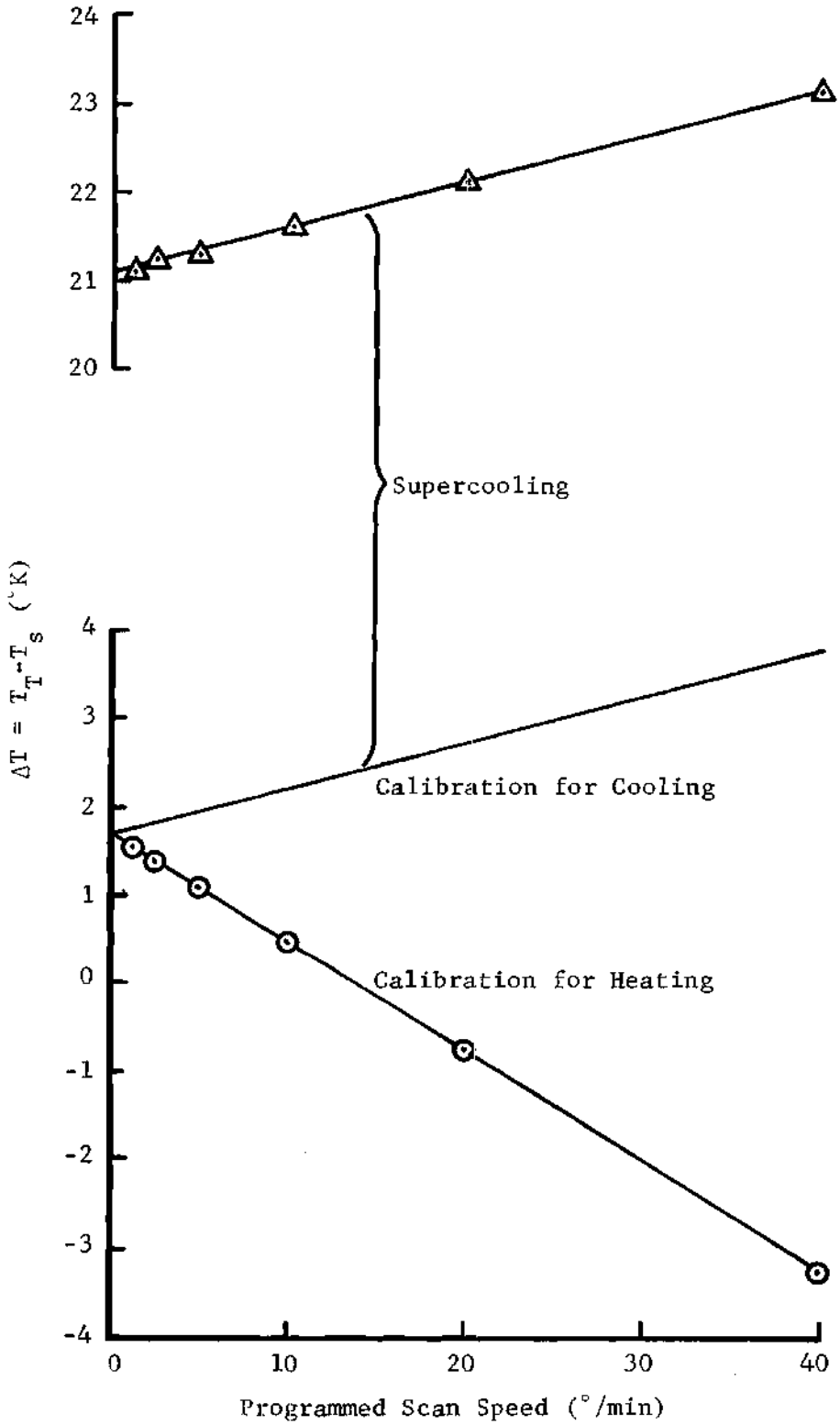

Figure 39. Calibration of Standard Sample Temperature at Tin Transition

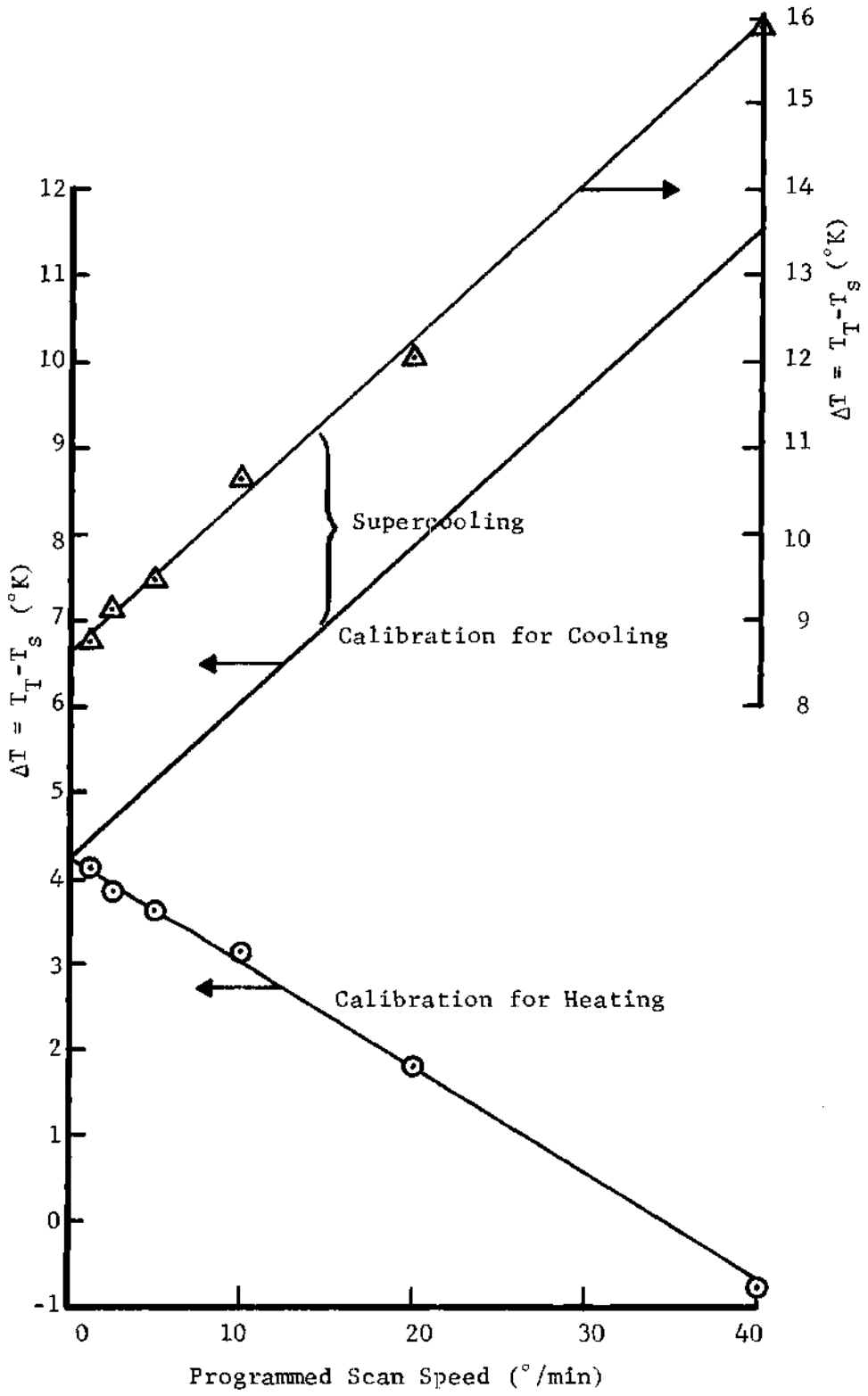

Figure 40. Calibration of Standard Sample Temperature at Lead Transition

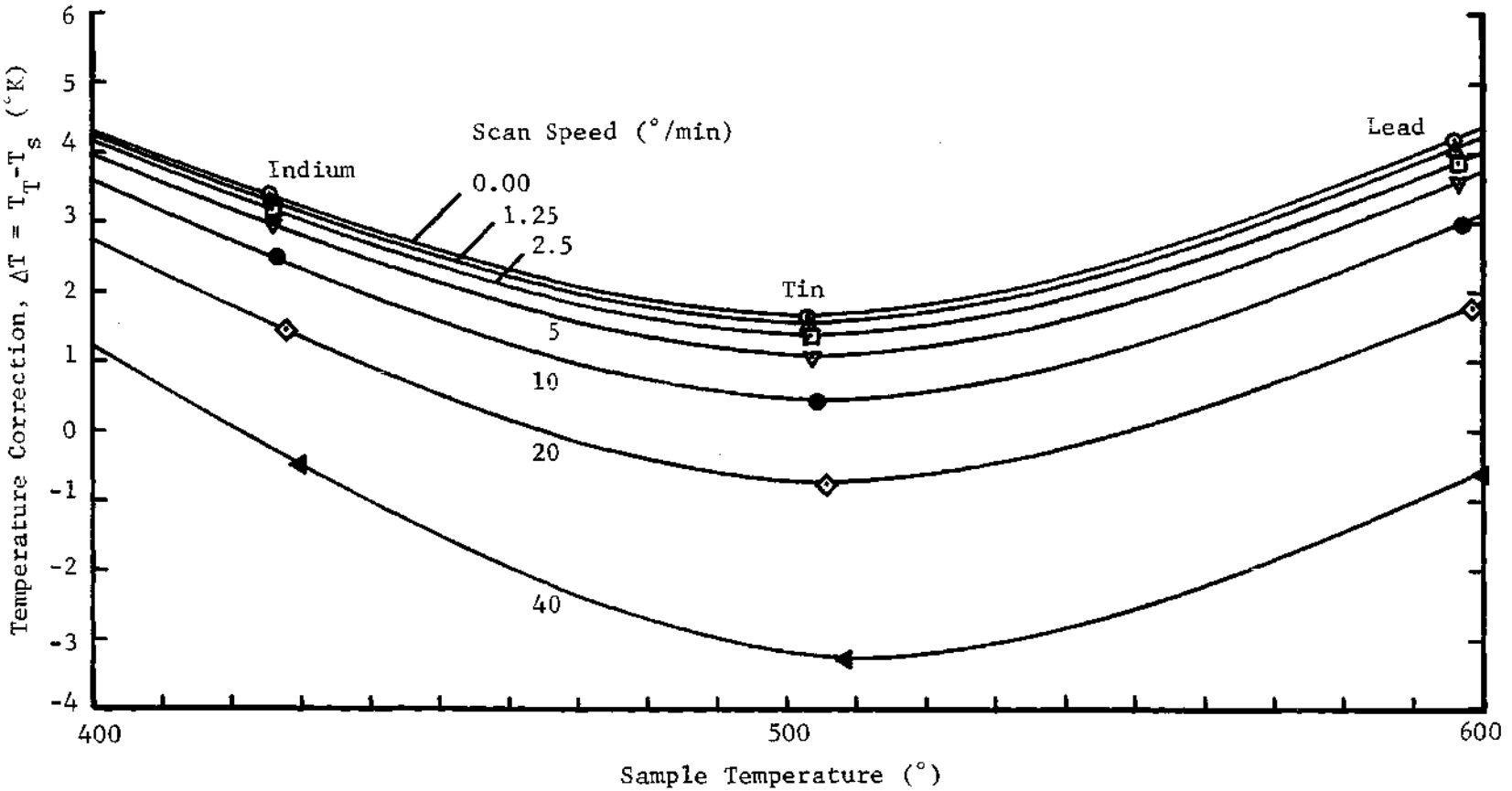

Figure 41. Standard Temperature Calibration and Correction Curves for Various Heating Scan Speeds

appearance of a spike of high amplitude and narrow width. See Figure 42. Thus, correction for thermal lag must be accomplished through sample weight (m_s) and specific heat (C_{p_s}) as follows:

$$T_s = T_p - m_s C_{p_s} \frac{dT_p}{dt} R_o \qquad \text{(D-6)}$$

Fortunately, $m_s C_{p_s} dT_p/dt$ amounts to less than 0.1° and can be neglected, and T_s essentially equals T_p. T_s was determined at six scan speeds for each of the three standards: indium, tin, and lead. If T_s at each scan speed does not correspond to the true solidification temperature (T_T) of that standard sample, it is corrected by an amount equal to their difference:

$$\Delta T = T_T - T_s \ . \qquad \text{(D-7)}$$

Graphs of correction temperature (ΔT) verses scan speed for indium, tin, and lead are shown in Figures 38, 39, and 40 respectively. These correction curves for the cooling mode of operation require an adjustment for the degree of supercooling below the solidification point. For zero scan speed, the temperature correction (ΔT) should be the same for both heating and cooling modes of operation. Since all standard samples were observed to solidify rapidly at all scan speeds, no kinetic adjustment in supercooling has been assumed at any scan speed. Hence, the apparent temperature correction curve has been shifted parallel to itself by an amount equal to the minimum degree of supercooling at zero scan speed to obtain the actual "Calibration for Cooling" curve. A set of correction curves for various cooling scan speeds is shown in Figure 43. Although similar in shape, these temperature correction curves for cooling scan speeds are not a mirror image

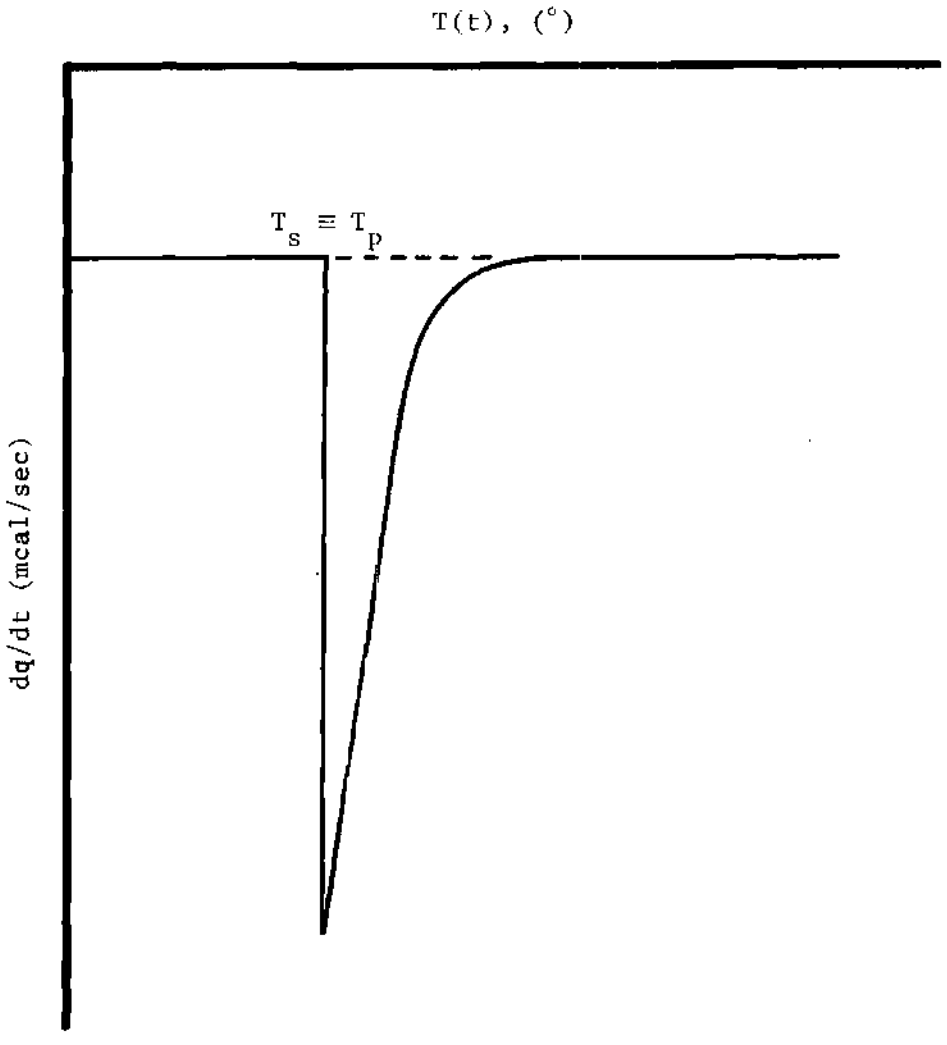

Figure 42. Typical Standard Freezing Thermogram

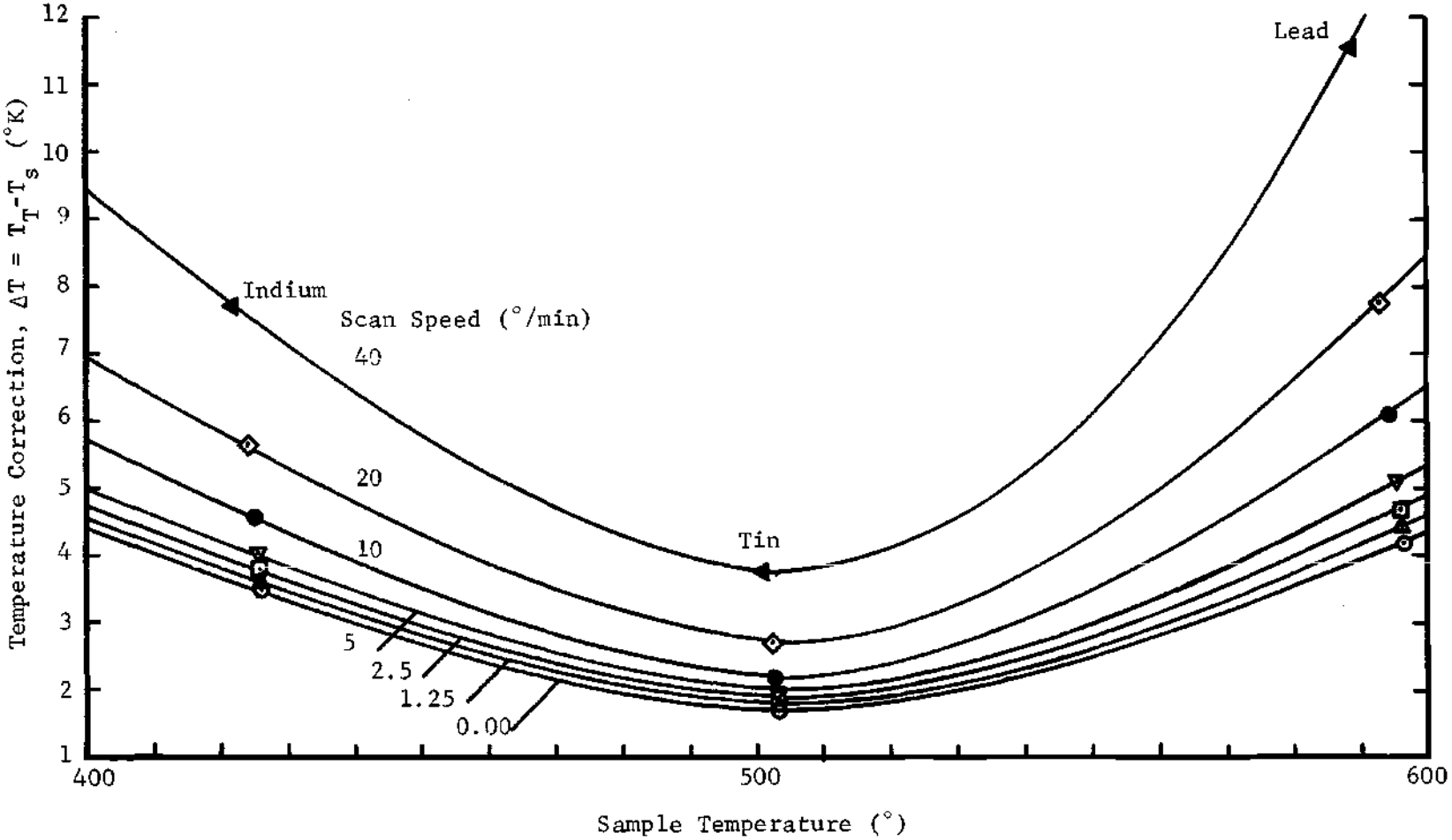

Figure 43. Standard Temperature Calibration and Correction Curves for Various Cooling Scan Speeds

of the correction curves for heating scan speeds. Thus separate sample temperature correction curves must be developed at all desired scan speeds for both heating and cooling modes. Again, this dependence of temperature correction on scan speed has not been generally noted before.

Correction of DSC Thermograms

The temperature correction sequence and impact that these correction and calibration techniques have on heating and cooling thermograms on polymeric materials is illustrated in Figures 44 and 45 respectively. By comparison, the amount of thermal lag in cooling scans is substantially greater than in heating scans (not shown for obvious reasons).

The thermograms shown in Figures 44 and 45 were run without using a heat transfer fluid in the holders in order to maximize the corrections, thus spreading out the various corrected thermograms and making the correction procedure easier to visualize and comprehend. By using a heat transfer fluid to reduce the thermal lag, the thermal resistance correction ($T_p \rightarrow T_s$) is only 1/3 of the amount shown.

Because polymers do not melt or solidify at a specific temperature but do so over a temperature range, only the baseline temperatures bracketing such a range are recorded. Correction for thermal lag crystallization or melting thermograms is accomplished through Equation (D-6) which is repeated here for convenience:

$$T_s = T_p - m_s C_{p_s} \frac{dT_p}{dt} R_o \qquad (D\text{-}6)$$

For any particular polymer, the thermal lag for cooling scans varied from

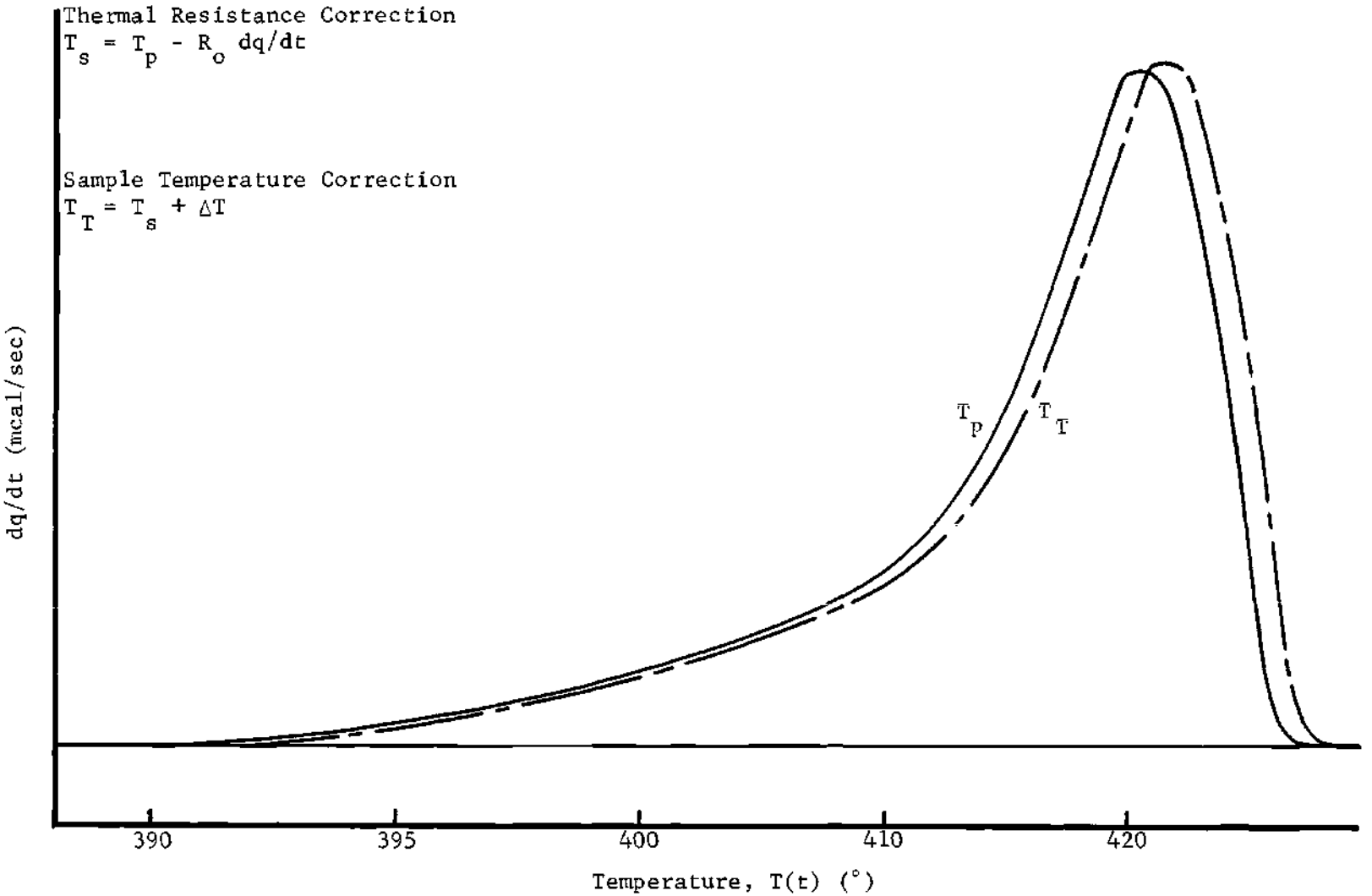

Figure 44. Temperature Correction Sequence and Impact on Melt Thermograms

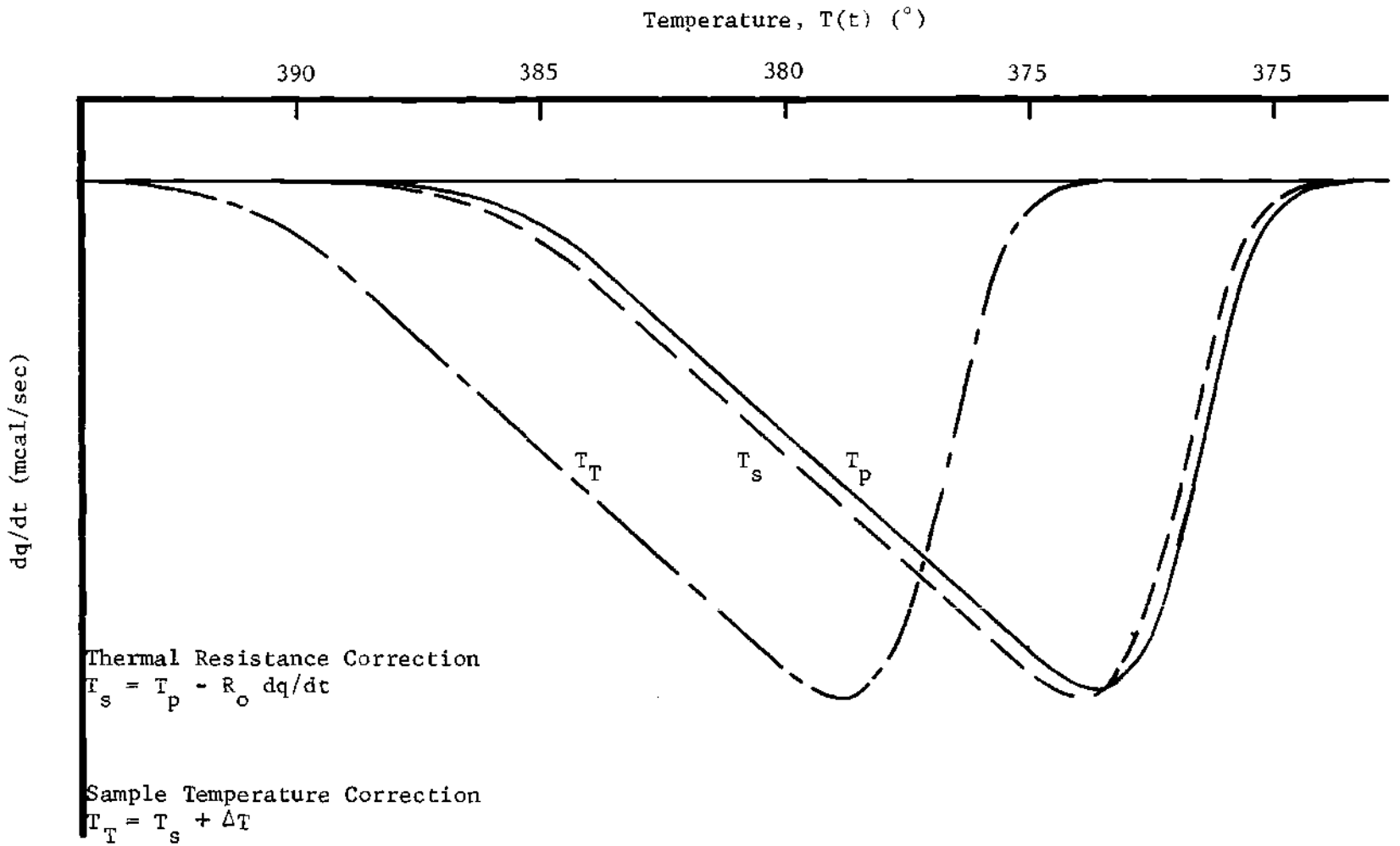

Figure 45. Temperature Correction Sequence and Impact on Cooling Thermograms

$<0.01^{\circ}$ to 0.50°; and for heating scans, <0.1 to 0.30°. Correction for thermal lag in the peak temperature of the cooling scan is handled as follows:

$$T_s = T_p - R_o \frac{dq}{dt} \qquad \text{(D-8)}$$

where dq/dt is the amplitude of the thermogram peak above its baseline. The thermal lag varied from $<0.10^{\circ}$ to $\sim 2.50^{\circ}$.

APPENDIX E

QUANTITATIVE STEREOLOGY

Stereology is the study of the structure of matter in three dimensions at the microscopic level, based on the examination of two dimensional sections through the material. (72)

The analysis of the geometric properties and characteristics of particle and grain elements within bounded surfaces and volumes can be approached in several ways. A grain or particle may be analyzed as a separate entity, and its average properties examined without regard to its surroundings. Alternatively, grains and particles and their surrounding matrix may be considered "in toto" and average properties obtained for the overall aggregate. When considering the bulk properties of a typical planar section containing grains or particles, an average distance through these randomly oriented elements is more meaningful than an overall dimension. Such an averaged distance is the mean intercept length, $\bar{L}_3$, where the subscript refers to the dimensionality of the measured grain or particle. (76) Following is an explanation of the physical nature of $\bar{L}_3$.

Imagine an irregularly shaped, convex grain through which lines are passed at all possible locations and angles. The intercept lengths will vary from zero to a maximum at a particular location and direction. Thus the mean value of the intercept length ($\bar{L}_3$) will lie somewhere between these two extremes. In the case of spherically-shaped particles,

the mean intercept length is equal to two thirds the sphere diameters. (76)

Uniform Spherical Grains

The mean intercept length is defined for a single grain or an aggregate of grains uniform in size as:

$$L_3 = \frac{1}{N} \Sigma (L_3)_i \qquad \text{(E-1)}$$

where $(L_3)_i$ are the intercept lengths measured from N random penetrations of the grains by a straight test line. Based on a relationship developed by Tomkeieff (72,76), the surface-to-volume ratio (S/V) of isolated, convex or concave bodies is related to the mean intercept length through the body by:

$$\bar{L}_3 = 4V/S \qquad \text{(E-2)}$$

In the case of uniform, spherical grains, the diameter is related to the surface-to-volume ratio through:

$$\frac{V}{S} = \frac{D}{6} \qquad \text{(E-3)}$$

Substituting into Equation (E-2) and rearranging gives:

$$D = \frac{3}{2} \bar{L}_3 \qquad \text{(E-4)}$$

Equations (E-1) and (E-4) are sufficient to determine the diameter of isolated, uniform, spherical grains dispersed in a homogeneous phase. This is the case and consequently the technique applied in determining the spherulite diameters of high density polyethylene and poly(ethylene

terephthalate) samples.

Uniform Non-Spherical Grains

In polypropylene, nylon 6, and nylon 66 the spherulite morphology is uniform but non-spherical in shape (space-filling contiguous grains). To satisfy the basic theory of the Avrami and volumetric growth relations, an equivalent sphere diameter must be resolved. For this purpose the mean intercept length is unsatisfactory since it cannot be directly related to a corresponding sphere diameter. The technique used to obtain an equivalent sphere diameter for these three polymers is explained in the ensuing paragraphs.

It is necessary to determine the grain population density (number per unit volume, N_V), and the equivalent diameter (D). The number of grains per volume (N_V) is defined as:

$$N_V = \pi N_A^2/4N_L \qquad \text{(E-5)}$$

and the equivalent diameter is defined as:

$$D = 4N_L/\pi N_A \qquad \text{(E-6)}$$

where N_A is the number of interceptions of grains per unit test area, and N_L is the number of interceptions of grains per length of test line. (76)

For space-filling, contiguous grains, N_A is defined as:

$$N_A = N_T/A_T \qquad \text{(E-7)}$$

with:

$$N_T = N_W + \frac{1}{2} N_i \qquad \text{(E-8)}$$

where N_W is the number of grains lying wholly within the test area A_T, and N_i is the number of grains intercepted by the test area perimeter. If enough perimeter grains are intercepted, on the average, they will be divided in half. (76)

The procedure for a given test area (A_T) is: 1) determine N_W and N_i for calculating N_A, and 2) randomly draw test lines extending completely across the test area to determine N_L.

As defined in Equations (E-5) and (E-6), N_v and D are calculated from statistically exact relationships for grain of regular shapes, thus any discrepency in correlation between N_v and D must be attributable to: 1) limitations in the quantity of experimental data, and 2) the accuracy of magnification corrections applied to the photomicrographs. Since D is one dimensional, less error should result in resolving D. Then a consistent value for N_v can be obtained through:

$$N_v = .74\ (6/\pi\ D^3) \qquad \text{(E-9)}$$

Equation (E-9) is the preferred method for obtaining N_v and has been used in characterizing polypropylene, nylon 6, and nylon 66.

APPENDIX F

CRYSTALLIZATION AND MELT THERMOGRAM DATA

A tabulation of pertinent DSC thermogram data for each of the six polymers under study is given in Tables 6 through 11. For each polymer the data are tabulated relative to the programmed, crystallization scan speed listed in the first column. A zero scan speed denotes isothermal crystallization data. The second column gives the actual sample scan speed at which the data were collected.

Figure 46 illustrates the source of the following quantities reported in the tables for crystallization:

1) T_i, temperature at start of crystallization exotherm
2) T_{peak}, temperature at peak of crystallization exotherm
3) T_F, temperature at finish of crystallization exotherm
4) β, degree of crystallinity up to T_{peak}
5) X_w, total degree of crystallinity up to T_F

Similarly, Figure 47 illustrates the source of the following quantities reported in the tables for melting:

1) T_i, temperature at start of melt endotherm
2) T_F, temperature at finish of melt endotherm
3) X_w, total degree of crystallinity up to T_F

All of the reported data has been corrected according to the procedures

presented in Appendix D.

The accuracy of the experimental data has been determined to be as follows:

1) D_s, $\pm.01$ to $\pm.1$ for 1.25 to 40.°/minute, respectively

2) T_i, $\pm 1.0^{\circ}$

3) T_{peak}, $\pm 1.0^{\circ}$

4) T_F, $\pm 2.0^{\circ}$

5) β, $\pm.02$

6) X_w, $\pm.03$

Table 6. Crystallization and Melt Thermogram Data: High Density Polyethylene

Crystallization Data

Scan Speed (°/min)		Temperature (°K)			Crystallinity	
D_p	D_s	T_i	T_{peak}	T_F	β	X_w
1.25	1.25	398	395	392	.29	.56
2.5	2.41	397	395	389	.33	.64
5.	4.89	397	393	381	.33	.67
10.	9.74	396	391	377	.33	.69
20.	18.7	395	391	362	.34	.72
40.	36.9	395	389	359	.39	.78
0.	0.	395	395	395	.24	.50

Melt Data

Scan Speed (°/min)		Temperature (°K)		Crystallinity
Cryst	Melt	T_i	T_F	X_w
1.25	19.4	389	413	.68
2.5	19.0	385	415	.71
5.	19.1	384	412	.72
10.	19.1	383	410	.72
20.	19.0	382	410	.70
40.	19.0	381	409	.68
0	19.0	385	412	.73

Table 7. Crystallization and Melt Thermogram Data: Polypropylene

Crystallization Data

Scan Speed (°/min)		Temperature (°K)			Crystallinity	
D_p	D_s	T_i	T_{peak}	T_F	β	X_w
1.25	1.21	400	392	387	.32	.49
2.5	2.44	398	388	384	.35	.48
5.	4.90	399	385	381	.35	.47
10.	9.30	395	381	375	.34	.47
20.	18.8	394	377	369	.34	.47
40.	37.6	389	374	362	.30	.47
0.	0.	395	395	395	.28	.50

Melt Data

Scan Speed (°/min)		Temperature (°K)		Crystallinity
Cryst	Melt	T_i	T_F	X_w
1.25	19.0	388	439	.55
2.5	19.3	384	440	.54
5.	19.1	384	441	.51
10.	19.0	384	439	.52
20.	19.0	384	439	.48
40.	19.0	384	440	.47
0.	19.1	396	439	.51

Table 8. Crystallization and Melt Thermogram Data: Poly (ethylene terephthalate), Mylar 700S

Crystallization Data

Scan Speed (°/min)		Temperature (°K)			Crystallinity	
D_p	D_s	T_i	T_{peak}	T_F	β	X_w
1.25	1.23	499	494	490	.09	.18
2.5	2.45	499	491	484	.10	.18
5.	4.64	494	485	479	.11	.20
10.	9.68	489	478	470	.11	.18
20.	19.1	484	469	455	.10	.19
40.	38.1	482	458	437	.12	.24
0.	0.	492	492	492	.13	.27
0.	0.	482	482	482	.13	.29

Melt Data

Scan Speed (°/min)		Temperature (°K)		Crystallinity
Cryst	Melt	T_i	T_F	X_w
1.25	19.9	489	532	.33
2.5	19.9	471	533	.38
5.	19.9	478	536	.34
10.	20.6	490	538	.30
20.	20.2	488	535	.31
40.	19.9	481	535	.33
0.	20.2	492	532	.33
0.	19.9	480	536	.33

Table 9. Crystallization and Melt Thermogram Data: Poly (ethylene terephthalate), Monsanto

Crystallization Data

Scan Speed (°/min)		Temperature (°K)			Crystallinity	
D_p	D_s	T_i	T_{peak}	T_F	β	χ_w
1.25	—	—	—	—	—	—
2.5	2.46	498	488	475	.15	.30
5.	4.80	498	485	467	.13	.30
10.	9.70	492	476	457	.12	.29
20.	19.2	488	471	447	.14	.31
40.	37.5	484	460	421	.13	.33
0.	0.	492	492	492	.11	.30
0.	0.	482	482	482	.10	.27

Melt Trace

Scan Speed (°/min)		Temperature (°K)		Crystallinity
Cryst	Melt	T_i	T_F	χ_w
1.25	—	—	—	—
2.5	20.0	477	542	.34
5.	20.1	479	544	.33
10.	20.2	496	545	.29
20.	20.1	489	543	.30
40.	19.6	481	545	.28
0.	20.0	492	543	.34
0.	19.9	483	542	.30

Table 10. Crystallization and Melt Thermogram Data: Polycaprolactam, Nylon 6

Crystallization Data

Scan Speed (°/min)		Temperature (°K)			Crystallinity	
D_p	D_s	T_i	T_{peak}	T_F	β	x_w
1.25	—	—	—	—	—	—
2.5	2.41	465	455	447	.13	.23
5.	4.82	468	440	440	.22	.33
10.	9.54	465	440	426	.19	.31
20.	19.4	464	433	411	.19	.29
40.	37.4	465	421	392	.19	.30
0.	0.	462	462	462	.11	.26

Melt Data

Scan Speed (°/min)		Temperature (°K)		Crystallinity
Cryst	Melt	T_i	T_F	x_w
1.25	—	—	—	—
2.5	19.8	472	511	.23
5.	20.0	472	517	.26
10.	19.9	471	519	.26
20.	19.6	470	512	.28
40.	19.6	463	511	.28
0.	19.6	464	513	.31

Table 11. Crystallization and Melt Thermogram Data: Poly (hexamethylene adipamide), Nylon 66

Crystallization Data

Scan Speed (°/min)		Temperature (°K)			Crystallinity	
D_p	D_s	T_i	T_{peak}	T_F	β	χ_w
1.25	–	–	–	–	–	–
2.5	2.50	513	501	494	.19	.30
5.	5.00	511	496	488	.19	.29
10.	9.80	512	488	475	.18	.29
20.	19.5	513	486	467	.20	.31
40	38.1	504	474	439	.16	.32
0.	0.	512	512	512	.11	.20

Melt Data

Scan Speed (°/min)		Temperature (°K)		Crystallinity
Cryst	Melt	T_i	T_F	χ_w
1.25	–	–	–	–
2.5	20.2	493	564	.32
5.	20.2	490	554	.34
10.	20.3	489	560	.32
20.	20.4	500	559	.26
40.	20.4	500	563	.29
0.	20.3	501	558	.30

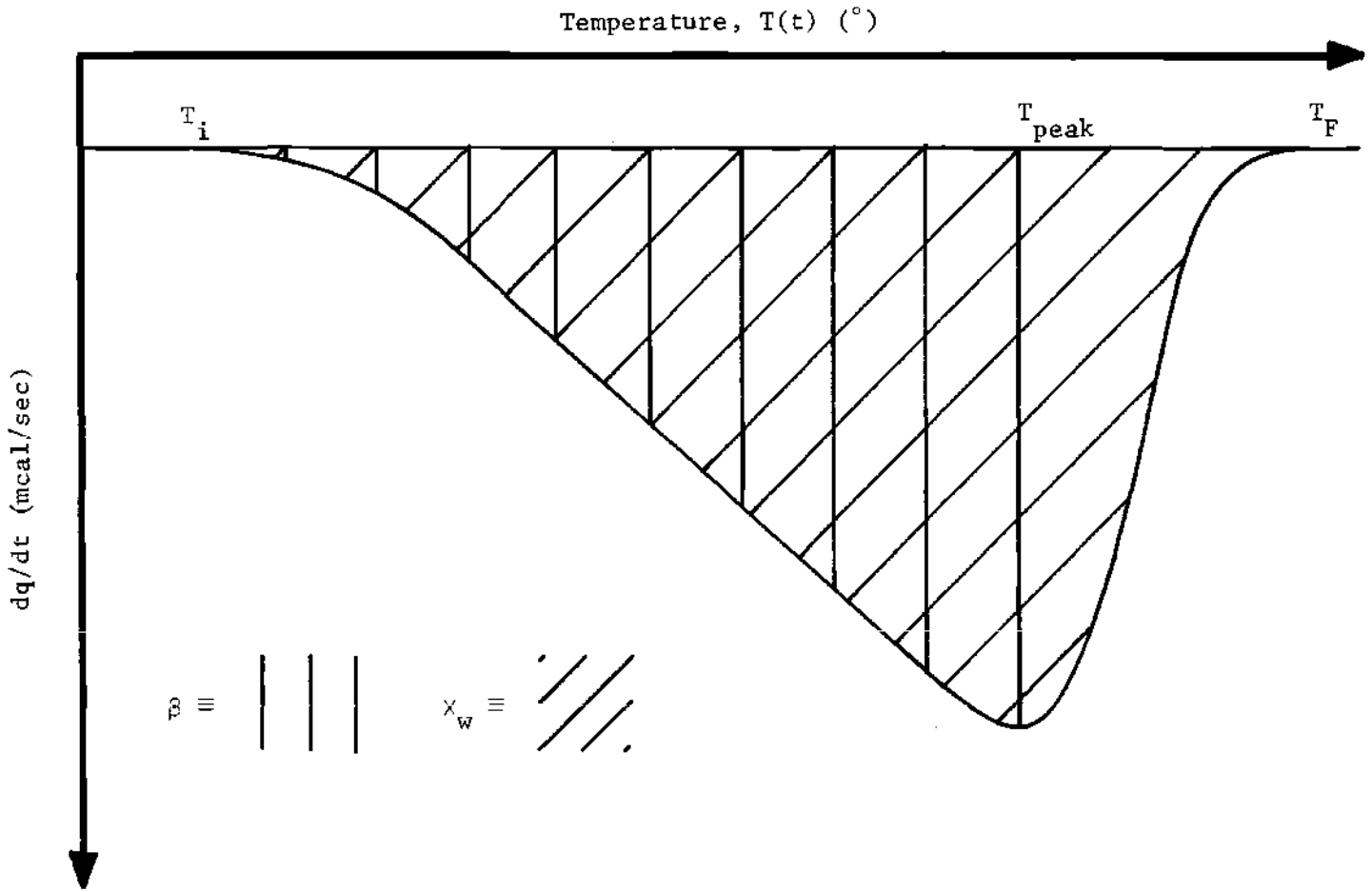

Figure 46. Origin of Crystallization Thermogram Data

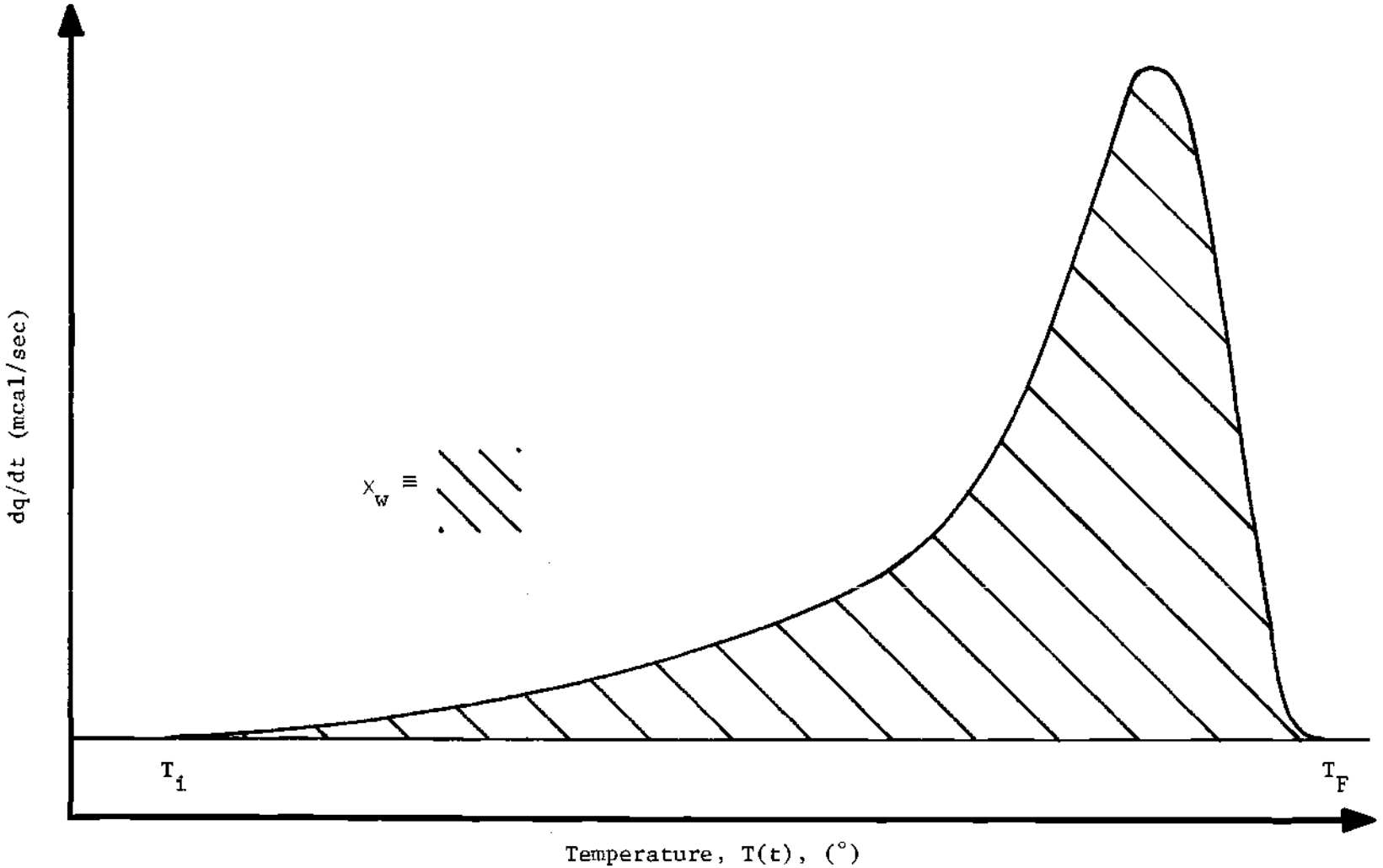

Figure 47. Origin of Melt Thermogram Data

APPENDIX G

DENSITOMETRY DATA

A tabulation of the densitometry data for the polyolefins, polyesters, and polyamides is given in Tables 12, 13, and 14 respectively. The data are tabulated relative to crystallization scan speed, D_p and D_s, to aid in relating crystallinity data (χ_w) calculated from density data to similar data calculated from thermal data given in Appendix F.

Crystallinity was calculated as follows:

$$\chi_w = \frac{\rho - \rho_m}{\rho_c - \rho_m} \qquad \text{(G-1)}$$

where ρ_c and ρ_m are the 100% crystalline and 100% melt densities respectively. They are given for each polymer in Appendix H.

The accuracy of the experimental and calculated data has been determined to be as follows:

1) ρ, $\pm .001$

2) χ_w, $\sim \pm .002$

Table 12. Densitometry Data: Polyolefins

Programmed Scan Speed	High Density Polyethylene			Polypropylene		
D_p (°/min)	D_s (°K/min)	ρ (gm/cc)	X_w	D_s (°K/min)	ρ (gm/cc)	X_w
1.25	1.25	.968	.679	1.21	.910	.606
2.5	2.41	.968	.679	2.44	.909	.592
5.	4.89	.966	.662	4.90	.908	.577
10.	9.74	.964	.647	9.30	.905	.535
20.	18.7	.963	.638	18.8	.903	.507
40.	36.9	.961	.622	37.6	.902	.493
0.	0. (395)	.967	.670	0. (395)	.908	.577

Table 13. Densitometry Data: Polyesters*

Programmed Scan Speed	Mylar 700S			Monsanto Grade		
D_p (°/min)	D_s (°K/min)	ρ (gm/cc)	X_w	D_s (°K/min)	ρ (gm/cc)	X_w
1.25	1.23	1.375	.333	—	—	—
2.5	2.45	1.376	.342	2.46	1.375	.333
5.	4.64	1.375	.333	4.80	1.374	.325
10.	9.68	1.376	.342	9.70	1.370	.292
20.	19.1	1.374	.325	19.2	1.374	.325
40.	38.1	1.374	.325	37.5	1.372	.308
0.	0. (492)	1.376	.342	0. (492)	1.374	.325
0.	0. (482)	1.375	.333	0. (482)	1.374	.317

*Poly(ethylene terephthalates)

Table 14. Densitometry Data: Polyamides

Programmed Scan Speed D_p (°/min)	Nylon 6*			Nylon 66**		
	D_s (°K/min)	ρ (gm/cc)	X_w	D_s (°K/min)	ρ (gm/cc)	X_w
1.25	—	—	—	—	—	—
2.5	2.41	1.134	.353	2.50	1.144	.378
5.	4.82	1.140	.396	5.00	1.142	.367
10.	9.54	1.136	.367	9.80	1.135	.332
20.	19.4	1.131	.332	19.5	1.130	.306
40.	37.4	1.129	.318	38.1	1.124	.276
0.	0. (462)	1.142	.409	0. (512)	1.143	.372

* Polycaprolactam

** Poly(hexamethylene adipamide)

APPENDIX H

QUANTITATIVE STEREOLOGY DATA

It is difficult to assess the accuracy of the spherulite diameters given in the following tables because of limitations in the quantity of experimental data and calculations based on statistically exact relationships.

As discussed in Appendix E, two techniques were used to measure spherulite diameters. For polyethylene and poly(ethylene terephthalate), spherulite size was determined through a technique of measuring the intercept lengths (L_3) of uniform spherical grains. The accuracy can be assess by determining just how accurate L_3 for any particular spherulite can be measured. Thus, the spherulite diameters reported for polyethylene and poly(ethylene terephthalate) has been calculated to have a 5% variation.

Assessment of the accuracy of spherulite diameters reported for polypropylene, nylon 6, and nylon 66 is even more difficult. The technique used for measuring uniform, non-sherical grains involves simply a counting of the number of spherulites within a test area and along test lines. These are explicit measurements. Thus accuracy is solely dependent on the quantity of data taken, size of the test area, and length of test line. All of these parameters were maximized for collecting the stereology data. It was observed that the larger the test area, the smaller was the variation in spherulite size per test area. Based on such data, the spherulite diameters for polypropylene, nylon 6 and 66 have a 6% variation.

Table 15. Impingement Spherulite Diameters: Polyolefins

Programmed Scan Speed D_p (°/min)	High Density Polyethylene D_s (°K/min)	High Density Polyethylene D_i (μ)	Polypropylene D_s (°K/min)	Polypropylene D_i (μ)
1.25	1.25	74	1.21	168
2.5	2.41	70	2.44	176
5	4.89	65	4.90	170
10	9.74	61	9.30	167
20	18.7	62	18.8	144
40	36.9	62	37.6	106
0.	0. (395)	64	0. (395)	147

Table 16. Impingement Spherulite Diameter: Polyesters*

Programmed Scan Speed D_p (°/min)	Mylar 700S D_s (°K/min)	Mylar 700S D_i (μ)	Monsanto Grade D_s (°K/min)	Monsanto Grade D_i (μ)
1.25	1.23	19.	—	—
2.5	2.45	23.	2.45	25.
5.	4.64	—	4.80	—
10.	9.68	20.	9.70	23.
20.	19.1	22.	19.2	—
40.	38.1	—	37.5	17.
0.	0. (492)	20.	0. (492)	—
0.	0. (482)	22.	0. (482)	21.

* Poly(ethylene terephthalate)

Table 17. Impingement Spherulite Diameter: Polyamides

Programmed Scan Speed D_p (°/min)	Nylon 6*		Nylon 66**	
	D_s (°K/min)	D_i (μ)	D_s (°K/min)	D_i (μ)
1.25	—	—	—	—
2.5	2.41	176	2.50	209
5.	4.82	168	5.00	189
10.	9.54	164	9.80	176
20.	19.4	154	19.5	155
40.	37.4	132	38.1	115
0.	0. (462)	169	0. (512)	209

* Polycaprolactam

**Poly(hexamethylene adipamide)

APPENDIX I

POLYMER THERMAL AND PHYSICAL PROPERTIES

The thermal and physical properties — thermodynamic melt temperatures, glass transition, latent heat of crystallization, melt and crystalline densities, monomolecular layer dimensions, and chain fold energies — for each polymer are tabulated in Tables 18-22 with accompanying source references.

The crystalline densities (ρ_c) were calculated from unit cell dimensions and the number of monomer units per unit cell.

The monomolecular layer thickness (b_o) and width (a_o) are assumed to be the nearest distance between carbon atoms in the molecular backbone in different molecules. These distances (a_o and b_o) can be calculated from the unit cell dimensions projected onto the (001) plane. For example, in polyethylene crystal growth by chain folding is in the [110] direction; and hence, a_o and b_o are defined as shown in Figure 48. Since crystal growth directions for the other polymers could not be found, values for a_o and b_o for these polymers were determined through reference to their respective unit cells and by assuming analagous crystal growth patterns.

The surface energy parameters (σ and σ_e) can be determined by a variety of techniques. (34,47) The values selected are all based on experimental determinations of σ_e and/or $\sigma\sigma_e$.

Table 18. Thermal-Physical Properties of High Density Polyethylene

Parameter	Value	Units	Reference
T_m	415.	°K	8
T_g	231.	°K	16
ΔH_c	68.4	cal/gm	6,48,86
ρ_m	.8838	gm/cm^3	34
ρ_c	1.0075	gm/cm^3	9
b_o	4.13×10^{-8}	cm	9
a_o	4.46×10^{-8}	cm	9
σ	10.25	$ergs/cm^2$	*
σ_e	57.0	$ergs/cm^2$	8
$\sigma\sigma_e$	584.0	$ergs^2/cm^4$	34

*calculated

Table 19. Thermal-Physical Properties of Polypropylene

Parameter	Value	Units	Reference
T_m	447.	°K	55
T_g	267.	°K	55
ΔH_c	45.	cal/gm	55
ρ_m	.867	gm/cm^3	82
ρ_c	.938	gm/cm^3	52
b_o	5.40×10^{-8}	cm	52
a_o	3.35×10^{-8}	cm	52
σ	9.54	$ergs/cm^2$	31
σ_e	47.7	$ergs/cm^2$	32
$\sigma\sigma_e$	455.	$ergs^2/cm^2$	*

*calculated

Table 20. Thermal-Physical Properties of Poly(ethylene terephthalate)

Parameter	Value	Units	Reference
T_m	540.	°K	85
T_g	353.	°K	61
ΔH_c	30.	cal/gm	19,67
ρ_m	1.335	gm/cm^3	15,77
ρ_c	1.455	gm/cm^3	15,67,77
b_o	4.04×10^{-8}	cm	15
a_o	5.76×10^{-8}	cm	15
σ	5.	$ergs/cm^2$	85
σ_e	40.	$ergs/cm^2$	85
$\sigma\sigma_e$	200.	$ergs^2/cm^4$	*

*calculated

Table 21. Thermal-Physical Properties of Polycaprolactam, Nylon 6

Parameter	Value	Units	Reference
T_m	505	°K	45
T_g	323	°K	61
ΔH_c	45.3	cal/gm	13,36,45,49
ρ_m	1.0840	gm/cm^3	45,77
ρ_c	1.2255	gm/cm^3	45,77
b_o	8.62×10^{-8}	cm	10
a_o	8.83×10^{-8}	cm	10
σ	8.	$ergs/cm^2$	47
σ_e	60.	$ergs/cm^2$	47
$\sigma\sigma_e$	480.	$ergs^2/cm^4$	47

Table 22. Thermal-Physical Properties of Poly (hexamethylene adipamide), Nylon 66

Parameter	Value	Units	Reference
T_m	545.	°K	47
T_g	330.	°K	77
ΔH_c	46.6	cal/gm	36,49
ρ_m	1.07	gm/cm^3	77
ρ_c	1.266	gm/cm^3	10
b_o	4.77×10^{-8}	cm	10
a_o	4.04×10^{-8}	cm	10
σ	8.5	$ergs/cm^2$	47
σ_e	42.35	$ergs/cm^2$	47
$\sigma\sigma_e$	360.	$ergs^2/cm^4$	47

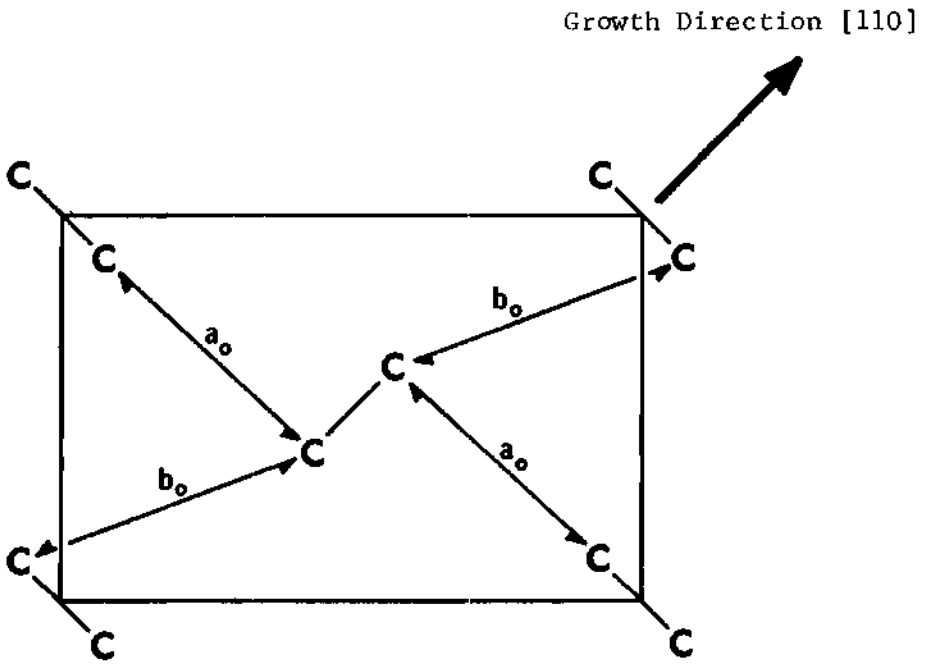

Figure 48. The (001) Plane of the Polyethylene Unit Cell (9)

Table 23. Transient Heat Conduction Data: Polyolefins

Parameter	Value	Units	Reference
High Density Polyethylene			
T_{eject}	360.	°K	*
C_{p_c}	.5	cal/gm/°K	54
C_{p_m}	.6	cal/gm/°K	54
k_p	7.8×10^{-4}	cal·cm/sec/cm^2/°K	57
c_2	171.	°K	*
X_w	.69	–	*
Polypropylene			
T_{eject}	360.	°K	*
C_{p_c}	.5	cal/gm/°K	55
C_{p_m}	.6	cal/gm/°K	55
k_p	3.4×10^{-4}	cal·cm/sec/cm^2/°K	57
c_2	147.	°K	*
X_w	.475	–	*

* Experimental

Table 24. Transient Heat Conduction Data: Polyesters**

Parameter	Value	Units	Reference
	Mylar 700S		
T_{eject}	430.	°K	*
C_{p_c}	.27	cal/gm/°K	77
C_{p_m}	.37	cal/gm/°K	77
k_p	3.7×10^{-4}	cal·cm/sec/cm^2/°K	69
c_2	103.5	°K	*
X_w	.30	–	*
	Monsanto Grade		
T_{eject}	430.	°K	*
C_{p_c}	.27	cal/gm/°K	77
C_{p_m}	.37	cal/gm/°K	77
k_p	3.7×10^{-4}	cal·cm/sec/cm^2/°K	69
c_2	103.5	°K	*
X_w	.28	–	*

* Experimental

** Poly(ethylene terephthalate)

Table 25. Transient Heat Conduction Data: Polyamides

Parameter	Value	Units	Reference
Nylon 6**			
T_{eject}	390.	°K	*
C_{p_c}	.6	cal/gm/°K	18
C_{p_m}	.65	cal/gm/°K	18
k_p	5.0×10^{-4}	cal·cm/sec/cm^2/°K	57
c_2	150	°K	*
χ_w	.29	—	*
Nylon 66***			
T_{eject}	440.	°K	*
C_{p_c}	.65	cal/gm/°K	17
C_{p_m}	.70	cal/gm/°K	17
k_p	5.8×10^{-4}	cal·cm/sec/cm^2/°K	57
c_2	116.5	°K	*
χ_w	.29	—	*

* Experimental

** Polycaprolactam

***Poly(hexamethylene adipamide)

APPENDIX K

COMPUTER PROGRAMS

```
C     CRYSTALLIZATION SIMULATION OF HOMOGENEOUS POLYMERS
C     CRYSTALLINITY THROUGH THE 'MODIFIED' AVRAMI RELATION
C     D. G. BRIGHT
C     GEORGIA INSTITUTE OF TECHNOLOGY;  JUNE, 1975
C
C     POLYMER TEMPERATURE,K - T
C     THERMODYNAMIC MELT TEMPERATURE, K - TM
C     GLASS TRANSITION TEMPERATURE,K - TG
C
C     OVERAL SCAN SPEED, DEG K/MIN - DSO
C     AVE PRIMARY SCAN SPEED, DEG K/MIN - DSAVEP
C     AVE SECONDARY SCAN SPEED, DEG K/MIN - DSAVES
C
C     HEAT OF CRYSTALLIZATION, MCAL/MG - LAMBDA
C     100% CRYSTALLINE DENSITY,GM/CM3 - RHOC
C
C     PRIMARY NUCLEATION CONSTANT - N1
C     SECONDARY NUCLEATION CONSTANT - N2
C
C     DEGREE OF CRYSTALLINITY - CHI
C     MAXIMUM DEGREE OF CRYSTALLINITY - CHIW
C
C     MONOMOLECULAR LAYER THICKNESS,CM - BO
C     MONOMOLECULAR LAYER WIDTH,CM - AO
C     LATERAL SURFACE FOLD ENERGY,ERGS/CM2 - SIGMA
C     END SURFACE FOLD ENERGY,ERG/CM2 - SIGMAE
C     FOLD ENERGY CONSTANTS - A1,A2
C     WLF CONSTANT - B
C     WLF PARAMETER,K - C2
C
C     BOLTZMANN'S CONSTANT, ERG/K - K
C     PLANCK'S CONSTANT,  ERG*SEC - H
C
C     TIME, SECONDS - TIME
C
      REAL LAMBDA,N1,N2,K
      DATA K,H,R ,PI /1.38E-16,6.624E-27,1.987  ,3.14159/
      DATA NCD,NPR /5,6/
      DATA BLANK /'    '/
C
      DIMENSION POLYME(20)
C
      COMMON  GO,A1,A2,B,C,TM,TG,C2,CHIW
C
   10 CONTINUE
      READ (NCD,1000) POLYME
      IF (POLYME(1) .EQ. BLANK) CALL EXIT
      READ (NCD,1100) BO,AO,SIGMA,SIGMAE,TM,TG,LAMBDA,RHOC
      READ (NCD,1100) TP ,TPEAK,TS ,DSO,DSAVEP,DSAVES,TIME1,
     2                TIME2
```

```
      READ (NCD,1100) DI,VO,CHIW,DT,DTIME,N1,N2,C2
C
      BO = BO*1.0E-08
      AO = AO*1.0E-8
      DHC = LAMBDA * 4.186E+07 * RHOC
      VO = VO * 1.0E+05
C
      WRITE (NPR,2000)
      WRITE (NPR,2200) POLYME
      WRITE (NPR,2400) TM,TG,LAMBDA,RHOC,BO,AO,SIGMA,SIGMAE,
     2                 TP,TPEAK,TS,DSO,DSAVEP,DSAVES,CHIW,
     3                 DI,C2,VO,N1,N2
C
C     CONSTANT INITIALIZATION
      A1 = 4.*BO*SIGMA*SIGMAE*TM**2/K/DHC
      A2 = AO*DHC/SIGMA/TM**2
      B = 4120./R
      C = 4./3.*PI*VO
C
C     VARIABLE INITIALIZATION
      TIME = BLANK
      T = TM
      DS = DSO
      DRDT = 0.0
      DRDTR = 0.0
      D = 0.0
      DHDT = 0.0
      DH = 0.0
      CHI = 0.0
      CHIA = 0.0
C
      WRITE (NPR,2000)
      WRITE (NPR,2200) POLYME
      WRITE (NPR,2300)
      WRITE (NPR,2100) TIME,T,DS,DRDT,D,DHDT,DH,CHI,CHIA
C
C
      II = 1
      DUM = ABS(DSO)
      IF = IFIX ((TM-TP )*60./DUM/DT)
      IC = 1
C
C     PRE-CRYSTALLIZATION, MONOMOLECULAR LAYER BUILD-UP
      DO 100 I=II,IF,IC
      T = T + DS*DT/60.
      IF (I .EQ. IF .AND. T .NE. TP)  DT=(T-DS*DT/60.-TP)/
     2                                   ABS(DS)*60.
      IF (I .EQ. IF .AND. I .NE. TP) T = TP
C     INSTANTANEOUS LAMELLAR GROWTH RATE, CM/SEC - DRDT
      GO = BO*K*T/H
```

```
      DRDT = G(T)
C     NET SPHERULITE DIAMETER,MICRONS - D
      D = D + (DRDT+DRDTR)*DT/1.0E-04
      DRDTR = DRDT
      WRITE (NPR,2100) TIME,T,DS,DRDT,D,DHDT,DH,CHI,CHIA
  100 CONTINUE
C
C
C
      II = 1
      DUM = ABS(DSAVEP)
      IF (DSAVEP .NE. 0.0) IF = IFIX((TP -TPEAK)*60./DUM/
     2                                DTIME/2.)
      IF (DSAVEP .EQ. 0.0) IF = IFIX(TIME1/DTIME/2.)
      IF (DSAVEP .EQ. 0.0) DS = 0.0
      IC = 1
C
      DDSDT = 4.*(DSO-DSAVEP)*DSAVEP/(TP -TPEAK)
      TIME = 0.0
      DHDTR = 0.0
C
C     PRIMARY CRYSTALLIZATION
      DO 200 I=II,IF,IC
      TIME = TIME + DTIME
      DS = DS + DDSDT*DTIME/60.
      T = T + DS*DTIME/60.
C     INSTANTANEOUS LAMELLAR GROWTH RATE, CM/SEC - DRDT
      GO = BO*K*T/H
      DRDT = G(T)
C     NET SPHERULITE DIAMETER,MICRONS - D
      D = D + (DRDT+DRDTR)*DTIME/1.0E-04
      DRDTR = DRDT
C     ENTHALPY VIA LATENT HEAT OF CRYSTALLIZATION
      DHDT = RHOC*LAMBDA*DXDT(TIME,T,DS,N1)
C     ACCUMMULATION OF LATENT HEAT OF CRYSTALLIZATION
      DH = DH + DTIME*(DHDT+DHDTR)/2.
      DHDTR = DHDT
C     DEGREE OF CRYSTALLINITY
      CHI = DH/RHOC/LAMBDA
      CHIA = CHIW*(1.-EXP(-C*DRDT**N1*TIME**N1))
      WRITE (NPR,2100) TIME,T,DS,DRDT,D,DHDT,DH,CHI,CHIA
  200 CONTINUE
C
      II = IF + IC
      IF = 2*IF
      IC = 1
C
      DO 300 I=II,IF,IC
      TIME = TIME + DTIME
      DS = DS - DDSDT*DTIME/60.
```

```
      T = T + DS*DTIME/60.
C     INSTANTANEOUS LAMELLAR GROWTH RATE, CM/SEC - DRDT
      GO = BO*K*T/H
      DRDT = G(T)
C     NET SPHERULITE DIAMETER,MICRONS - D
      D = D + (DRDT+DRDTR)*DTIME/1.0E-04
      DRDTR = DRDT
C     ENTHALPY VIA LATENT HEAT OF CRYSTALLIZATION
      DHDT = RHOC*LAMBDA*DADT(TIME,T,DS,N1)
C     ACCUMMULATION OF LATENT HEAT OF CRYSTALLIZATION
      DH = DH + DTIME*(DHDT+DHDTR)/2.
      DHDTR = DHDT
C     DEGREE OF CRYSTALLINITY
      CHI = DH/RHOC/LAMBDA
      CHIA = CHIW*(1.-EXP(-C*DRDT**N1*TIME**N1))
      WRITE (NPR,2100) TIME,T,DS,DRDT,D,DHDT,DH,CHI,CHIA
  300 CONTINUE
C
C
C
      II = 1
      DUM = ABS(DSAVES)
      IF (DSAVES .NE. 0.0) IF = IFIX((TPEAK-TS )*60./DUM/
     2                                DTIME/2.)
      IF (DSAVES .EQ. 0.0) IF = IFIX(TIME2/DTIME/2.)
      IF (DSAVES .EQ. 0.0) DS = 0.0
      IC = 1
C
      DDSDT = 4.*(DSO-DSAVES)*DSAVES/(TPEAK-TS)
C
C     SECONDARY CRYSTALLIZATION
      DO 400 I=II,IF,IC
      TIME = TIME + DTIME
      DS = DS + DDSDT*DTIME/60.
      T = T + DS*DTIME/60.
C     INSTANTANEOUS LAMELLAR GROWTH RATE, CM/SEC - DRDT
      GO = BO*K*T/H
      DRDT = G(T)
C     NET SPHERULITE DIAMETER,MICRONS - D
      D = D + (DRDT+DRDTR)*DTIME/1.0E-04
      DRDTR = DRDT
C     ENTHALPY VIA LATENT HEAT OF CRYSTALLIZATION
      DHDT = RHOC*LAMBDA*DADT(TIME,T,DS,N2)
C     ACCUMMULATION OF LATENT HEAT OF CRYSTALLIZATION
      DH = DH + DTIME*(DHDT+DHDTR)/2.
      DHDTR = DHDT
C     DEGREE OF CRYSTALLINITY
      CHI = DH/RHOC/LAMBDA
      CHIA = CHIW*(1.-EXP(-C*DRDT**N2*TIME**N2))
      WRITE (NPR,2100) TIME,T,DS,DRDT,D,DHDT,DH,CHI,CHIA
```

```
  400 CONTINUE
C
      II = IF + IC
      IF = 2*IF
      IC = 1
C
      DO 500 I=II,IF,IC
      TIME = TIME + DTIME
      DS = DS - DDSDT*DTIME/60.
      T = T + DS*DTIME/60.
C     INSTANTANEOUS LAMELLAR GROWTH RATE, CM/SEC - DRDT
      GO = BO*K*T/H
      DRDT = G(T)
C     NET SPHERULITE DIAMETER,MICRONS - D
      D = D + (DRDT+DRDTR)*DTIME/1.0E-04
      DRDTR = DRDT
C     ENTHALPY VIA LATENT HEAT OF CRYSTALLIZATION
      DHDT = RHOC*LAMBDA*DXDT(TIME,T,DS,N2)
C     ACCUMMULATION OF LATENT HEAT OF CRYSTALLIZATION
      DH = DH + DTIME*(DHDT+DHDTR)/2.
      DHDTR = DHDT
C     DEGREE OF CRYSTALLINITY
      CHI = DH/RHOC/LAMBDA
      CHIA = CHIW*(1.-EXP(-C*DRDT**N2*TIME**N2))
      WRITE (NPR,2100) TIME,T,DS,DRDT,D,DHDT,DH,CHI,CHIA
  500 CONTINUE
      GO TO 10
C
 1000 FORMAT (20A4)
 1100 FORMAT (8F10.0)
 2000 FORMAT (1H1)
 2100 FORMAT (10X,F5.0,F10.2,F10.5,E15.8,3F10.2,2F10.5)
 2200 FORMAT (1H0, 9X,20A4,/)
 2300 FORMAT (10X,'THETA       TS       DS              G,9X,
     A'DIAMETER      DHDT        H          X          XA',/)
 2400 FORMAT(1H0,
     1    9X,'THERMODYNAMIC MELT TEMPERATURE,K          ',E15.8,
     A//,10X,'THERMODYNAMIC GLASS TRANSITION,K         ',E15.8,
     B//,10X,'LATENT HEAT OF CRYSTALLIZATION,MCAL/MG   ',E15.8,
     C//,10X,'100% CRYSTALLINE DENSITY,GM/CM3          ',E15.8,
     D//,10X,'MONOMOLECULAR LAYER THICKNESS,CM         ',E15.8,
     E//,10X,'MONOMOLECULAR LAYER WIDTH,CM             ',E15.8,
     F//,10X,'LATERAL SURFACE FOLD ENERGY,ERGS/CM2     ',E15.8,
     G//,10X,'END SURFACE FOLD ENERGY,ERGS/CM2         ',E15.8,
     H//,10X,'INCIPIENT CRYSTALLIZATION TEMPERATURE,K  ',E15.8,
     I//,10X,'PEAK CRYSTALLIZATION TEMPERATURE,K       ',E15.8,
     J//,10X,'FINAL CRYSTALLIZATION TEMPERATURE,K      ',E15.8,
     K//,10X,'OVERALL SCAN SPEED ,DEG K/MIN            ',E15.8,
     L//,10X,'AVE PRIMARY SCAN SPEED, DEG K/MIN        ',E15.8,
     M//,10X,'AVE SECONDARY SCAN SPEED, DEG K/MIN      ',E15.8,
```

```
     N//,10X,'MAXIMUM CRYSTALLINITY                          ',E15.8,
     O//,10X,'SPHERULITE DIAMETER, MICRONS                   ',E15.8,
     P//,10X,'WLF PARAMETER, DEG K                           ',E15.8,
     Q//,10X,'ACTIVE NUCLEATION SITES/VOLUME,1/CM3           ',E15.8,
     R//,10X,'PRIMARY NUCLEATION CONSTANT                    ',E15.8,
     S//,10X,'SECONDARY NUCLEATION CONSTANT                  ',E15.8)
      END
      FUNCTION DXDT (TIME,T,DS,N)
      REAL N
      COMMON GO,A1,A2,B,C,TM,TR,C2,CHIW
C     DIFFERENTIATED FORM OF THE 'MODIFIED' AVRAMI RELATION
C
      TERM1 = C * (G(T))**N * TIME**N
      TERM2 = 1./TIME
      TERM3 = DS/T/60.
      TERM4 = A1*((2.*TM-3.*T)/T**3/(TM-T)**2)*DS/60.  +
     1        A2*(TM-2.*T)*DS/60.
      IF (T .GE. TR+100.)
     1    TERM5 = B*((2.*(TR+100.)**2-(TR+100.)*(C2+100.))/
     2              (C2+100.)**3)*DS/T/60.
      IF (T .LT. TR+100.)
     1    TERM5 = B*((2.*T**2 - T*(C2+T-TR))/(C2+T-TR)**3)*
     2              DS/T/60.
      TERM6 = EXP(-TERM1)
C
      DXDT = N*CHIW*TERM1*(TERM2+TERM3+TERM4+TERM5)*TERM6
      RETURN
      END
      FUNCTION G (T)
C     THE HOFFMAN GROWTH RATE EXPRESSION
      COMMON GO,A1,A2,B,C,TM,TG,C2
C
      TERM2 = A1/T**2/(TM-T) + 2. - A2*T*(TM-T)
      IF (T .GE. TG+100.) TERM3 = B*(TG+100.)**2/(C2+100.)
     2                            **2/T
      IF (T .LT. TG+100.) TERM3 = B*T**2/(C2+T-TG)**2/T
C
      G = GO * EXP(-TERM2) * EXP(-TERM3)
      RETURN
      END
```

```
C      CRYSTALLIZATION SIMULATION OF HOMOGENEOUS POLYMERS
C      CRYSTALLINITY THROUGH THE VOLUMETRIC GROWTH RELATION
C      D.G. BRIGHT
C      GEORGIA INSTITUTE OF TECHNOLOGY;  JULY, 1975
C
C      POLYMER TEMPERATURE,K - T
C      THERMODYNAMIC MELT TEMPERATURE, K - TM
C      GLASS TRANSITION TEMPERATURE,K - TG
C
C      OVERAL SCAN SPEED, DEG K/MIN - DSO
C      AVE PRIMARY SCAN SPEED, DEG K/MIN - DSAVEP
C      AVE SECONDARY SCAN SPEED, DEG K/MIN - DSAVES
C
C      HEAT OF CRYSTALLIZATION, MCAL/MG - LAMBDA
C      100% CRYSTALLINE DENSITY,GM/CM3 - RHOC
C
C      PRIMARY NUCLEATION CONSTANT - N1
C      SECONDARY NUCLEATION CONSTANT - N2
C
C      DEGREE OF CRYSTALLINITY - CHI
C      MAXIMUM DEGREE OF CRYSTALLINITY - CHIW
C
C      MONOMOLECULAR LAYER THICKNESS,CM - BO
C      MONOMOLECULAR LAYER WIDTH,CM - AO
C      LATERAL SURFACE FOLD ENERGY,ERGS/CM2 - SIGMA
C      END SURFACE FOLD ENERGY,ERG/CM2 - SIGMAE
C      FOLD ENERGY CONSTANTS - A1,A2
C      WLF CONSTANT - B
C      WLF PARAMETER,K - C2
C
C      BOLTZMANN'S CONSTANT, ERG/K - K
C      PLANCK'S CONSTANT,  ERG*SEC - H
C
C      TIME, SECONDS - TIME
C
       REAL LAMBDA,N1,N2,K
       DATA K,H,R ,PI /1.38E-16,6.624E-27,1.987  ,3.14159/
       DATA NCD,NPR /5,6/
       DATA BLANK /'    '/
C
       DIMENSION POLYME(20)
C
       COMMON /AREA1/ PI,CHIW
       COMMON /AREA2/ GO,A1,A2,B,C,TM,TG,C2
C
   10  CONTINUE
       READ (NCD,1000) POLYME
       IF (POLYME(1) .EQ. BLANK) CALL EXIT
       READ (NCD,1100) BO,AO,SIGMA,SIGMAE,TM,TG,LAMBDA,RHOC
       READ (NCD,1100) TP ,TPEAK,TS ,DSO,DSAVEP,DSAVES,TIME1,
```

```
     2                  TIME2
      READ (NCD,1100) DI,VO,CHIW,DT,DTIME,N1,N2,C2
C
      BO = BO*1.0E-08
      AO = AO*1.0E-8
      DHC = LAMBDA * 4.186E+07 * RHOC
      VO = VO * 1.0E+05
C
      WRITE (NPR,2000)
      WRITE (NPR,2200) POLYME
      WRITE (NPR,2400) TM,TG,LAMBDA,RHOC,BO,AO,SIGMA,SIGMAE,
     2                 TP,TPEAK,TS,DSO,DSAVEP,DSAVES,CHIW,
     3                 DI,C2,VO,N1,N2
C
C     CONSTANT INITIALIZATION
      A1 = 4.*BO*SIGMA*SIGMAE*TM**2/K/DHC
      A2 = AO*DHC/SIGMA/TM**2
      B = 4120./R
      C = 4./3.*PI*VO
C
C     VARIABLE INITIALIZATION
      TIME = BLANK
      T = TM
      DS = DSO
      DRDT = 0.0
      DRDTR = 0.0
      D = 0.0
      DHDT = 0.0
      DH = 0.0
      CHI = X(DI,1)
      CHIR = 0.0
      CHIA = 0.0
C
      WRITE (NPR,2000)
      WRITE (NPR,2200) POLYME
      WRITE (NPR,2300)
      WRITE (NPR,2100) TIME,T,DS,DRDT,D,DHDT,DH,CHI,CHIA
C
C
      II = 1
      DUM = ABS(DSO)
      IF = IFIX ((TM-TP )*60./DUM/DT)
      IC = 1
C
C     PRE-CRYSTALLIZATION, MONOMOLECULAR LAYER BUILD-UP
      DO 100 I=II,IF,IC
      T = T + DS*DT/60.
      IF (I .EQ. IF .AND. T .NE. TP)  DT=(T-DS*DT/60.-TP)/
     2                                   ABS(DS)*60.
      IF (I .EQ. IF .AND. T .NE. TP) T = TP
```

```
C       INSTANTANEOUS LAMELLAR GROWTH RATE, CM/SEC - DRDT
        GO = BO*K*T/H
        DRDT = G(T)
C       NET SPHERULITE DIAMETER,MICRONS - D
        D = D + (DRDT+DRDTR)*DT/1.0E-04
        DRDTR = DRDT
C       ACCUMMULATION OF LATENT HEAT OF CRYSTALLIZATION
        DH = RHOC * LAMBDA * X(D,2)
C       DEGREE OF CRYSTALLINITY
        CHI = DH/RHOC/LAMBDA
        CHIA = CHIW*(1.-EXP(-C*DRDT**N1*TIME**N1))
C       ENTHALPY VIA LATENT HEAT OF CRYSTALLIZATION
        DHDT = RHOC * LAMBDA * (CHI-CHIR)/DT
        CHIR = CHI
        WRITE (NPR,2100) TIME,T,DS,DRDT,D,DHDT,DH,CHI,CHIA
  100 CONTINUE
C
C
C
        II = 1
        DUM = ABS(DSAVEP)
        IF (DSAVEP .NE. 0.0) IF = IFIX((TP -TPEAK)*60./DUM/
       2                                        DTIME/2.)
        IF (DSAVEP .EQ. 0.0) IF = IFIX(TIME1/DTIME/2.)
        IF (DSAVEP .EQ. 0.0) DS = 0.0
        IC = 1
C
        DDSDT = 4.*(DSO-DSAVEP)*DSAVEP/(TP -TPEAK)
        TIME = 0.0
        DHDTR = 0.0
C
C       PRIMARY CRYSTALLIZATION
        DO 200 I=II,IF,IC
        TIME = TIME + DTIME
        DS = DS + DDSDT*DTIME/60.
        T = T + DS*DTIME/60.
C       INSTANTANEOUS LAMELLAR GROWTH RATE, CM/SEC - DRDT
        GO = BO*K*T/H
        DRDT = G(T)
C       NET SPHERULITE DIAMETER,MICRONS - D
        D = D + (DRDT+DRDTR)*DTIME/1.0E-04
        DRDTR = DRDT
C       ACCUMMULATION OF LATENT HEAT OF CRYSTALLIZATION
        DH = RHOC * LAMBDA * X(D,2)
C       DEGREE OF CRYSTALLINITY
        CHI = DH/RHOC/LAMBDA
        CHIA = CHIW*(1.-EXP(-C*DRDT**N1*TIME**N1))
C       ENTHALPY VIA LATENT HEAT OF CRYSTALLIZATION
        DHDT = RHOC * LAMBDA * (CHI-CHIR)/DTIME
        CHIR = CHI
```

```
      WRITE (NPR,2100) TIME,T,DS,DRDT,D,DHDT,DH,CHI,CHIA
  200 CONTINUE
C
      II = IF + IC
      IF = 2*IF
      IC = 1
C
      DO 300 I=II,IF,IC
      TIME = TIME + DTIME
      DS = DS - DDSDT*DTIME/60.
      T = T + DS*DTIME/60.
C     INSTANTANEOUS LAMELLAR GROWTH RATE, CM/SEC - DRDT
      GO = BO*K*T/H
      DRDT = G(T)
C     NET SPHERULITE DIAMETER,MICRONS - D
      D = D + (DRDT+DRDTR)*DTIME/1.0E-04
      DRDTR = DRDT
C     ACCUMMULATION OF LATENT HEAT OF CRYSTALLIZATION
      DH = RHOC * LAMBDA * X(D,2)
C     DEGREE OF CRYSTALLINITY
      CHI = DH/RHOC/LAMBDA
      CHIA = CHIW*(1.-EXP(-C*DRDT**N1*TIME**N1))
C     ENTHALPY VIA LATENT HEAT OF CRYSTALLIZATION
      DHDT = RHOC * LAMBDA * (CHI-CHIR)/DTIME
      CHIR = CHI
      WRITE (NPR,2100) TIME,T,DS,DRDT,D,DHDT,DH,CHI,CHIA
  300 CONTINUE
C
C
C
      II = 1
      DUM = ABS(DSAVES)
      IF (DSAVES .NE. 0.0) IF = IFIX((TPEAK-TS )*60./DUM/
     2                                DTIME/2.)
      IF (DSAVES .EQ. 0.0) IF = IFIX(TIME2/DTIME/2.)
      IF (DSAVES .EQ. 0.0) DS = 0.0
      IC = 1
C
      DDSDT = 4.*(DSO-DSAVES)*DSAVES/(TPEAK-TS)
C
C     SECONDARY CRYSTALLIZATION
      DO 400 I=II,IF,IC
      TIME = TIME + DTIME
      DS = DS + DDSDT*DTIME/60.
      T = T + DS*DTIME/60.
C     INSTANTANEOUS LAMELLAR GROWTH RATE, CM/SEC - DRDT
      GO = BO*K*T/H
      DRDT = G(T)
C     NET SPHERULITE DIAMETER,MICRONS - D
      D = D + (DRDT+DRDTR)*DTIME/1.0E-04
```

```
      DRDTR = DRDT
C     ACCUMMULATION OF LATENT HEAT OF CRYSTALLIZATION
      DH = RHOC * LAMBDA * X(D,2)
C     DEGREE OF CRYSTALLINITY
      CHI = DH/RHOC/LAMBDA
      CHIA = CHIW*(1.-EXP(-C*DRDT**N2*TIME**N2))
C     ENTHALPY VIA LATENT HEAT OF CRYSTALLIZATION
      DHDT = RHOC * LAMBDA * (CHI-CHIR)/DTIME
      CHIR = CHI
      WRITE (NPR,2100) TIME,T,DS,DRDT,D,DHDT,DH,CHI,CHIA
  400 CONTINUE
C
      II = IF + IC
      IF = 2*IF
      IC = 1
C
      DO 500 I=II,IF,IC
      TIME = TIME + DTIME
      DS = DS - DDSDT*DTIME/60.
      T = T + DS*DTIME/60.
C     INSTANTANEOUS LAMELLAR GROWTH RATE, CM/SEC - DRDT
      GO = BO*K*T/H
      DRDT = G(T)
C     NET SPHERULITE DIAMETER,MICRONS - D
      D = D + (DRDT+DRDTR)*DTIME/1.0E-04
      DRDTR = DRDT
C     ACCUMMULATION OF LATENT HEAT OF CRYSTALLIZATION
      DH = RHOC * LAMBDA * X(D,2)
C     DEGREE OF CRYSTALLINITY
      CHI = DH/RHOC/LAMBDA
      CHIA = CHIW*(1.-EXP(-C*DRDT**N2*TIME**N2))
C     ENTHALPY VIA LATENT HEAT OF CRYSTALLIZATION
      DHDT = RHOC * LAMBDA * (CHI-CHIR)/DTIME
      CHIR = CHI
      WRITE (NPR,2100) TIME,T,DS,DRDT,D,DHDT,DH,CHI,CHIA
  500 CONTINUE
      GO TO 10
C
 1000 FORMAT (20A4)
 1100 FORMAT (8F10.0)
 2000 FORMAT (1H1)
 2100 FORMAT (10X,F5.0,F10.2,F10.5,E15.8,3F10.2,2F10.5)
 2200 FORMAT (1H0, 9X,20A4,/)
 2300 FORMAT (10X,'THETA       TS       DS              G,9X,
     A'DIAMETER       DHDT         H          X          XA',/)
 2400 FORMAT(1H0,
     1    9X,'THERMODYNAMIC MELT TEMPERATURE,K        ',E15.8,
     A//,10X,'THERMODYNAMIC GLASS TRANSITION,K       ',E15.8,
     B//,10X,'LATENT HEAT OF CRYSTALLIZATION,MCAL/MG ',E15.8,
     C//,10X,'100% CRYSTALLINE DENSITY,GM/CM3        ',E15.8,
```

```
     D//,10X,'MONOMOLECULAR LAYER THICKNESS,CM          ',E15.8,
     E//,10X,'MONOMOLECULAR LAYER WIDTH,CM              ',E15.8,
     F//,10X,'LATERAL SURFACE FOLD ENERGY,ERGS/CM2      ',E15.8,
     G//,10X,'END SURFACE FOLD ENERGY,ERGS/CM2          ',E15.8,
     H//,10X,'INCIPIENT CRYSTALLIZATION TEMPERATURE,K',E15.8,
     I//,10X,'PEAK CRYSTALLIZATION TEMPERATURE,K        ',E15.8,
     J//,10X,'FINAL CRYSTALLIZATION TEMPERATURE,K       ',E15.8,
     K//,10X,'OVERALL SCAN SPEED ,DEG K/MIN             ',E15.8,
     L//,10X,'AVE PRIMARY SCAN SPEED, DEG K/MIN         ',E15.8,
     M//,10X,'AVE SECONDARY SCAN SPEED, DEG K/MIN       ',E15.8,
     N//,10X,'MAXIMUM CRYSTALLINITY                     ',E15.8,
     O//,10X,'SPHERULITE DIAMETER, MICRONS              ',E15.8,
     P//,10X,'WLF PARAMETER, DEG K                      ',E15.8,
     Q//,10X,'ACTIVE NUCLEATION SITES/VOLUME,1/CM3      ',E15.8,
     R//,10X,'PRIMARY NUCLEATION CONSTANT               ',E15.8,
     S//,10X,'SECONDARY NUCLEATION CONSTANT             ',E15.8)
      END
      FUNCTION X (D,I)
      COMMON /AREA1/ PI,CHIW
C
C     THE VOLUMETRIC GROWTH RELATION
C
      GO TO (100,200),I
C     INITIALIZATION
  100 RI = D/2.
      RM = SQRT(2.) * RI
      HI = (1. - SQRT(2.)/2.) * RI
      VSI = PI * HI**2 * (3.*RI - HI) / 3.
      VCI = PI * (RM - (RI-HI))**3 / 3.
      VII = VCI - VSI
      VT = 4./3.*PI*RI**3 + 1.03*6.*VII
      X = 0.0
      RETURN
C
  200 IF (D/2. .GT. RI) GO TO 300
C
C     SPHERULITE GROWTH TO IMPINGEMENT
      R = D/2.
      V = 4./3.*PI*R**3
      X = CHIW * V/VT
      RETURN
C     SPHERULITE GROWTH INTO INTER-SPHERULITIC REGIONS
  300 R = D/2.
      IF (R .GT. RM) R = RM
      H = (RI - SQRT(R**2 - RI**2))/SQRT(2.) - (RM - R)
      VS = PI * H**2 * (3.*R - H) / 3.
      VC = PI * (RM - (R-H))**3 / 3.
      VI = VC - VS
      V = 4./3.*PI*RI**3 + 1.03*6.*(VII - VI)
      X = CHIW * V/VT
```

```
      RETURN
      END
      FUNCTION G (T)
      COMMON /AREA2/ GO,A1,A2,B,C,TM,TG,C2
C
C     THE HOFFMAN GROWTH RATE EXPRESSION
      TERM2 = A1/T**2/(TM-T) + 2. - A2*T*(TM-T)
      IF (T .GE. TG+100.) TERM3 = B*(TG+100.)**2/(C2+100.)
     2                            **2/T
      IF (T .LT. TG+100.) TERM3 = B*T**2/(C2+T-TG)**2/T
C
      G = GO * EXP(-TERM2) * EXP(-TERM3)
      RETURN
      END
```

```
C      TRANSIENT HEAT CONDUCTION IN BULK SOLIDIFIED POLYMERS
C      D.G. BRIGHT
C      GEORGIA INSTITUTE OF TECHNOLOGY;  AUGUST, 1975
C
C      POLYMER TEMPERATURE,K - T
C      THERMODYNAMIC MELT TEMPERATURE,K - TM
C      GLASS TRANSITION TEMPERATURE,K - TG
C      COOLANT TEMPERATURE,K - TC
C      EJECTION TEMPERATURE,K - TEJECT
C
C      POLYMER SCAN SPEED,K/MINUTE - DS
C
C      LATENT HEAT OF CRYSTALLIZATION,MCAL/G - LAMBDA
C      100% CRYSTALLINE SPECIFIC HEAT,CAL/GM/K - CPC
C      100% MELT SPECIFIC HEAT,CAL/GM/K - CPM
C
C      100% CRYSTALLINE DENSITY,GM/CM3 - RHOC
C      100% MELT DENSITY,GM/CM3 - RHOM
C
C      DEGREE OF CRYSTALLINITY - CHI
C      MAXIMUM DEGREE OF CRYSTALLINITY - CHIW
C
C      MONOMOLECULAR LAYER THICKNESS,CM - BO
C      MONOMOLECULAR LAYER WIDTH,CM - AO
C      LATERAL SURFACE FOLD ENERGY,ERGS/CM2 - SIGMA
C      END SURFACE FOLD ENERGY,ERG/CM2 - SIGMAE
C      FOLD ENERGY CONSTANTS - A1,A2
C      WLF CONSTANT - B
C      WLF PARAMETER,K - C2
C
C      BOLTZMANN'S CONSTANT, ERG/K - K
C      PLANCK'S CONSTANT,  ERG*SEC - H
C
C      TIME, SECONDS - TIME
C
       REAL LAMBDA,KP,KMW,K
C
       COMMON /AREA1/ BO,K,H,A1,A2,B,TM,TG,C2
       COMMON /AREA2/ NX,T(25,2),DC(25),TC
       COMMON /AREA3/ AC(25),BC(25),CC(25)
       COMMON /AREA4/ RHOC,RHOM,CPC,CPM,LAMBDA
       COMMON /AREA5/ KP,KMW,DXP,DXMW,HI
       COMMON /AREA6/ DTIME,DS(25),DRDTR(25),D(25),CHIR(25),
     1                KEY(25),DRDTT
       COMMON /AREA7/ CHIW,PI
C
       DATA K,H,R ,PI /1.38E-16,6.624E-27,1.987  ,3.14159/
       DATA NCD,NPR /5,6/
       DATA BLANK /'    '/
C
```

```
      DIMENSION POLYME(20)
C
   10 CONTINUE
      READ (NCD,1000) POLYME
      IF (POLYME(1) .EQ. BLANK) CALL EXIT
      READ (NCD,1100) BO,AO,SIGMA,SIGMAE,TM,TG,LAMBDA,CHIW
      READ (NCD,1100) RHOC,RHOM,CPC,CPM
      READ (NCD,1100) KP,KMW,DXP,DXMW,HI
      READ (NCD,1100) TC,TEJECT,XN,DTIME,TIME,C2,DRDTT
C
      II = 1
      IF = IFIX(TIME)
      IC = IFIX(DTIME)
      NX = IFIX(XN)
      KPRINT = 5
C
C     CONSTANT INITIALIZATION
      AO = AO*1.0E-8
      BO = BO*1.0E-08
      DHC = LAMBDA * 4.186E+07 * RHOC
      A1 = 4.*BO*SIGMA*SIGMAE*TM**2/K/DHC
      A2 = AO*DHC/SIGMA/TM**2
      B = 4120./R
      KP = KP * 1.0E-04
      KMW = KMW * 1.0E-04
      HI = HI * 1.0E-04
      DRDTT = DRDTT * 1.0E-05
C
      WRITE (NPR,2100)
      WRITE (NPR,2200) POLYME
      WRITE (NPR,2400) TM,TG,LAMBDA,CPC,CPM,RHOC,RHOM,CHIW,
     1                 BO,AO,SIGMA,SIGMAE,C2
      WRITE (NPR,2500) KP,KMW,DXP,DXMW,HI,DRDTT,TC,TEJECT
C
C     VARIABLE INITIALIZATION
      TIME = 0.0
      DO 100 I=1,NX
      T(I,1) = TM
      DS(I) = 0.0
      D(I) = 0.0
      KEY(I) = 0
      DRDTR(I) = 0.0
      CHIR(I) = 0.0
  100 CONTINUE
C
      WRITE (NPR,2100)
      WRITE (NPR,2000) TIME
      WRITE (NPR,2000) (T(I,1),I=1,NX)
      WRITE (NPR,2000) (DS(I),I=1,NX)
      WRITE (NPR,2000) (D(I),I=1,NX)
```

```
      WRITE (NPR,2000) (CHIR(I),I=1,NX)
C
      DO 400 J=IT,IF,IC
      TIME = TIME + DTIME
      CALL ABCC
      CALL DCOEFF
      CALL ALGOR
      CALL DTDT
      IF (J .NE. KPRINT .AND. T(NX,2) .GT. TEJECT) GO TO 400
      KPRINT = KPRINT + 5
      WRITE (NPR,2000) TIME
      WRITE (NPR,2000) (T(I,2),I=1,NX)
      WRITE (NPR,2000) (DS(I),I=1,NX)
      WRITE (NPR,2000) (D(I),I=1,NX)
      WRITE (NPR,2000) (CHIR(I),I=1,NX)
      IF (T(NX,2) .LE. TEJECT) GO TO 10
  400 CONTINUE
      GO TO 10
C
 1000 FORMAT (20A4)
 1100 FORMAT (8F10.0)
 2000 FORMAT (12F10.3)
 2100 FORMAT (1H1)
 2200 FORMAT (1H0, 9X,20A4,/)
 2400 FORMAT (1H0,
     1    9X,'THERMODYNAMIC MELT TEMPERATURE,K          ',E15.8,
     A//,10X,'THERMODYNAMIC GLASS TRANSITION,K          ',E15.8,
     B//,10X,'LATENT HEAT OF CRYSTALLIZATION,MCAL/MG    ',E15.8,
     C//,10X,'100% CRYSTALLINE CP,CAL/GM/K              ',E15.8,
     D//,10X,'100% MELT CP,CAL/GM/K                     ',E15.8,
     E//,10X,'100% CRYSTALLINE DENSITY,GM/CM3           ',E15.8,
     F//,10X,'100% MELT DENSITY,GM/CM3                  ',E15.8,
     G//,10X,'MAXIMUM CRYSTALLINITY                     ',E15.8,
     H//,10X,'MONOMOLECULAR LAYER THICKNESS,CM          ',E15.8,
     I//,10X,'MONOMOLECULAR LAYER WIDTH,CM              ',E15.8,
     J//,10X,'LATERAL SURFACE FOLD ENERGY,ERGS/CM2      ',E15.8,
     K//,10X,'END SURFACE FOLD ENERGY,ERGS/CM2          ',E15.8,
     L//,10X,'WLF PARAMETER,K                           ',E15.8)
 2500 FORMAT (
     1 /,10X,'POLYMER K,CAL*CM/SEC/CM2/K                ',E15.8,
     A//,10X,'MOLD WALL K,CAL*CM/SEC/CM2/K              ',E15.8,
     B//,10X,'POLYMER SLAB INCREMENT,CM                 ',E15.8,
     C//,10X,'MOLD WALL THICKNESS,CM                    ',E15.8,
     D//,10X,'HEAT TRANSFER COEFF,CAL/SEC/CM2/K         ',E15.8,
     E//,10X,'INSTANTANEOUS TEST GROWTH RATE,CM/SEC     ',E15.8,
     F//,10X,'COOLANT TEMPERATURE,K                     ',E15.8,
     G//,10X,'EJECTION TEMPERATURE,K                    ',E15.8)
      END
```

```
      SUBROUTINE ABCC
      REAL KP,KMW
      COMMON /AREA2/ NX
      COMMON /AREA3/ AC(25),BC(25),CC(25)
      COMMON /AREA4/ RHOC,RHOM,CPC,CPM
      COMMON /AREA5/ KP,KMW,DXP,DXMW,HI
      COMMON /AREA6/ DTIME,DS(25),DRDTR(25),D(25),CHIR(25)
      COMMON /AREA7/ CHIW
C
      DO 500 I=1,NX
C
      RHO = RHOC*CHIR(I)/CHIW + RHOM*(CHIW-CHIR(I))/CHIW
      CP = CPC*CHIR(I)/CHIW + CPM*(CHIW-CHIR(I))/CHIW
C
C     CALCULATE CONSTANTS IN MATRIX EQUATIONS
      ALPHA = KP/RHO/CP
      UPSILO = ALPHA*DTIME/DXP**2
      PSI = (1.+KMW/HI/DXMW)*(KP/KMW*DXMW/2./DXP)
C
C     CALCULATE MATRIX COEFFICIENTS
      IF (I .GT. 1) GO TO 200
      AC(1) = 0.0
      BC(1) = -(2.+2.*UPSILO+UPSILO/PSI)
      CC(1) = 2.*UPSILO
      GO TO 500
  200 IF (I .EQ. NX) GO TO 300
      AC(I) = UPSILO
      BC(I) = -(2.+2.*UPSILO)
      CC(I) = UPSILO
      GO TO 500
  300 CONTINUE
      AC(NX) = 2.*UPSILO
      BC(NX) = -(2.+2.*UPSILO)
      CC(NX) = 0.0
  500 CONTINUE
      RETURN
      END
      SUBROUTINE DCOEFF
      REAL LAMBDA,KP,KMW
C
      COMMON /AREA1/ BO,K,N,A1,A2,B,TM,TG,C2
      COMMON /AREA2/ NX,T(25,2),DC(25),TC
      COMMON /AREA4/ RHOC,RHOM,CPC,CPM,LAMBDA
      COMMON /AREA5/ KP,KMW,DXP,DXMW,HI
      COMMON /AREA6/ DTIME,DS(25),DRDTR(25),D(25),CHIR(25),
     1               KEY(25),DRDTT
      COMMON /AREA7/ CHIW
C
      DIMENSION DIR(25)
C
```

```
      DO 400 I=1,NX
      DUM1 = T(I,1)
      IF (T(I,1) .GE. TM) GO TO 300
C     INSTANTANEOUS LAMELLAR GROWTH RATE,CM/SEC - DRDT
      DRDT = G(DUM1)
C
      IF (DRDT .GE. DRDTT .AND. KEY(I) .EQ. 1) GO TO 100
      IF (DRDT .LT. DRDTT .AND. KEY(I) .EQ. 1) GO TO 100
      IF (DRDT .LT. DRDTT .AND. KEY(I) .EQ. 0) GO TO 200
C     IMPINGEMENT DIAMETER,MICRONS - DI
      DUM2 = DS(I)
      DUM2 = ABS(DUM2)
      DI = DIAMET(DUM2)
      DIR(I) = DI
      CHI = X(DI,1,I)
      KEY(I) = 1
C
  100 CONTINUE
C     NET SPHERULITE DIAMETER,MICRONS - D
      D(I) = D(I) + (DRDT+DRDTR(I))*DTIME/1.0E-04
      DRDTR(I) = DRDT
      IF (D(I) .GT. SQRT(2.)*DIR(I)) D(I) = SQRT(2.)*DIR(I)
      DUM3 = D(I)
C     DEGREE OF CRYSTALLINITY - CHI
      CHI = X(DUM3,2,I)
C     INSTANTANEOUS HEAT GENERATION RATE,CAL/CM3/SEC - DHDT
      DHDT = RHOC*LAMBDA*(CHI-CHIR(I))/DTIME
      GO TO 400
C
  200 CONTINUE
      DRDTR(I) = DRDT
  300 CONTINUE
      DHDT = 0.0
C
  400 CONTINUE
      RHO = RHOC*CHIR(I)/CHIW + RHOM*(CHIW-CHIR(I))/CHIW
      CP = CPC*CHIR(I)/CHIW + CPM*(CHIW-CHIR(I))/CHIW
      ALPHA = KP/RHO/CP
      UPSILO = ALPHA*DTIME/DXP**2
      PSI = (1.+KMW/HI/DXMW)*(KP/KMW*DXMW/2./DXP)
      CHIR(I) = CHI
C
      IF (I .EQ. 1)
     2   DC(I) = -(2.-2.*UPSILO-UPSILO/PSI)*T(I,1) -
     3           2.*UPSILO*T(I+1,1) - 2.*UPSILO/PSI*TC -
     4                                2.*DHDT    *DTIME/RHO/CP
      IF (I .GT. 1 .AND. I .LT. NX)
     2   DC(I) = -UPSILO*T(I-1,1) - (2.-2.*UPSILO)*T(I,1)
     3           -UPSILO*T(I+1,1) -2.*DHDT    *DTIME/RHO/CP
      IF (I .EQ. NX)
```

```
     2   DC(I) = -2.*UPSILO*T(I-1,1) - (2.-2.*UPSILO)*T(I,1)
     3           -2.*DHDT    *DTIME/RHO/CP
  500 CONTINUE
      RETURN
      END
      FUNCTION X (D,J,I)
      COMMON /AREA7/ CHIW,PI
C
      DIMENSION RI(25),RM(25),VII(25),VT(25)
C
C     THE VOLUMETRIC GROWTH RELATION
      GO TO (100,200),J
C     INITIALIZATION
  100 RI(I) = D/2.
      RM(I) = SQRT(2.) * RI(I)
      HI = (1.-SQRT(2.)/2.) * RI(I)
      VSI = PI * HI**2 * (3.*RI(I) - HI) / 3.
      VCI = PI * (RM(I) - (RI(I) - HI))**3 / 3.
      VII(I) = VCI - VSI
      VT(I) = 4./3.*PI*RI(I)**3 + 1.03*6.*VII(I)
      X = 0.0
      RETURN
C
  200 IF (D/2. .GT. RI(I)) GO TO 300
C
C     SPHERULITE GROWTH TO IMPINGEMENT
      R = D/2.
      V = 4./3.*PI*R**3
      X = CHIW * V/VT(I)
      RETURN
C
C     SPHERULITE GROWTH INTO INTER-SPHERULITIC REGIONS
  300 R = D/2.
      IF (R .GT. RM(I)) R = RM(I)
      H = (RI(I)-SQRT(R**2-RI(I)**2))/SQRT(2.) - (RM(I)-R)
      VS = PI * H**2 * (3.*R - H) / 3.
      VC = PI * (RM(I) - (R-H))**3 / 3.
      VI = VC - VS
      V = 4./3.*PI*RI(I)**3 + 1.03*6.*(VII(I)-VI)
      X = CHIW * V/VT(I)
      RETURN
      END
      FUNCTION G (T)
      REAL K
      COMMON /AREA1/ BO,K,H,A1,A2,B,TM,TG,C2
C
C     THE HOFFMAN GROWTH RATE EXPRESSION
      TERM1 = BO*K*T/H
      TERM2 = A1/T**2/(TM-T) + 2. - A2*T*(TM-T)
      IF (T .GE. TG+100.) TERM3 = B*(TG+100.)**2/(C2+100.)
```

```
     2                                  **2/T
      IF (T .LT. TG+100.) TERM3 = B*T**2/(C2+T-TG)**2/T
C
      G = TERM1 * EXP(-TERM2) * EXP(-TERM3)
      RETURN
      END
      SUBROUTINE ALGOR
      COMMON /AREA2/ NX,T(25,2),DC(25)
      COMMON /AREA3/ AC(25),BC(25),CC(25)
C
      DIMENSION BETA(25),GAMMA(25)
C
C     THE SOLUTION ALGORITHM
C     CALCULATE RECURSION PARAMETERS
      BETA(1) = BC(1)
      GAMMA(1) = DC(1)/BETA(1)
      DO 100 I=2,NX
      BETA(I) = BC(I)-AC(I)*CC(I-1)/BETA(I-1)
      GAMMA(I) =(DC(I)-AC(I)*GAMMA(I-1))/BETA(I)
  100 CONTINUE
C
C     CALCULATE TEMPERATURES
      T(NX,2) = GAMMA(NX)
      NDUM = NX - 1
      DO 200 II=1,NDUM
      I = NX - II
      T(I,2) = GAMMA(I) -CC(I)*T(I+1,2)/BETA(I)
  200 CONTINUE
      RETURN
      END
      SUBROUTINE DTDT
      COMMON /AREA2/ NX,T(25,2)
      COMMON /AREA6/ DTIME,DS(25)
C
C     POLYMER COOLING SCAN SPEED
      DO 100 I=1,NX
      DS(I) = (T(I,2)-T(I,1))/DTIME*60.
      T(I,1) = T(I,2)
  100 CONTINUE
      RETURN
      END
```

```
      FUNCTION DIAMET(DS)
C     SPHERULITE IMPINGEMENT DIAMETER, MICRONS
C     HIGH DENSITY POLYETHYLENE, MARLEX 6050
      DIAMET = 62.
      IF (DIAMET .LT. 1.0) DIAMET = 1.0
      RETURN
      END
      FUNCTION DIAMET(DS)
C     SPHERULITE IMPINGEMENT DIAMETER, MICRONS
C     POLYPROPYLENE, MARLEX HGZ-050-02
      DIAMET = 180.7 - 1.940*DS
      IF (DIAMET .LT. 1.0) DIAMET = 1.0
      RETURN
      END
      FUNCTION DIAMET(DS)
C     SPHERULITE IMPINGEMENT DIAMETER, MICRONS
C     POLY(ETHYLENE TEREPHTHALATE), DU PONT MYLAR 700S
      DIAMET = 21.
      IF (DIAMET .LT. 1.0) DIAMET = 1.0
      RETURN
      END
      FUNCTION DIAMET(DS)
C     SPHERULITE IMPINGEMENT DIAMETER, MICRONS
C     POLY(ETHYLENE TEREPHTHALATE), MONSANTO FIBER GRADE
      DIAMET = 25.7 - .242*DS
      IF (DIAMET .LT. 1.0) DIAMET = 1.0
      RETURN
      END
      FUNCTION DIAMET(DS)
C     SPHERULITE IMPINGEMENT DIAMETER, MICRONS
C     POLYCAPROLACTUM, NYLON 6, ALLIED CHEMICAL 'PLASKON'
      DIAMET = 173.5 - 1.107*DS
      IF (DIAMET .LT. 1.0) DIAMET = 1.0
      RETURN
      END
      FUNCTION DIAMET(DS)
C     SPHERULITE IMPINGEMENT DIAMETER, MICRONS
C     POLY(HEXAMETHYLENE ADIPAMIDE), NYLON 66,
C     DU PONT 'ZYTEL'
      DIAMET = 198. - 2.178*DS
      IF (DIAMET .LT. 1.0) DIAMET = 1.0
      RETURN
      END
```

BIBLIOGRAPHY

1. Adams, J.A. and D.F. Rogers, "Transient Conduction," Computer-Aided Heat Transfer Analysis, McGraw-Hill: New York (1973) pp. 176-209.

2. Annual Book of ASTM Standards, Part 35, ASTM: Philadelphia (1975) pp. 475-80.

3. Avrami, M., "Kinetics of Phase Change. I General Theory," J. Chem. Phys., 7, 1103-12 (1939).

4. Avrami, M., "Kinetics of Phase Change. II Transformation - Time Relation for Random Distribution of Nuclei," J. Chem. Phys., 8, 212-24 (1940).

5. Avrami, M., "Kinetics of Phase Change. III Granulation, Phase Change, and Microstructure," J. Chem. Phys., 9, 177-84 (1941).

6. Bair, H.E., T.W. Huseby, and R. Salovey, "Equilibrium Melting Temperature and Surface Free Energy of Polyethylene Single Crystals," Am. Chem. Soc. J., 9 (1), 795-805 (1968).

7. Brennan, W.P., et al., "Thermal Resistance Factor in Differential Scanning Calorimetry," Analytical Calorimetry, 2, edited by R.S. Porter and J.F. Johnson, Plenum Press: New York (1968) pp. 441-54.

8. Brown, R.G. and R.K. Eby, "Effect of Crystallization Conditions and Heat Treatment on Polyethylene: Lamellar Thickness, Melting Temperature, and Density," J. Appl. Phys., 35 (4), 1156-61 (1964).

9. Bunn, C.W., "The Crystal Structure of Long-Chain Normal Paraffin Hydrocarbons. The 'Shape' of the $>CH_2$ Groups." Trans. Faraday Soc., 35, 482-91 (1939).

10. Bunn, C.W. and E.V. Garner, "The Crystal Structures of Two Polyamides (Nylons)," Proc. Royal Soc. (London), 189A, 39-49 (1947).

11. Carnahan, B., H.A. Luther, and J.O. Wilkes, Applied Numerical Methods, Wiley: New York (1969) pp. 429-451.

12. Carslaw, H.S. and J.C. Jaeger, Conduction of Heat in Solids, Oxford University Press: London (1947) p. 27.

13. Caughey, E.C., Allied Chemical, private communication.

14. Crank, J. and P. Nicolson, "A Practical Method for Numerical Evaluation of Solutions of Partial Differential Equations of the Heat-Conduction

Type," Proc. Cambridge Philos. Soc., 43, 50-67 (1947).

15. Daubeney, R. de P., C.W. Bunn and C.J. Brown, "The Crystal Structure of Polyethylene Terephthalate," Proc. Royal Soc. (London), 226A, 531-41 (1954).

16. Davis, G.T. and R.K. Eby, "The Glass Transition of Polyethylene: Volume Relaxation," Polymer Conference Series, Crystallinity, Univ. Utah, July (1973).

17. Dole, M. and R.C. Wilhoit, "Specific Heat of Synthetic High Polymers. II Polyhexamethylene adipamide and Sebacamide," J. Phys. Chem., 57, 14-21 (1953).

18. Dole, M., et al., "Specific Heat of Synthetic High Polymers: IV Polycaprolactam," J. Phys. Chem., 59, 1015-8 (1955).

19. Dole, M. and B. Wunderlich, "The Melting Range of Semicrystalline Copolymers," J. Polymer Sci., 24, 139-42 (1957).

20. Echert, E.R.G. and R.M. Drake, Heat and Mass Transfer, McGraw-Hill: New York (1959) pp. 27-31.

21. Evans, U.R., "The Laws of Expanding Circles and Spheres in Relation to the Lateral Growth of Surface Films and the Grain-Size of Metals," Trans. Faraday Soc. (London), 41, 365-74 (1945).

22. Ferry, J.D., Viscoelastic Properties of Polymers, Wiley: New York (1961) pp. 215-8.

23. Gloor, W E., "Heat Transfer Calculations in Crystalline Plastics," Soc. Plastics Eng. Trans., 3, 270-7 (1963).

24. Gornick, F., "Computer Analysis of Polymer Cooling Curves in a DTA Experiment," Am. Chem. Soc., Div. Polymer Chem., 8 (1), 262-8 (1967).

25. Gornick, F., "Computer Analysis of Polymer Cooling Curves in a DTA Experiment. I. Self-Heating Effects," J. Polymer Sci.: C, (25), 121-43 (1968).

26. Gray, A.P., "A Simple Generalized Theory for the Analysis of Dynamic Thermal Measurement," Analytical Calorimetry, 1, edited by R.S. Porter and J.F. Johnson, Plenum Press: New York (1970) pp. 209-18.

27. Gurney, H.D. and J. Lurie, "Charts for Estimating Temperature Distributions in Heating and Cooling Solid Shapes," Ind. Eng. Chem., 15 (11), 1170-2 (1923).

28. Henke, S.J., C.E. Smith, and R.F. Abbott, "Effect of Mold Temperature on the Morphology and Properties of Polypropylene: I A Propylene-Ethylene Copolymer," Polymer Eng. Sci., 15 (2), 79-83 (1975).

29. Hester, R.D., "A Morphological Study of the Initial Cold Drawing Deformation in the Superstructure of Bulk Crystallized Linear Polyethylene," Ph.D. Thesis, Georgia Institute of Technology, Atlanta, Georgia, 1974.

30. Hoffman, J D., "Thermodynamic Driving Force in Nucleation and Growth Processes," J. Chem. Phys., 28, 1192-3 (1958).

31. Hoffman, J.D. and J.I. Lauritzen, Jr., "Crystallization of Bulk Polymers with Chain Folding: Theory of Growth of Lamellar Spherulites," J. Res. NBS, 65A (4), 297-336 (1961).

32. Hoffman, J.D. and J.J. Weeks, "Melting Process and Equilibrium Melting Temperature of Polychorotrifluoroethylene," J. Res. NBS, 66A (1), 13-28 (1962).

33. Hoffman, J.D. and J.J. Weeks, "Rate of Spherulitic Crystallization with Chain Folds in Polychlorotrifluoroethylene," J. Chem. Phys., 37 (8), 1723-71 (1962).

34. Hoffman, J.D., "Theoretical Aspects of Polymer Crystallization with Chain Folds: Bulk Polymers," Soc. Plastics Eng. Trans., 4, 315-62 (1964).

35. Holmes, D.R., C.W. Bunn, and D.J. Smith, "The Crystal Structure of Polycaproamide: Nylon 6," J. Polymer Sci., 17, 159-77 (1955).

36. Inoue, M., "Studies on Crystallization of High Polymers by Differential Thermal Analysis," J. Polymer Sci.: A, 1, 2697-2709 (1963).

37. Instructions, Differential Scanning Calorimeter: DSC-1B, Perkin-Elmer Corp., Norwalk, Conn. (February, 1968).

38. Kamal, M.R. and S. Kenig, "The Injection Molding of Thermoplastics Part I: Theoretical Model," Polymer Eng. Sci., 12 (4), 294-301 (1972).

39. Keith, H.D. and F.J. Padden, Jr., "A Phenomenological Theory of Spherulitic Crystallization," J. Appl. Phys., 34 (8), 2409-21 (1963).

40. Keith, H.D. and F.J. Padden, Jr., "Spherulitic Crystallization from the Melt. I. Fractionation and Impurity Segregation and Their Influence on Crystalline Morphology," J. Appl. Phys., 35 (4), 1270-85 (1964).

41. Keith, H.D. and F.J. Padden, Jr., "Spherulite Crystallization from the Melt. II. Influence of Fractionation and Impurity Segregation on the Kinetics of Crystallization," J. Appl. Phys., 35 (4), 1286-96 (1964).

42. Keith, H.D., F.J. Padden, Jr. and R.G. Vadinsky, "Intercrystalline Links: Critical Evaluation," J. Appl. Phys., 42 (12), 4585-92 (1971).

43. Kenig, S. and M.R. Kamal, "Cooling Molded Parts-A Rigorous Analysis," Soc. Plastics Eng. J., 26, 50-7 (1970).

44. Lauritzen, J.I. and J.D. Hoffman, "Theory of Formation of Polymer Crystals with Folded Chains in Dilute Solution," J. Res. NBS, 64A (1), 73-102 (1960).

45. Liberti, F.N. and B. Wunderlich, "Melting of Polycaprolactam," J. Polymer Sci.: A-2, 6, 833-48 (1968).

46. Lindenmeyer, P.H., "Why do Polymer Molecules Fold," Polymer Eng. Sci., 14 (6), 456-63 (1974).

47. Magill, J.H., "Crystallization of Polyamides II - Nylon 6 and Nylon 66," Polymer, 6, 367-71 (1965).

48. Mandelkern, L., A.L. Allou and M. Gopalan, "Enthalpy of Fusion of Linear Polyethylene," J. Phys. Chem., 72 (1), 309-18 (1968).

49. Marx, P., et al., "Specific Heat of Synthetic High Polymers: IV Polycaprolactam," J. Phys. Chem., 59, 1015-8 (1955).

50. Milby, R.V., Plastics Technology, McGraw-Hill: New York (1973) pp. 363-5.

51. McKelvey, J.M., Polymer Processing, Wiley: New York (1962) pp. 40-8.

52. Natta, G. and P. Carradini, "Structure and Properties of Isotactic Polypropylene," Nuovo Cimento, Suppl., 15 (1), 40-51 (1960).

53. O'Neill, M.J., "The Analysis of a Temperature Controlled Scanning Calorimetry," Anal. Chem., 36 (7), 1238-45 (1964).

54. Passaglia, E. and H.K. Kevorkian, "The Heat Capacity of Linear and Branched Polyethylene," J. Appl. Polymer Sci., 7, 119-32 (1963).

55. Passaglia, E. and H.K. Kevorkian, "Specific Heat of Atactic and Isotactic Polypropylene and Entropy of Glass," J. Appl. Phys., 34, 90-7 (1963).

56. Pella, E. and M. Nebuloni, "Temperature Measurements with a Differential Calorimeter," J. Therm. Anal., 3, 229-46 (1971).

57. Perry, J.H., Chemical Engineers' Handbook, McGraw-Hill: New York (1963) pp. 23.54-5.

58. Price, F P., "Some Comments on the 'Avrami' Equation," J. Appl. Phys.,

56 (10), 3014-16 (1965).

59. Price, F.P., "Kinetics of Crystallization," Encycl. Polymer Sci. Tech., 8, 63-80 (1968).

60. Progelhof, R.C and J.L. Throne, "Cooling of Crystalline Forms with Developing Density Profiles," Soc. Plastics Eng. 33rd ANTEC, 21, 455-8 (1975).

61. Radriquez, F., Principles of Polymer Science, McGraw-Hill: New York (1970) p. 421.

62. Schwenker, R.F. and J.C. Whitwell, "Differential Enthalpic Analysis as a Calorimetric Method: Evaluation by a Statistical Design," Analytical Calorimetry, 1, edited by R.S Porter and J.F. Johnson, Plenum Press: New York (1968) pp. 249-57.

63. Selby, S.M., CRC Standard Mathematical Tables, 14th ed., The Chemical Rubber Company: Cleveland, Ohio (1965) p. 495.

64. Sharples, A.A., "Crystallinity," Polymer Science, 1, edited by A.D. Jenkins, Elsevier Pub.: New York (1972) pp. 251-320.

65. Sifleet, W.L., "Unsteady Heat Transfer in a Crystallizing Polymer," M.S.Ch.E., Ohio University, 1970.

66. Sifleet, W.L., N. Dinos, and J.R. Collier, "Unsteady-State Heat Transfer in a Crystallizing Polymer," Polymer Eng. Sci., 13 (1), 10-16 (1973).

67. Smith, C.W. and M. Dole, "Specific Heat of Synthetic High Polymer. VII Polyethylene Terephthalate," J. Polymer Sci., 20, 37-40 (1956).

68. Tannenbaum, M. and M. Hershenson, "The Finest Grain Yet," Camera 35, 16 (3), 44-5 (1972).

69. Technical Information Bulletine M-2D, E.I. duPont de Nemours & Co., Inc., Wilmington, Delaware.

70. Thermal Analysis Newsletter, (5), Perkin-Elmer Corp.

71. Thin Sectioning and Associated Technics for Electron Microscopy, Ivan Sorvall, Inc., Norwalk, Connecticut, (1967).

72. Tomkeieff, S.I., "Linear Intercept, Areas and Volumes," Nature, 155, 24 (1945).

73. Tung, L.H. and W.C. Taylor, "An Imapproved Method of Preparing Density Gradient Tubes," J. Polymer Sci., 21, 144-7 (1956).

74. Turnbull, D. and J.C. Fisher, "Rate of Nucleation in Condensed Systems,"

J. Chem. Phys., 17 (1), 71-3 (1949).

75. Turnbull, D., "Kinetics of Heterogeneous Nucleation," J. Chem. Phys., 18 (2), 198-203 (1950).

76. Underwood, E.E., Quantitative Stereology, Addison-Wesley: Reading, Mass. (1970).

77. Van Krevelen, D.W., Properties of Polymers, Elsevier Publishing Co.: Amsterdam (1972) pp. 386-93.

78. Van Vlack, L.H., Elements of Material Science, Addison-Wesley: Reading, Mass. (1964) pp. 60-1, 379.

79. Watkins, N.C. and D. Hansen, "Morphology of Melt-Crystallized Polyethyleneterephthalate," Text. Res. J., 38, 388-94 (1968).

80. Watson, E.S., et al., "A Differential Scanning Calorimetry for Qualitative Differential Thermal Analysis," Anal. Chem., 36 (7), 1233-8 (1964).

81. Wiley, R.E., "Setting Up a Density Gradient Laboratory," Plastics Tech., 8, 31-41 (1962).

82. Wilkinson, R.W. and M. Dole, "Specific Heat of Synthetic High Polymers. X. Isotactic and Atactic Polypropylene," J. Polymer Sci., 58, 1089-1106 (1962).

83. Williams, M.L., "The Temperature Dependence of Mechanical and Electrical Relaxations in Polymers," J. Phys. Chem., 59, 95-6 (1955).

84. Williams, M.L., R.F. Landel, and J.D. Ferry, "The Temperature Dependence of Relaxation Mechanisms in Amorphous Polymers and Other Glass-forming Liquids," Am. Chem. Soc. J., 77 (3), 3701-6 (1955).

85. Wunderlich, B., "Theory of Cold Crystallization of High Polymers," J. Chem. Phys., 29 (1), 1395-1404 (1958).

86. Wunderlich, B and C.M. Cormier, "Heat of Fusion of Polyethylene," J. Polymer Sci.: A-2, 5, 987-8 (1967).

VITA

Donald Gene Bright was born on November 14, 1944 in Greensboro, North Carolina to Dallas W. Bright and Virginia M. Fitch. He attended grammar school in Greensboro and graduated from Guilford High School, Guilford College, North Carolina in 1963. He received a Bachelor of Science degree in Chemical Engineering from North Carolina State University in 1967. Upon graduation he worked for Air Products & Chemicals, Inc., Allentown, Pennsylvania as a staff engineer. In 1968 he was transferred to the Houdry Process and Chemical Division where he worked as a process design engineer for one year and then as a process development engineer for two years. He entered graduate school at Villanova University, Villanova, Pennsylvania in 1971 and received a Master of Chemical Engineering degree in 1972. In September of that year he entered the Georgia Institute of Technology as a candidate for the Ph.D. degree in Chemical Engineering.